

# Cooperative Control of Networked Robotic Systems



Yiannis Stergiopoulos

Department of Electrical and Computer Engineering

University of Patras, Greece

Ph.D. Dissertation

Dissertation No: 321

September 2014

---

## ΠΙΣΤΟΠΟΙΗΣΗ

Η παρούσα διδακτορική διατριβή με θέμα:  
:«**Συνεργατικός Έλεγχος Δικτυωμένων Ρομποτικών Συστημάτων**»

Του ΣΤΕΡΓΙΟΠΟΥΛΟΥ ΙΩΑΝΝΗ του ΒΑΣΙΛΕΙΟΥ, Διπλωματούχου Ηλεκτρολόγου Μηχανικού & Τεχνολογίας Υπολογιστών παρουσιάστηκε δημοσίως στο Τμήμα Ηλεκτρολόγων Μηχανικών & Τεχνολογίας Υπολογιστών του Πανεπιστημίου Πατρών την 30<sup>η</sup> Σεπτεμβρίου 2014 και εξετάστηκε και εγκρίθηκε από την ακόλουθη Εξεταστική Επιτροπή:

**Ευάγγελος Δερματάς**, Αναπληρωτής Καθηγητής Τμήματος Ηλεκτρολόγων Μηχανικών & Τεχνολογίας Υπολογιστών, Πολυτεχνικής. Σχολής, Πανεπιστημίου Πατρών

**Νικόλαος Κούσουλας**, Καθηγητής Τμήματος Ηλεκτρολόγων Μηχανικών & Τεχνολογίας Υπολογιστών, Πολυτεχνικής. Σχολής, Πανεπιστημίου Πατρών

**Σταμάτιος Μάνεσης**, Καθηγητής Τμήματος Ηλεκτρολόγων Μηχανικών & Τεχνολογίας Υπολογιστών, Πολυτεχνικής. Σχολής, Πανεπιστημίου Πατρών

**Κωνσταντίνος Μουστάκας**

Επίκουρος Καθηγητής Τμήματος Ηλεκτρολόγων Μηχανικών και Τεχνολογίας Υπολογιστών, Πολυτεχνικής. Σχολής, Πανεπιστημίου Πατρών

**Σωτήριος Νικολετσέας**

Αναπληρωτής Καθηγητής Τμήματος Μηχανικών Ηλεκτρονικών Υπολογιστών και Πληροφορικής, Πολυτεχνικής. Σχολής, Πανεπιστημίου Πατρών

**Νικόλαος Παπανικολόπουλος**

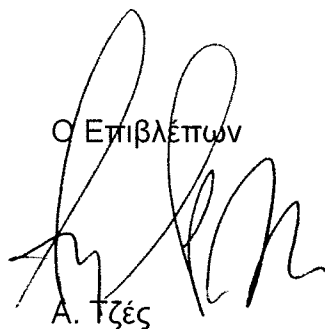
Καθηγητής Τμήματος Computer Science & Engineering, University of Minnesota, Η.Π.Α.

**Αντώνιος Τζες**

Καθηγητής Τμήματος Ηλεκτρολόγων Μηχανικών και Τεχνολογίας Υπολογιστών, Πολυτεχνικής. Σχολής, Πανεπιστημίου Πατρών

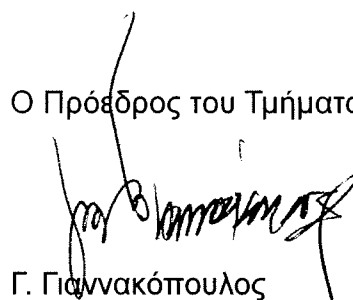
Πάτρα 30 Σεπτεμβρίου 2014

Ο Επιβλέπων



A. Τζές

Ο Πρόεδρος του Τμήματος



Γ. Γιαννακόπουλος

---

## **Abstract**

The main scope of this thesis is the design and analysis of distributed control strategies for achieving optimum area coverage in mobile sensor networks. Due to the numerous applications of the latter in missions as area exploration, environmental sampling, patrolling, or even security, a large part of the scientific community has turned its interest on developing methods for achieving optimum, if possible, sensing environmental perception by groups of autonomous mobile agents. Such robotic teams, randomly deployed in areas of interest initially, are designed to coordinate their motion in a distributed manner, rather than via a global supervisory system, in order to succeed in the corresponding mission objective.

At the first stages of this thesis, the coverage problem of an area of interest by a group of identical nodes is examined from a numerical point of view. The mobile nodes are considered to be governed by simple discrete-time kinodynamic motion, while their sensing performance is assumed radial, range-limited, uniform around the node. As a first approach, the optimum direction at each time step for optimum deployment achievement is determined based on proper distance-based space partitioning techniques. The developed concept allows for gradual increase in the covered area among consecutive steps, although suffers from allowing motion of one node at a time.

In the sequel, the aforementioned concept is extended to the case of heterogeneous networks, where heterogeneity lays mainly in the unequal limited-range of the sensing performance of the nodes. In addition, extension to continuous-time allows for simultaneous motion of the nodes, increasing drastically the convergence time towards the optimal state, especially for large-scale networks. An alternate partitioning of the space is developed that is mainly based on the nodes' footprints, rather than their spatial positions only. The resulting assigned cells form the main

core for the coordination algorithm proposed, in order to distributedly organize the mobile swarm to achieve optimum sensing performance.

Motivated by the high-degree anisotropy that governs the sensing domains of certain types of sensors, i.e. directional microphones for sound sensing mainly for security applications, or even the radiation patterns of directional antennas in communication-coverage scenarios, our research is extended beyond the standard disc model of sensing. Based on certain properties for planar convex curves, a distributed strategy is developed for networks characterized by convex sensing domains of same orientation. Although convexity of the sensing sets may seem to impose a high level restriction to the overall setup, in fact can be assigned as the maximal convex inscribed set in any (originally) anisotropic pattern. The control scheme is further extended, in the sequel, for the case of adding an extra degree of freedom to the node's mobility abilities, incorporating different and time-varying orientations among the nodes patterns. The resulting scheme is proven to lead anisotropic networks in optimum configurations, considering their sensing footprints, by properly controlling both the nodes' positions and orientations, via an innovative pattern-based partitioning scheme of the sensed space.

The thesis ends by examining the case where radio-range constraints are imposed on inter-agents communication. In the majority of the related works, this issues is usually overcome by allowing RF range as double the sensing one, guaranteeing that way distributed nature of the control schemes. The proposed scheme allows for uncorrelated RF and sensing ranges in the network, while guarantees convergence of the network towards the optimal state, via simultaneous preservation of a-priori imposed radio-range constraints. Concluding remarks along with comparative discussion are presented in the last chapter, where future research plans and ways to improve the already developed schemes are proposed.

*To my family*

for their love, patience and support throughout all these years

---



## Acknowledgements

This is the time where a stage of your life ends, while a new one just begins, and you realize that the larger part of what you have achieved in these years are is cause of certain people that were always by your side, supporting you, guiding you, understanding you, in every moment of your life. Let me devote some space in trying to express my “thank you” to those people.

I feel really honored for having the opportunity to meet in my very early academic years Anthony Tzes, professor of the Department and supervisor of this thesis, with whom i work with for over ten years, since the times i was an undergraduate student in this Department. He has always been by my side, since my first research stages, up to the final preparations, devoting a great part of his time in discussions over research plans, supporting me at the times where i really needed, not only as an academic but as a close person as well. I believed in you, you believed in our work. I thank you for all you have done for me.

I would like to thank the professors of the seven member committee, Nikos Kousoulas, Nikos Papanikolopoulos, Stamatis Manesis, Konstantinos Moustakas, Sotiris Niko-letseas, Vaggelis Dermatas, for the time they provided in closely revising this thesis, as well as their insightful comments in the discussions we had in order to make it stronger up to its current form. A special “thank you” to prof. Manesis, for all the times we have spent these years, by allowing me to know him better.

I am proud for being a member of the “guys of the SAE LAB”. We have spent much time together, living nice and bad moments. It is Marialena Vagia, my “roommate”, sharing same office for many years, knowing me in any mood. It is Themis Kolyvas and Yannis Koveos, to whom i still owe a “board presentation”. It is Vasso Reppa and Nancy Panousopoulou, the ladies that organized us when needed. I’ll still be your “little-john”. It is Eleni Kelasidi, Kostalexis and John Arvanitakis (*aka* the coordinator). We shared so much with Eleni. It is the

“new blood”, Nikos Evaggeliou, Ranis Tsilomitrou, George Andrikopoulos. Yian-nis Kantaros, Christos Papachristos, Kostis Giannousakis, Stathis Kountouras. It is Michalis Thanou, Michalis that sadly left us so early. It is these people that “secretly” keep working in the labs, not being know to everyone, yet they are that much important to me.

I thank my friends that aren't in the academic circle anymore. Thodoris, my friend and roommate for so many years. Always being next to me when I needed. I owe you a lot. Niki, friend since the undergraduate days. I was so sad when you moved to Athens permanently. Billy, always by me, getting me back on track when not focused.

Last but not least is Vassilis, Vivi, Fanis. They are my family. It is them that supported me all these years that I've been away from home. They gave everything for my studies, in especially hard times. This work is dedicated to you for being always here, by my side.

# Contents

<b>List of Figures</b>	<b>ix</b>
<b>1 Introduction</b>	<b>1</b>
1.1 Subject of the Thesis . . . . .	1
1.2 Structure of Thesis . . . . .	2
<b>2 Directional–Search Approach for Area Coverage</b>	<b>5</b>
2.1 Introduction . . . . .	5
2.2 Preliminaries . . . . .	6
2.2.1 Coverage problem setup . . . . .	6
2.2.2 Control policies for coverage optimization . . . . .	8
2.2.3 Spatial Voronoi tessellation . . . . .	9
2.3 Proposed Coordination Scheme . . . . .	11
2.3.1 Main concept . . . . .	11
2.3.2 Local Delaunay graph alteration . . . . .	12
2.3.3 Coordination algorithm . . . . .	14
2.3.4 Issues concerning spatial information exchange . . . . .	17
2.3.4.1 Connectivity with current Delaunay neighbors . . . . .	17
2.3.4.2 Guaranteeing connectivity with all possible future Delaunay neighbors . . . . .	19
2.3.5 Simulation results . . . . .	22
2.4 Conclusions . . . . .	26
<b>3 Coverage by Heterogeneous Networks</b>	<b>27</b>
3.1 Introduction . . . . .	27
3.2 Preliminaries — Motivation . . . . .	28

## CONTENTS

---

3.2.1	Main Assumptions . . . . .	28
3.2.2	Properties of Voronoi diagram for homogeneous networks . . . . .	29
3.2.3	Application in heterogeneous networks . . . . .	31
3.3	Proposed Partitioning of the Space . . . . .	32
3.3.1	Basic concept . . . . .	32
3.3.2	Development of the proposed space–partitioning technique . . . . .	33
3.3.2.1	Case I: The nodes’ sensing regions do not overlap . . . . .	35
3.3.2.2	Case II: The boundaries of the nodes’ sensing regions intersect . . . . .	35
3.3.2.3	Case III: A node’s sensing region is subset of the other’s pattern . . . . .	36
3.3.3	Properties of the proposed partitioning scheme . . . . .	36
3.3.3.1	Properties of proposed partitioning for heterogeneous and homogeneous networks . . . . .	36
3.3.3.2	Discussion on physical properties of the proposed scheme . . . . .	38
3.3.3.3	Discussion on degenerate cases arising from the proposed scheme . . . . .	39
3.3.4	Numerical results . . . . .	42
3.4	Proposed Algorithm for Optimum Area Coverage . . . . .	44
3.4.1	Preliminaries . . . . .	44
3.4.2	Coordination Algorithm Development . . . . .	46
3.4.3	Connectivity Issues . . . . .	49
3.4.3.1	Case A: A–priori knowledge of the maximum sensing radius among all nodes of the network . . . . .	50
3.4.3.2	Case B: A–priori knowledge of the sensing–radii–set of the network . . . . .	51
3.4.4	Simulation Studies . . . . .	53
3.5	Conclusions . . . . .	56
<b>4</b>	<b>Area Coverage by Anisotropic Networks</b>	<b>57</b>
4.1	Introduction . . . . .	57
4.2	Preliminaries — Motivation . . . . .	58
4.2.1	Main Assumptions and Definitions . . . . .	58
4.2.2	On Non–Uniform Sensing Patterns . . . . .	59
4.3	Optimum Coverage in Anisotropic Networks . . . . .	60

4.3.1	Space Partitioning . . . . .	60
4.3.2	Spatially Distributed Coordination Algorithm . . . . .	63
4.3.3	Distributedness Issues . . . . .	64
4.3.4	Numerical studies . . . . .	66
4.4	Extensions via Allowing Rotation of the Footprints . . . . .	71
4.4.1	Motivation . . . . .	71
4.4.2	Problem Statement . . . . .	73
4.4.3	Proposed Pattern-based Partitioning . . . . .	74
4.4.3.1	Related Approaches . . . . .	75
4.4.3.2	Proposed Partitioning . . . . .	76
4.4.4	Distributed Motion Coordination . . . . .	78
4.4.5	Simulation Studies . . . . .	81
4.5	Conclusions . . . . .	85
<b>5</b>	<b>Coverage with Constraints in the Communication Range</b>	<b>87</b>
5.1	Introduction . . . . .	87
5.2	Problem Setup — Preliminaries on Connectivity . . . . .	88
5.2.1	Coverage Problem Formulation . . . . .	88
5.2.2	Radio Connectivity Issues . . . . .	91
5.3	Distributed Control for Optimum Coverage while Maintaining Network Con- nectivity . . . . .	95
5.3.1	Motivation for extension of existing control laws . . . . .	96
5.3.2	Proposed Control Scheme – Modifications . . . . .	97
5.3.3	Further heuristic extension . . . . .	104
5.4	Conclusions . . . . .	108
<b>6</b>	<b>Thesis Summary and Future Research Plans</b>	<b>109</b>
6.1	Research Contribution . . . . .	109
6.2	Extensions of current research . . . . .	110
	<b>References</b>	<b>115</b>

## CONTENTS

---

# List of Figures

2.1	Voronoi diagram [left] and Delaunay graph [right] for a set of nodes in a compact domain. . . . .	10
2.2	Characterization of the different regions concerning a node and its Voronoi cell.	11
2.3	Alteration of the Delaunay neighbors of a node caused by the motion of the latter.	12
2.4	Illustrative example for definition of $V_j^{r,k}  _{\mathcal{G}_i^k}$ sets. . . . .	14
2.5	Worst case scenario for the existence of a node $m$ that is to enter $\mathcal{N}_i^{k+1}$ . . . . .	20
2.6	Communication radius of the node-to-move (red color) required in order to guarantee connectivity: (a) with $\mathcal{N}_i^k$ , (b) with $\mathcal{N}_i^{k+1}$ , for a given node's motion (worst case scenario). . . . .	21
2.7	Sparse-network case study: [Left] Initial network configuration. [Middle] Network evolution through time. [Right] Final network optimum state. [Bottom] Percentage of covered area w.r.t. time. . . . .	24
2.8	Congested-network case study: [Left] Initial network configuration. [Middle] Network evolution through time. [Right] Final network optimum state. [Bottom] Percentage of covered area w.r.t. time. . . . .	25
3.1	Inappropriateness of standard Voronoi tessellation when dealing with heterogeneous networks. . . . .	32
3.2	Notations for definition of $\tilde{H}_{ij}$ halfplanes. . . . .	33
3.3	Space-partitioning based on the radii and relative positioning of a pair of nodes.	34
3.4	Space-partitioning via the proposed algorithm for a network consisting of three nodes in order to show the existence of sole cells. . . . .	40
3.5	Voronoi partitioning via the standard [left] and modified [right] technique for a heterogeneous network to emphasize in the degenerate cases arisen. . . . .	41

## LIST OF FIGURES

---

3.6	Voronoi partitioning via the standard [left] and proposed [right] technique for a heterogeneous network consisted of $n = 7$ nodes (Case Study 1). . . . .	42
3.7	Voronoi partitioning via the standard [left] and proposed [right] technique for a heterogeneous network consisted of $n = 16$ nodes (Example 2). . . . .	43
3.8	Decomposition of the set $\partial\tilde{V}_i^r$ into mutually disjoint sets. . . . .	48
3.9	Graphical representation of $\tilde{n}_i, \tilde{n}_j$ at the common boundary $\partial\tilde{V}_i \cap \partial\tilde{V}_j$ for the degenerate case where $x_i \notin \tilde{V}_i$ . . . . .	49
3.10	Graphical representation of the worst case scenario determination during the radio-range adjustment scheme. . . . .	52
3.11	Case Study I — Coordination results derived via standard [top row] and modified [bottom row] Voronoi partitioning, respectively. [Left column] Initial network configuration. [Middle column] Network evolution through time. The black circles (blue squares) represent the nodes' final (initial) positions. [Right column] Final network state. . . . .	54
3.12	Percentage of covered area w.r.t. time for standard [blue line] and modified [red line] Voronoi partitioning utilization in the control law. Left (Right) part stands for Case Study I (II). . . . .	55
3.13	Case Study II — Coordination results derived via standard [top row] and modified [bottom row] Voronoi partitioning, respectively. [Left column] Initial network configuration. [Middle column] Network evolution through time. The black circles (blue squares) represent the nodes' final (initial) positions. [Right column] Final network state. . . . .	56
4.1	Graphical example to indicate the benefits arisen by allowing non-node-centered sensing domains in coverage applications. [Left] The node's patterns are the antenna's radiation pattern in T-mote Sky platforms as provided in [1]. [Right] The node's pattern is a typical cardioid footprint of directional microphones as provided in [2]. . . . .	60
4.2	Illustrative examples of the partitioning of the sensed domain of a network via Definition 4.3 for RF (left) and acoustic (right) devices, based on their approximation as of Figure 4.1. . . . .	62
4.3	Graphical example of defining the topological worst case scenario among two arbitrary nodes in order to determine the communication radius bound. . . . .	65



4.4	Sensing pattern of the nodes utilized in the simulations, defined as the union of sequential Bézier curves. . . . .	67
4.5	Case Study I — Coordination results derived via control schemes (4.6) [top row] and (4.5) [bottom row], respectively. [Left column] Initial network configuration. [Middle column] Network evolution through time. The black circles (blue squares) represent the nodes' final (initial) positions. [Right column] Final network state. . . . .	68
4.6	Percentage of sensed area w.r.t. time for Case Study I [left] and II [right], when control schemes (4.6) [blue line] and (4.5) [red line] are applied, respectively. The black dotted line represents the maximum possible coverage ratio in each case. . . . .	69
4.7	Case Study II — Coordination results derived via control schemes (4.6) [top row] and (4.5) [bottom row], respectively. [Left column] Initial network configuration. [Middle column] Network evolution through time. The black circles (blue squares) represent the nodes' final (initial) positions. [Right column] Final network state. . . . .	70
4.8	Case Study III — Coordination results derived via control schemes (4.6) [top row] and (4.5) [bottom row], respectively. [Left column] Initial network configuration. [Middle column] Network evolution through time. The black circles (blue squares) represent the nodes' final (initial) positions. [Right column] Final network state. . . . .	71
4.9	Percentage of sensed area w.r.t. time for Case Study III, when control schemes (4.6) [blue line] and (4.5) [red line] are applied, respectively. . . . .	72
4.10	Graphical representation of the evolution of suggested techniques for non-uniform sensor footprints. . . . .	73
4.11	Graphical representation of the need for alternate partitioning in non-uniform sensor networks. (a) Anisotropic heterogeneous network approximated with disc-model. (b) Corresponding power diagram based on the approximation of node-centered maximal inscribed circles. (c) Real network's coverage via the original non-uniform patterns, as evaluated through the simultaneously sensed and assigned cells. . . . .	75
4.12	Illustrative example indicating the partitioning of the sensed space via the proposed technique. . . . .	77

## LIST OF FIGURES

---

4.13	Decomposition of $\partial W_i$ into mutually disjoint sets. . . . .	79
4.14	Notations concerning the proof of the main theorem. . . . .	80
4.15	Normalized patterns used in the first [left] and second [right] simulation study, respectively, along with their maximal inscribed node-centered discs. . . . .	82
4.16	[Case-Study 1]: Coordination results derived via control schemes (4.6) [top row] and (4.13)–(4.14) [bottom row], respectively. [Left column] Initial network configuration. [Middle column] Network evolution through time. The black circles (blue squares) represent the nodes’ final (initial) positions. [Right column] Final network state. . . . .	83
4.17	[Case-Study 1]: [Left] Evolution of covered area percentage w.r.t. time evaluated via the non-uniform original patterns. Blue (Red) line corresponds to top (bottom) row of Fig. 4.16. [Right] Evolution of nodes’ orientation w.r.t. time corresponding to the bottom row of Fig. 4.16. . . . .	84
4.18	[Case-Study 2]: Coordination results derived via control schemes (4.6) [top row] and (4.13)–(4.14) [bottom row], respectively. [Left column] Initial network configuration. [Middle column] Network evolution through time. The black circles (blue squares) represent the nodes’ final (initial) positions. [Right column] Final network state. . . . .	85
4.19	[Case-Study 2]: [Left] Evolution of covered area percentage w.r.t. time evaluated via the non-uniform original patterns. Blue (Red) line corresponds to top (bottom) row of Fig. 4.18. [Right] Evolution of nodes’ orientation w.r.t. time corresponding to the bottom row of Fig. 4.18. . . . .	86
5.1	Graphical representation of the Delaunay [left] and $2r$ -limited Delaunay [right] neighbors in a sensor network. . . . .	90
5.2	Example of area-optimal configurations achieved via (4.6) for an arbitrary sensor network. . . . .	90
5.3	Graphical representation of the need for multi-hopping in order to acquire sufficient information for distributed $V_i^r$ evaluation. . . . .	92
5.4	Evolution of $\mathcal{D}_i^N$ -set identification during a time-step interval $T$ . The 3-hops neighbors of the yellow diamond-shaped node are identified sequentially (red ones) via chained neighbors-transmission. The repeated RX/TX process takes place during the time-step interval $T$ . . . . .	94

5.5 Graphical illustration of the connectivity-oriented motivation for demanding motion of one node at each step in a simple network of two nodes. . . . . 94

5.6 Graphical representation of topologies where connectivity among  $2r$ -limited Delaunay neighbors cannot be forced. . . . . 95

5.7 Coordination results derived via Algorithm 5.2. [Left] Initial network configuration. [Right] Final network state. Communication graph indicates 2-hops connectivity among the  $2r$ -limited Delaunay neighbors. . . . . 97

5.8 Categorization of nodes into interior and exterior ones. Blue (red) dots represent the interior (exterior) ones. . . . . 98

5.9 Graphical depiction of the suboptimal directions allowed in chapter 5 to avoid deadend-configurations, while preserving connectivity. . . . . 99

5.10 Notations concerning the proof of Lemma 5.1 . . . . . 102

5.11 Converged state along with communication graph when 1-hop [left], 2-hops [middle] and 3-hops [right] connectivity is demanded. . . . . 103

5.12 Effect of allowed number of hops for connectivity preservation in coverage performance [1-hop:blue, 2-hops:green, 3-hops:black]. . . . . 104

5.13 Categorization of nodes into interior(exterior)[boundary] nodes, denoted with blue(red)[black] dots. . . . . 106

5.14 Coordination results derived via the heuristically extended control scheme. [Left] Initial network configuration. [Middle] network evolution. [Right] Final network state. . . . . 107

5.15 Percentage of sensed area during network evolution. Blue (green) line corresponds to Fig. 5.14 (5.11). . . . . 107

## LIST OF FIGURES

---

# List of Algorithms

2.1	Communication Range Adjustment for Connectivity with $\mathcal{N}_i^k$ . . . . .	19
2.2	Communication Range Adjustment Algorithm for Connectivity with $\mathcal{F}_i^k$ . . . . .	23
3.1	Distributed Radio–Range Adjustment Scheme for Heterogeneous Networks . . . . .	53
5.1	Identification of $\mathcal{N}_i^{2r}$ neighbors via multi–hopping for fixed RF range . . . . .	93
5.2	Motion planning for coverage control in networks under non–trivial communication constraints (base pattern) . . . . .	96
5.3	Proposed control scheme based on interior/exterior nodes–categorization . . . . .	100

## LIST OF ALGORITHMS

---

# 1

## Introduction

### 1.1 Subject of the Thesis

Distributed coordination of robotic swarms has been studied widely in the last years due its direct application in missions where human interference involves risk or is even prohibited, while on-time detection of certain events is crucial [3, 4]. Mobile platforms with sensing, computational and communication capabilities are in most cases spread in areas of interest in order to investigate various physical quantities [5] and/or even take responsibility of surveying the area assuming applications related to environmental sensing [6], patrolling [7], exploration [8, 9], precaution [10] or even security [11]. In most cases, these tasks are almost impossible to be carried out by a single robotic agent, while a properly organized team benefits from robustness in nodes' failure and allows flexibility of the network [12]. Thus, efficiently designed cooperative strategies can lead the network in an optimal state, dependent on a predefined aggregate criterion [13].

We focus in utilization of mobile robotic teams in coverage/surveillance applications mainly. Mobility offers the advantage of allowing to the members of the team to evolve in space through time autonomously and seek the optimum configuration that would serve the common purpose. In either case, the mobile platforms are equipped with appropriate means for inter-agents communication, along with sensing devices such as microphones, cameras, humidity/temperature sensors, smoke detectors and others, dependent on the application. Information exchange along with mobility provide the major advantage of allowing the network to reconfigure itself in case of topological alteration and adapt to the current purpose, as in search and rescue missions.

It is essential though that the corresponding control laws that serve towards the aggregate

## 1. INTRODUCTION

---

criterion are decentralized in the sense that they should not demand global information, but only from nodes in the proximity neighborhood of each agent [14]. Partitioning of the space is the core in distributed control, allowing proper assignments of regions among the nodes, so that individual action serves the global network performance. This thesis serves towards the development of distributed control strategies for mobile teams that are able to lead the network towards area-optimal topological configurations.

We mainly emphasize in issues that arise by assuming non-trivial sensing models, as directed by the sensor type itself in most applications. Starting from the standard uniform radial model, we extend the results for nodes with unequal ranges via properly partitioning the space among the members of the team in a pattern-based framework. Control strategies are presented that lead the nodes in area-optimal topology. The concept is generalized for sensors with arbitrary footprints, where the space is tessellated in a non-distance-based manner. Communication issues that arise from the distributed demand of the corresponding laws are analyzed in order to maintain connectivity routes among the members during network's evolution.

### 1.2 Structure of Thesis

The remaining of the thesis is organized as follows. In chapter 2 the core coverage problem is examined for a group of nodes with uniform radial sensing patterns assuming discrete time evolution. Utilizing the main results of Euclidean Voronoi partitioning, proper analysis is performed in order for the node-to-move to acquire information from its current and future Delaunay neighbors, in order to guarantee strict increase in the overall network's performance between sequential time steps via its motion.

In chapter 3 networks with inherent heterogeneity are examined, where the latter is captured in the different ranges that the various sensors of the nodes can sense. The discrete evolution model is abandoned, allowing for faster convergence rates in the overall network's performance. Insisting in convex partitioning of the space, while emphasizing in the pattern-based approach, a control strategy has been developed for leading a group of nodes towards locally optimal topology.

Inspired by the highly anisotropic nature of certain sensors, the case of nodes with non-radial footprints is examined in chapter 4. Utilizing special properties for planar strictly convex curves we develop a partitioning scheme of the sensed space, for the case of nodes with common orientation. A distributed coordination law based on the aforementioned tessellation is



presented, able to organize the nodes in an area–optimum configuration. In order to amend for dropping the somehow conservative restriction of common headings, an extra rotational degree of freedom is added in the kinematic model. An innovative partitioning technique is developed in the sequel, along with an appropriate law that serves the coverage problem, properly controlling both the nodes translation and headings towards the converged optimal topology.

Chapter 5 revisits the discrete model for the motion of the nodes. Unlike previous works that assume the RF range at least equal to twice the sensing one, we impose non–trivial constraints concerning connectivity among the agents. Considering the uniform radial model, we design a control law that is able to guarantee monotonic increase in the network’s coverage performance, while simultaneously maintain end–to–end connectivity among the agents during evolution, by properly adding/removing communication links, given the a–priori fixed RF range.

The thesis ends with concluding remarks in chapter 6, followed by discussion on how the current results can be extended for future research.

## 1. INTRODUCTION

---

## 2

# Directional–Search Approach for Area Coverage

## 2.1 Introduction

Area–coverage of a certain region by a set of mobile nodes can be examined via the “bin packing” or “disc covering” problem. According to the first approach, the goal is to find the nodes’ maximum sensing range (considered equal for all members of the network) such that there exists a configuration where the nodes are deployed in the interior of a region of interest covering the maximum possible area with no overlapping among their sensing patterns. On the other hand, the “disc covering” problem is posed as finding the minimum sensing range of the nodes in a way that all parts of the region of interest are sensed by at least one node.

In both algorithms, the sensing radius of the nodes is considered as a variable and the goal is to determine the nodes’ positions and radius in order to fulfill the appropriate area–related demand [15]. We assume the nodes’ sensing pattern to be fixed, seeking to define (locally) optimal positions such that the sensed area of the region of interest is maximized.

The centralized coverage problem has been examined from an instantaneous coverage point of view (*aka* awareness control) by [8], where the agents coordinate their motion such that all points in the environment are surveyed through time by an equal amount, resulting in a fully scanned area in finite time. Centroidal Voronoi schemes (CVT) have been developed for the distortion–minimization criterion in [13, 16] so that the network converges to a topology that minimizes the sensing–uncertainty in the environment.

We initially examine the problem in discrete evolution time. The nodes are equipped with

## 2. DIRECTIONAL-SEARCH APPROACH FOR AREA COVERAGE

---

radio transceivers with variable range, apart from the fixed-range sensors, leading in a hybrid coverage/connectivity research approach.

Considering optimum coverage of a certain region of interest by a set of nodes with sensing capabilities, the main problem lays in defining the optimum network configuration such that the sensing overlapping is minimized. Apart from that, since the nodes in most practical scenarios represent mobile robotic vehicles, a set of non-colliding trajectories is required so that the nodes can reach that optimum state. Centralized coordination frameworks though suffer from computational complexity, while they are characterized by the lack of adaptation to possible network alteration.

In this chapter coverage optimization is performed distributedly by the nodes, leading the network toward the optimum state, based on Voronoi partitioning of the space. Algorithmic implementations on the communication range adjustment (considering connectivity issues) are presented, along with corresponding bounds on them for connectivity preservation with the appropriate subset of nodes. Despite the absence of a centralized coordinator, the proposed scheme is built in a way such that the total area covered by the network is increasing from one step to another. Decision for motion is taken by the nodes autonomously, while assumptions concerning knowledge of current and future Delaunay neighbors are examined in detail, providing the corresponding communication radii needed for them to hold.

## 2.2 Preliminaries

### 2.2.1 Coverage problem setup

Let the region under surveillance  $\Omega$  be a convex compact set in  $\mathbb{R}^2$ . Suppose that  $n$  is the number of available mobile nodes responsible for the sensing coverage of  $\Omega$ . Let us define the set  $I_n = \{i \in \mathbb{N} : i \leq n\}$  for any  $n \in \mathbb{N}$ . The agents are considered to move on the  $\mathbb{R}^2$  Euclidean configuration space and their positions are denoted as  $x_i \in \mathbb{R}^2$ ,  $i \in I_n$ . The following assumptions are made for the network.

**Assumption 2.1.** *The nodes are supposed to move in the interior of  $\Omega \subset \mathbb{R}^2$  through two control inputs each,  $u_i \in \mathbb{R}^2$ ,  $i \in I_n$ , while obeying the discrete evolutionary equation*

$$x_i^{k+1} = x_i^k + u_i^k, \quad u_i, x_i \in \mathbb{R}^2, \quad i \in I_n. \quad (2.1)$$

*The superscript index denotes the corresponding time-step,  $k = 0, 1, 2, \dots$ , while only one node is supposed to move at each step.*

**Assumption 2.2.** Each node is supposed to have a uniform circular sensing pattern centered at its position  $x_i$  and is limited by a fixed maximum sensing radius  $r$ . The latter is the same for all nodes and the network is considered homogeneous, as far as concerns the nodes' sensing abilities. Let us denote as  $C_i$  the sensing region of each agent  $i$ , i.e.

$$C_i = \{x \in \mathbb{R}^2: \|x - x_i\| \leq r\}, \quad i \in I_n. \quad (2.2)$$

**Assumption 2.3.** Each node is supposed to be equipped with radio transceivers in order to be able to exchange spatial information with other members of the network. The radiation pattern  $S_i$  of the antennas is considered as a uniform circular one, centered at  $x_i$ , i.e.

$$S_i = \{x \in \mathbb{R}^2: \|x - x_i\| \leq R_i\}, \quad i \in I_n, \quad (2.3)$$

while the communication radii of the nodes,  $R_i$ , are considered to be adjustable.

As far as the motion of the nodes is concerned, the selection of the node-to-move must be performed by the nodes themselves, and not by a global supervisor, considering decentralized applications. This can be achieved by determining the corresponding node either in a cyclic or in a random manner. In the first case, an arbitrary node  $i$  moves only at time-steps  $k = i + p n$ ,  $p \in \mathbb{N}$ , while in the intermediate time-intervals it can be set in standby mode in order to preserve power. Alternatively, the node that is to perform possible motion can be chosen randomly by the group itself, where the random generators that run on each processor have the same "seed" value, so that at each step the node-to-move is unique and same for all members of the network.

The nodes are initially deployed randomly in  $\Omega$ . Considering coverage optimization scenarios, the goal is to find in a distributed way their optimal positions such that the area of the covered domain of  $\Omega$  by the network is the maximum possible. For a compact polygonal set  $P \subset \mathbb{R}^2$  let  $\partial P$  be its boundary. Then  $P$  is fully defined by the vertices of  $\partial P$  denoted as  $p_j$ ,  $j \in I_{N(P)}$ , where  $N(P)$  is the number of the latter's vertices.

From a numerical aspect, for any polygonal set  $P$ , the area-function  $\mathcal{A}(\cdot)$  is then defined as [16]

$$\mathcal{A}(P) = \frac{1}{2} \left\| \sum_{j \in I_{N(P)}} (p_j \times p_{j+1}) \right\|, \quad (2.4)$$

where  $\times$  corresponds to the cross-product of two vectors, the vertices  $p_j$  are set in counter-clockwise order and  $p_{N(P)+1} \equiv p_1$ , by convention. The main objective is to position the nodes

## 2. DIRECTIONAL-SEARCH APPROACH FOR AREA COVERAGE

---

at certain spatial coordinates such that the total region of  $\Omega$  surveyed by the network, i.e.  $\Omega \cap \bigcup_{i \in I_n} C_i$ , has the maximum possible area (at the optimal state), while providing at the same time non-degenerate trajectories for the nodes to reach that state.

### 2.2.2 Control policies for coverage optimization

In order to find the planar coordinates for each node  $x_i \in \Omega$ ,  $i \in I_n$  so that  $\mathcal{A}(\Omega \cap \bigcup_{i \in I_n} C_i)$  is optimized, a numerical approach will be followed. The aforementioned problem is a standard constrained numerical optimization one, the solution of which may converge to possible local extrema. Let  $X = (x_1^T, x_2^T, \dots, x_n^T)^T$  be the vector containing the coordinates of all agents,  $X \in \mathbb{R}^{2n}$ . The constraint  $x_i \in \Omega$ ,  $\forall i \in I_n$  can be cast in a linear compact form as  $A X \leq B$ , where the matrices  $A$ ,  $B$  are explicitly defined by the vertices  $\omega_j$  of  $\Omega$ ,  $j \in I_{N(\Omega)}$  [17]. Consequently, a centralized approach to the coverage problem can be defined as the solution of the following constrained optimization

$$\text{find } X: \quad \text{maximize } \mathcal{A}\left(\Omega \cap \bigcup_{i \in I_n} C_i\right), \quad \text{subject to } A X \leq B \quad (2.5)$$

Considering centralized optimization approaches, this is a computationally intensive problem to solve, due to the large number of its local extrema and the time it takes (for even a small number of nodes). Apart from that, one of the most significant disadvantages in these cases is its lack of adaptation. Consequently, in case the region of interest changes or if a node runs out of energy, then a new optimization should be performed for defining the “new” optimal positioning of the nodes, which may be disastrous in cases of emergency. On top of that, despite the centralized nature of the algorithms, global optimal solution is not guaranteed. Finally, it should be noted that, once the optimum network state is defined, path planning schemes must be applied afterwards so that the mobile agents can be able to reach this optimum, while avoiding collision with each other.

Distributed algorithms are faster from an implementation point of view and are adaptive by nature, since optimization is performed real-time individually by the members of the network itself. Each node self-organizes its action so that its motion contributes to network coverage, while decision is taken based only on local information, without the need of having global knowledge of the whole network’s state. Local information (obtained by radio transceivers attached on the nodes) is the one that poses the inherent adaptive nature of these algorithms, while the performed optimizations (executed on the on-board nodes’ processors) are by-far

less computationally intensive, making them applicable in real-time scenarios. Finally, one of the main differences, compared to the centralized approaches, is that the nodes do not focus in defining their final optimal positions, but they plan their positions at each time-step, such that (if possible) the total area coverage is an increasing function of time during this optimum-seeking procedure.

Considering the discussion above, it is clear that, although decentralized algorithms may converge to local extrema of (2.5), they are closer to real-time applications. What needs to be clearly defined is the term of “local information”, along with the coordination algorithm, according to which the nodes should organize their action in order to converge to a state where the total area covered by the network is optimal.

### 2.2.3 Spatial Voronoi tessellation

Considering the region under surveillance  $\Omega$ , a responsibility region can be assigned at each agent based on its spatial coordinates on the plane. The set of these regions is known as a Voronoi diagram [14]. For the convex compact set  $\Omega$  and the  $n$  nodes, the region under surveillance is partitioned into  $n$  convex compact subsets  $V_i$ ,  $i \in I_n$ , which are defined as

$$V_i = \{x \in \Omega: \|x - x_i\| \leq \|x - x_j\|, \forall j \in I_n\}, \quad i \in I_n. \quad (2.6)$$

The set  $V_i$  is known as the Voronoi cell of node  $i$ . It should be noted that a Voronoi diagram is a full tessellation of  $\Omega \subset \mathbb{R}^2$ , since  $\bigcup_{i \in I_n} V_i = \Omega$  and  $\text{Int } V_i \cap \text{Int } V_j = \emptyset, \forall i, j \in I_n, i \neq j$ , where  $\text{Int } \cdot$  is the interior of the set-argument. A Voronoi cell  $V_i$  is uniquely characterized by the set of its vertices  $v_{i,j}, j \in I_{N(V_i)}$ .

Two nodes that share an edge of their Voronoi cells (i.e. their Voronoi cells are adjacent) are considered as Delaunay neighbors [14]. The Delaunay neighbors  $\mathcal{N}_i$  of an arbitrary node  $i$  are then defined as

$$\mathcal{N}_i = \{j \in I_n: V_i \cap V_j \neq \emptyset \text{ non singleton}, j \neq i\}, \quad i \in I_n, \quad (2.7)$$

where  $a$  is an arbitrary point in  $\mathbb{R}^2$ . It should be noted that when  $V_i \cap V_j$  is a singleton, then the two nodes share a common Voronoi vertex (instead of a Voronoi edge) and are not considered as Delaunay neighbors. Figure 2.1 depicts the Voronoi diagram along with the corresponding Delaunay graph for a set of nodes in a compact region. It should be noted that node  $i$  itself is

## 2. DIRECTIONAL-SEARCH APPROACH FOR AREA COVERAGE

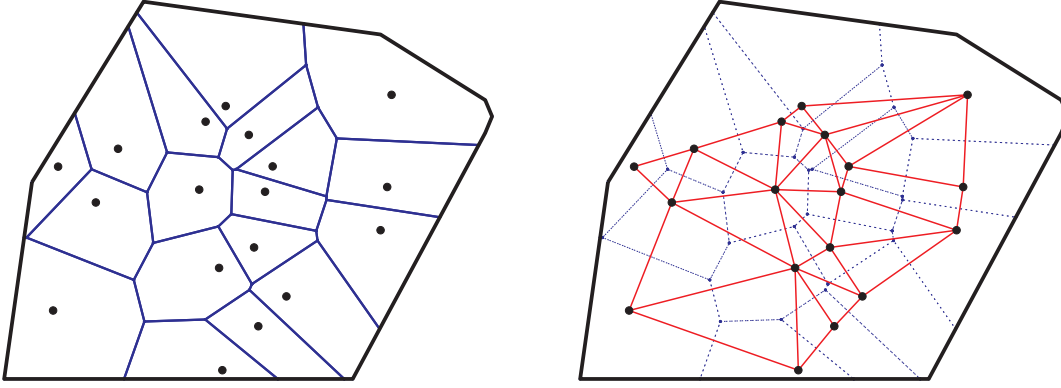


**Figure 2.1:** Voronoi diagram [left] and Delaunay graph [right] for a set of nodes in a compact domain.

not included into the set of its neighbors  $\mathcal{N}_i$ , as shown by (2.7). The edges of the Voronoi cell of an arbitrary node  $i$  that do not lay on the boundary of  $\Omega$  are then defined as

$$\Delta_{ij} = V_i \cap V_j, \quad i \in I_n, j \in \mathcal{N}_i. \quad (2.8)$$

In this work the agents move in a way to try and cover (ideally, if possible) the whole space  $\Omega$ , considering their limited sensing capabilities. Thus, the Voronoi tessellation alone is not sufficient for the motion algorithm, since it is based only on the nodes' positioning, but the sensing regions  $C_i$  should be taken into account. The  $r$ -limited Voronoi cells are then defined as

$$V_i^r = V_i \cap C_i, \quad i \in I_n. \quad (2.9)$$

An important property of these sets is that, since  $\Omega, V_i, C_i$  are convex sets, then  $V_i^r$  are all convex sets, too. However, they do not always consist a full tessellation of  $\Omega$ .

For each node, the unexploited regions of its sensing pattern (parts of the sensing region of the node that do not contribute to coverage of  $V_i$ ) are defined as

$$U_i = C_i \setminus V_i^r, \quad i \in I_n. \quad (2.10)$$

Although  $V_i, V_i^r \subseteq \Omega, \forall i \in I_n$  by definition, the same does not always hold for  $U_i$ , as concluded by (2.10) and (2.2). In fact, the set  $\bigcup_{i \in I_n} U_i$  corresponds to the parts of the nodes' sensing regions that overlap among each other or lay in the exterior of  $\Omega$ . However, the set  $U_i$  can be decomposed as a union of smaller sets which are disjoint among each other, as

$$U_i = U_i^\Omega \bigcup_{j \in \mathcal{N}_i} U_i^j, \quad i \in I_n, \quad (2.11)$$



where  $U_i^\Omega = C_i \setminus \Omega$ , i.e. parts of the sensing region that do not lay in  $\Omega$ , and  $U_i^j = U_i \cap V_j$ , i.e. parts of the node's unexploited regions that lay in the Voronoi cell of a neighbor node. The aforementioned definition along with its decomposition will be proven helpful in section 2.3.3. The above regions for an arbitrary node are shown graphically in Fig. 2.2.

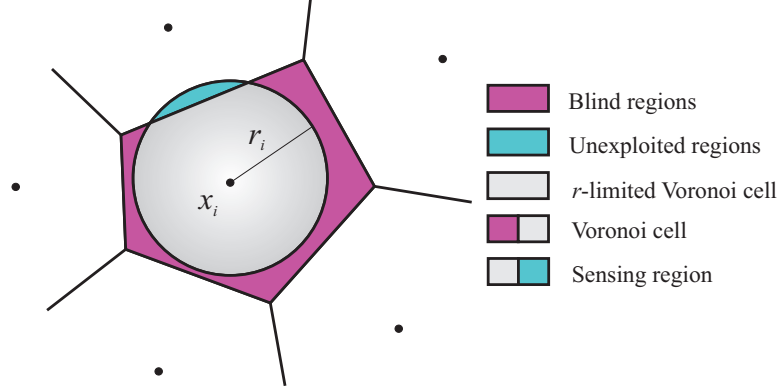


**Figure 2.2:** Characterization of the different regions concerning a node and its Voronoi cell.

Consequently, the area of the total region of  $\Omega$  surveyed by the network, can be written as

$$\mathcal{H} = \mathcal{A} \left( \Omega \cap \bigcup_{i \in I_n} C_i \right) = \sum_{i \in I_n} \mathcal{A}(V_i^r). \quad (2.12)$$

The main advantage in computation of  $\mathcal{H}$  via (2.12) is that, since  $\text{Int } V_i^r \cap \text{Int } V_j^r = \emptyset$ ,  $\forall i, j \in I_n$ ,  $i \neq j$ , the area covered by the network can be computed as the summation of the areas of the independent  $r$ -limited Voronoi cells, and thus leads in ease of implementation of decentralized techniques.

## 2.3 Proposed Coordination Scheme

### 2.3.1 Main concept

Considering sensing coverage applications, the nodes should one-by-one (Assumption 2.1) move to such spatial locations in a way that the total covered area  $\mathcal{H}$  of  $\Omega$  is non-decreasing as time evolves [18]. Taking into account that, in most practical scenarios, global knowledge of the network's state by a node is impossible (since that would lead to extremely large communication ranges), each node should have sufficient spatial information of the nodes in its neighborhood, in order to determine its position at the next step in a way that network's coverage will increase via its motion.

## 2. DIRECTIONAL-SEARCH APPROACH FOR AREA COVERAGE

However, considering (2.12), in order for the node-to-move to decide if its motion will contribute to coverage-increase at an arbitrary time-step, it should have appropriate knowledge of the state of the nodes whose Voronoi cells are to be affected via its motion. In fact, spatial information from these nodes is adequate in order for the node-to-move to take decision about the spot to move at, in a decentralized concept. Throughout the rest of the section, the index  $i$  will stand for the node-to-move at step  $k$ , and not for an arbitrary node.

### 2.3.2 Local Delaunay graph alteration

Considering the Voronoi space-partitioning defined in (2.6), the selected node should first define the region of responsibility (own Voronoi cell) that is assigned to it. The nodes are supposed to be capable of exchanging information concerning their spatial coordinates (Assumption 2.3). Taking into account the fact that no other node (apart from  $i$ ) moves at that time-step, the only part of the network that alters (considering coverage performance) are the Voronoi cells of the union of Delaunay neighbors of node  $i$  before and after its motion, along with the Voronoi cell of the moving node itself.

Let us denote as  $\mathcal{N}_i^k$  and  $\mathcal{N}_i^{k+1}$  the Delaunay neighbors of node  $i$  at steps  $k$  and  $k+1$ , which correspond to the time-instances before and after the motion of the latter, respectively. Figure 2.3 shows such a scenario, where a node moves in the interior of its Voronoi cell, resulting in alteration of its Delaunay neighbors. The red dot represents the node-to-move to the spot

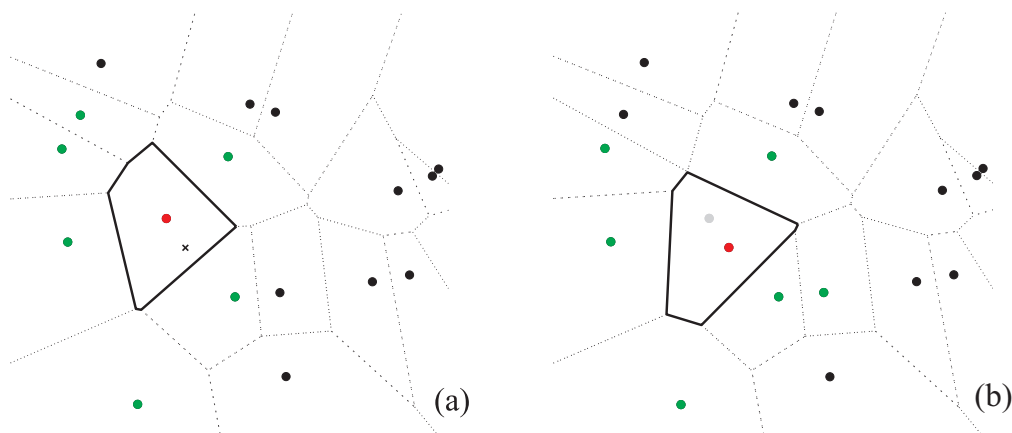


**Figure 2.3:** Alteration of the Delaunay neighbors of a node caused by the motion of the latter.

denoted with the  $\times$  sign in Fig. 2.3(a). Consider that Fig. 2.3(a) and 2.3(b) correspond to time-steps  $k$  and  $k+1$ , respectively. The green dots correspond to the Delaunay neighbors of

the red node in each case, i.e.  $\mathcal{N}_i^k$  (Fig. 2.3(a)) and  $\mathcal{N}_i^{k+1}$  (Fig. 2.3(b)). The grey sign at Fig. 2.3(b) corresponds to the position of the red node before its motion, i.e.  $x_i^k$ .

Each Delaunay neighbor of the red node is reflected on an edge of the latter's Voronoi cell. It is easy to see that if a node  $j \in \mathcal{N}_i^k$  is to leave the set  $\mathcal{N}_i$  at the next step, i.e.  $j \in \mathcal{N}_i^k \setminus \mathcal{N}_i^{k+1}$ , then the edge of the moving node's Voronoi cell that corresponds to that node degenerates into a vertex in the next step. In a similar manner, if a "new" node  $j \notin \mathcal{N}_i^k$  is to enter the set of the moving node's Delaunay neighbors after motion of the latter is performed, i.e.  $j \in \mathcal{N}_i^{k+1} \setminus \mathcal{N}_i^k$ , then a vertex of  $V_i$  will evolve into two vertices after its motion, adding  $\Delta_{ij}$  into the set of its Voronoi edges. Important is the fact that the rest of the network's state (considering Voronoi cell alteration), apart from the set  $\mathcal{N}_i^k \cup \mathcal{N}_i^{k+1} \cup \{i\}$ , does not alter at all. Indeed, if we suppose that the Voronoi cell of a node that does not belong in  $\mathcal{N}_i^k \cup \mathcal{N}_i^{k+1} \cup \{i\}$  alters, this means that a Delaunay neighbor of that node has moved and thus has perturbed a Voronoi edge. But, since the only node that moves is node  $i$ , then the aforementioned node should belong to the above set.

Suppose now that the possible motion of node  $i$  at step  $k$  is restricted in a convex compact subset of  $V_i^k$  denoted as  $W_i^k \subset V_i^k$ , containing  $x_i^k$ , i.e.  $x_i^k, x_i^{k+1} \in W_i^k$ . Let us define the set  $\mathcal{F}_i^k$  as

$$\mathcal{F}_i^k = \mathcal{N}_i^k \cup \{i\} \cup \bigcup_{x_i^{k+1} \in W_i^k} \mathcal{N}_i^{k+1}, \quad (2.13)$$

which corresponds to the union of the current (step  $k$ ) Delaunay neighbors of node  $i$ , the moving node itself, along with the union of all possible Delaunay neighbors at the next step for all possible node's motions in  $W_i^k$ .

**Lemma 2.1.** *The set  $\mathcal{F}_i^k$  contains the nodes of the network whose Voronoi cell is possibly affected by the motion of node  $i$ , given the restriction of  $x_i^{k+1} \in W_i^k$ .*

*Proof.* The proof is straightforward. □

**Assumption 2.4.** *The node-to-move  $i$  is considered to be able to exchange information at each time-step  $k$  with the nodes in the set  $\mathcal{F}_i^k$  for a given subset  $W_i^k \subset V_i^k$ .*

Information acquisition from a node's Delaunay neighbors is a non-restrictive assumption, which has appeared repeatedly in the existing literature [16, 19]. The main difference between the above assumption and the existing ones lays in the fact that the corresponding node-to-move needs connectivity with its current, along with its possible future Delaunay neighbors. Communication issues concerning Assumption 2.4 are to be examined in detail in section 2.3.4.

## 2. DIRECTIONAL-SEARCH APPROACH FOR AREA COVERAGE

It should be noted that the notation  $\mathcal{F}_i^k$  concerns motion at time-step  $k$ , while it is parameterized by the set  $W_i^k$  in which possible motion of node  $i$  is to be performed, i.e.  $x_i^{k+1} \in W_i^k$ .

### 2.3.3 Coordination algorithm

Let the notation  $q^\ell |_I$  stand for the evaluation of the arbitrary variable  $q$  at step  $\ell$  based on information from nodes in the set  $I \subseteq I_n$ . In the above notation it is implied that evaluation is performed by node  $i$  (i.e. node-to-move) at step  $k$  (i.e. before motion of the latter is performed). It should be noted that when  $\ell = k + 1$ , it is supposed that motion of node  $i$  is to be performed at a specified  $x_i^{k+1}$ . The aforementioned point is specified for evaluation purposes at step  $k$  and might not necessarily be the point at which node  $i$  decides to move at.

Considering Assumption 2.4, the  $r$ -limited Voronoi cell of a node  $j \in \mathcal{F}_i^k$  as evaluated by node  $i$  at step  $k$  is denoted as  $V_j^r |_{\mathcal{F}_i^k}$ . Considering coverage optimization scenarios, node  $i$  should move at a point  $x_i^{k+1}$  such that network's coverage will be increased at the maximum possible rate. Consequently, in order for the node-to-move to be able to evaluate its contribution to coverage-increase (via its motion), it should be able to evaluate  $\mathcal{H}^{k+1} - \mathcal{H}^k$  (for a given  $x_i^{k+1}$ ). However, since the latter has spatial information only of the nodes in  $\mathcal{F}_i^k$ , network's coverage-increase from its own point of view is provided as  $\mathcal{H}^{k+1} |_{\mathcal{F}_i^k} - \mathcal{H}^k |_{\mathcal{F}_i^k}$ . The above become clear via the following example.

Consider the homogeneous network shown in Fig. 2.4(a). The node to move  $i$  at the current

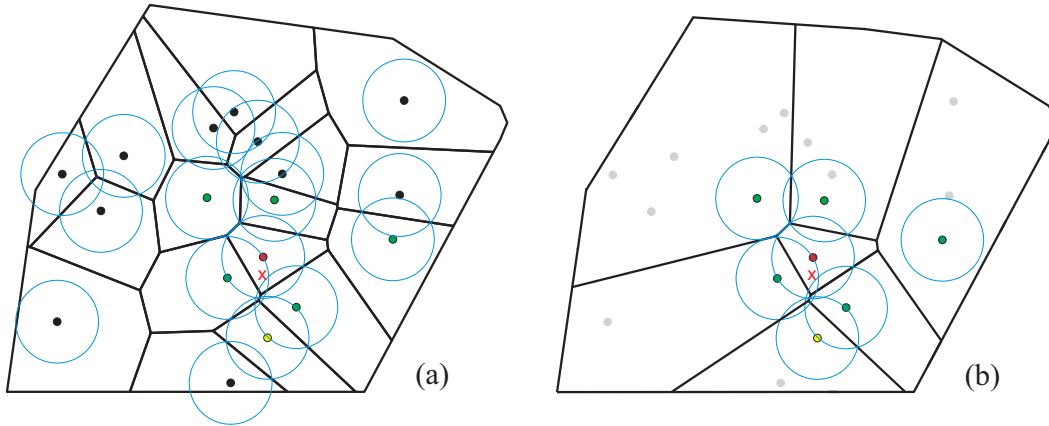


**Figure 2.4:** Illustrative example for definition of  $V_j^{r,k} |_{\mathcal{F}_i^k}$  sets.

step  $k$  is denoted by the red dot, while its supposed position at the next step (for evaluation purposes) is marked with an  $\times$  sign. The Delaunay neighbors of node  $i$  are denoted by green

dots, while the yellow dot corresponds to the future Delaunay neighbor of the latter at the next step (if the motion is performed at that point). Considering Assumption 2.4, node  $i$  is informed about existence of both yellow and green nodes, while connectivity issues for satisfying that assumption will be discussed later. The  $r$ -limited Voronoi cells of the nodes  $V_j^r$  are seen in Fig. 2.4(a) as the section of their Voronoi cells with the corresponding sensing patterns. However, since node  $i$  does not have any knowledge of existence of the rest network's nodes (apart from  $\mathcal{F}_i^k$ ), it can evaluate their  $r$ -limited Voronoi cells via Fig. 2.4(b). The grey dots in the latter denote the rest of the network's nodes that are not taken into account during the computation of the aforementioned cells. Similar procedure is followed by the moving node in order to evaluate  $V_j^{r,k+1} |_{\mathcal{F}_i^k}$ ; supposing that its position is that in the  $\times$  mark (for evaluation purposes only), it should compute the corresponding Voronoi tessellation and then follow the same procedure as before. Before proceeding to the main theorem, let us first prove the following lemma.

**Lemma 2.2.** *For each node  $j \in \mathcal{F}_i^k$ , it holds that*

$$\mathcal{A}\left(V_j^{r,\ell}\right) = \mathcal{A}\left(V_j^{r,\ell} |_{\mathcal{F}_i^k}\right) - \sum_{m \in \mathcal{N}_j^{\ell} \setminus \mathcal{F}_i^k} \mathcal{A}\left(U_j^{m,\ell}\right),$$

where  $\ell \in \{k, k+1\}$ .

*Proof.* Let us first examine the case  $\ell = k$ . Considering (2.10)–(2.11) and Fig. 2.2, for an arbitrary node  $j \in \mathcal{F}_i^k$ , it holds that

$$\begin{aligned} \mathcal{A}(C_j) &= \mathcal{A}\left(V_j^{r,k}\right) + \sum_{m \in \mathcal{N}_j^k} \mathcal{A}\left(U_j^{m,k}\right) + \mathcal{A}\left(U_j^{\Omega,k}\right) = \\ &= \mathcal{A}\left(V_j^{r,k}\right) + \sum_{m \in \mathcal{N}_j^k \cap \mathcal{F}_i^k} \mathcal{A}\left(U_j^{m,k}\right) + \sum_{m \in \mathcal{N}_j^k \setminus \mathcal{F}_i^k} \mathcal{A}\left(U_j^{m,k}\right) + \mathcal{A}\left(U_j^{\Omega,k}\right). \end{aligned}$$

Furthermore,  $\mathcal{A}(C_j)$  can be written as

$$\begin{aligned} \mathcal{A}(C_j) &= \mathcal{A}\left(V_j^{r,k} |_{\mathcal{F}_i^k}\right) + \sum_{m \in \mathcal{N}_j^k \cap \mathcal{F}_i^k} \mathcal{A}\left(U_j^{m,k} |_{\mathcal{F}_i^k}\right) + \mathcal{A}\left(U_j^{\Omega,k} |_{\mathcal{F}_i^k}\right) = \\ &= \mathcal{A}\left(V_j^{r,k} |_{\mathcal{F}_i^k}\right) + \sum_{m \in \mathcal{N}_j^k \cap \mathcal{F}_i^k} \mathcal{A}\left(U_j^{m,k}\right) + \mathcal{A}\left(U_j^{\Omega,k} |_{\mathcal{F}_i^k}\right), \end{aligned}$$

since the nodes  $m \in \mathcal{N}_j^k \cap \mathcal{F}_i^k$  are already known to node  $i$  (which performs the evaluation), i.e.  $\mathcal{N}_j^k \cap \mathcal{F}_i^k \subseteq \mathcal{F}_i^k$ .

Combining the above expressions for  $\mathcal{A}(C_j)$  results in

$$\mathcal{A}\left(V_j^{r,k}\right) = \mathcal{A}\left(V_j^{r,k} |_{\mathcal{F}_i^k}\right) - \sum_{m \in \mathcal{N}_j^k \setminus \mathcal{F}_i^k} \mathcal{A}\left(U_j^{m,k}\right) + \left(\mathcal{A}\left(U_j^{\Omega,k} |_{\mathcal{F}_i^k}\right) - \mathcal{A}\left(U_j^{\Omega,k}\right)\right).$$

However, since  $U_j^{\Omega,k} = C_j \setminus \Omega$  is dependent only on the sensing pattern and the region of interest, it holds that

$$\mathcal{A}\left(U_j^{\Omega,k} |_{\mathcal{F}_i^k}\right) = \mathcal{A}\left(U_j^{\Omega,k}\right),$$

and the result is proven.

The proof is identical for the case  $\ell = k+1$ . □

## 2. DIRECTIONAL-SEARCH APPROACH FOR AREA COVERAGE

**Theorem 2.1.** *If the node-to-move  $i$  has spatial information of the nodes in  $\mathcal{F}_i^k$ , then evaluation of the network's coverage-increase by ignoring the rest nodes in the network is the same as if the latter had been evaluated supposing existence of all the network's nodes, i.e.*

$$\mathcal{H}^{k+1} |_{\mathcal{F}_i^k} - \mathcal{H}^k |_{\mathcal{F}_i^k} = \mathcal{H}^{k+1} - \mathcal{H}^k. \quad (2.14)$$

*Proof.* Considering (2.12), it holds that

$$\begin{aligned} \mathcal{H}^{k+1} - \mathcal{H}^k &= \sum_{j \in I_n} \left[ \mathcal{A} \left( V_j^{r,k+1} \right) - \mathcal{A} \left( V_j^{r,k} \right) \right] = \\ &= \sum_{j \in \mathcal{F}_i^k} \left[ \mathcal{A} \left( V_j^{r,k+1} \right) - \mathcal{A} \left( V_j^{r,k} \right) \right] + \sum_{j \in I_n \setminus \mathcal{F}_i^k} \left[ \mathcal{A} \left( V_j^{r,k+1} \right) - \mathcal{A} \left( V_j^{r,k} \right) \right]. \end{aligned}$$

But the second summation in the expression above is equal to zero, according to Lemma 2.1.

Furthermore, substitution of  $\mathcal{A} \left( V_j^{r,k} \right), \mathcal{A} \left( V_j^{r,k+1} \right)$  from the result of Lemma 2.2 results in

$$\begin{aligned} \mathcal{H}^{k+1} - \mathcal{H}^k &= \sum_{j \in \mathcal{F}_i^k} \left[ \mathcal{A} \left( V_j^{r,k+1} |_{\mathcal{F}_i^k} \right) - \mathcal{A} \left( V_j^{r,k} |_{\mathcal{F}_i^k} \right) \right] - \\ &\quad \sum_{j \in \mathcal{F}_i^k} \left\{ \sum_{m \in \mathcal{N}_j^k \setminus \mathcal{F}_i^k} \left[ \mathcal{A} \left( U_j^{m,k+1} \right) - \mathcal{A} \left( U_j^{m,k} \right) \right] \right\}. \end{aligned}$$

However, the second term is consisted of the alteration in the unexploited regions of the nodes in  $\mathcal{F}_i^k$  that lay in the Voronoi cells of nodes that belong in  $\mathcal{N}_j^k \setminus \mathcal{F}_i^k$ . Thus, since the  $\Delta_{jm}$  edges are not altered ( $m \notin \mathcal{F}_i^k$ ), the aforementioned term is zero.

Consequently, it holds that

$$\mathcal{H}^{k+1} - \mathcal{H}^k = \sum_{j \in \mathcal{F}_i^k} \left[ \mathcal{A} \left( V_j^{r,k+1} |_{\mathcal{F}_i^k} \right) - \mathcal{A} \left( V_j^{r,k} |_{\mathcal{F}_i^k} \right) \right].$$

Without loss of generality, since node  $i$  does not have information of existence of the nodes  $I_n \setminus \mathcal{F}_i^k$ , their evaluated Voronoi cells can be arbitrarily be set to empty-sets, which results in

$$\begin{aligned} \mathcal{H}^{k+1} - \mathcal{H}^k &= \sum_{j \in \mathcal{F}_i^k} \left[ \mathcal{A} \left( V_j^{r,k+1} |_{\mathcal{F}_i^k} \right) - \mathcal{A} \left( V_j^{r,k} |_{\mathcal{F}_i^k} \right) \right] + \\ &\quad \sum_{j \in I_n \setminus \mathcal{F}_i^k} \left[ \mathcal{A} \left( V_j^{r,k+1} |_{\mathcal{F}_i^k} \right) - \mathcal{A} \left( V_j^{r,k} |_{\mathcal{F}_i^k} \right) \right] = \mathcal{H}^{k+1} |_{\mathcal{F}_i^k} - \mathcal{H}^k |_{\mathcal{F}_i^k}, \end{aligned}$$

and the result is proven.  $\square$

At this point, one can select the region  $W_i^k$  as a circular one as

$$W_i^k = \left\{ x \in \mathbb{R}^2 : \|x - x_i^k\| \leq \alpha d \left( x_i^k, V_i^k \right) \right\}, \quad (2.15)$$

where  $0 < \alpha \ll 1$  and  $d(x, M)$  is the distance of point  $x$  from the set  $M$  defined as

$$d(x, M) := \inf \{ \|x - y\| : y \in M \}. \quad (2.16)$$

It is clear that  $W_i^k$  expresses a disc centered at the agent's position. The advantage obtained by the selection of a circular region for  $W_i^k$  is its symmetry around  $x_i^k$ . It is easy to see that since  $x_i^{k+1} \in W_i^k$ , then the node-to-move performs its motion in the interior of its Voronoi cell,

leading so in non-singular paths (in terms of none coinciding nodes) for the nodes until the network reaches its optimum state.

Consequently, the destination point at which node  $i$  should move, i.e. the optimal  $x_i^{k+1} \in W_i^k$  denoted as  $x_i^{*k+1}$ , can be obtained numerically via solving at each step  $k$  the following optimization

$$\begin{aligned} & \text{find } x_i^{k+1} \in W_i^k : \\ & \text{maximize } \left\{ \mathcal{H}^{k+1} |_{\mathcal{F}_i^k} - \mathcal{H}^k |_{\mathcal{F}_i^k} \right\}, \\ & \text{subject to: } \mathcal{H}^{k+1} |_{\mathcal{F}_i^k} > \mathcal{H}^k |_{\mathcal{F}_i^k} \end{aligned} \quad (2.17)$$

either via gradient-based nonlinear constrained optimization schemes [20] or gridding on  $W_i^k$ . Considering Theorem 2.1 and (2.17), the area of the region surveyed by the network will be increased at each step in the maximum possible rate (due to the node's motion). The control action in (2.1) can be then selected as

$$u_i^k = x_i^{*k+1} - x_i^k, \quad (2.18)$$

where  $\|u_i\| \leq \alpha$ , as of (2.15). It is clear that in the case where any admissible motion of the node in  $W_i^k$  results in less or equal coverage area than that in the current step, then the node stays idle, since  $x_i^k \in W_i^k$ . Via the proposed scheme, it is guaranteed not only that the total area is increased in a monotonic manner, but with the highest possible rate, too.

### 2.3.4 Issues concerning spatial information exchange

As mentioned earlier, it is considered that node  $i$  should be able to receive spatial information from the set of nodes  $\mathcal{F}_i^k$  (Assumption 2.4). This section is dedicated into deriving a lower bound on the communication radius of the node-to-move in order for the assumption to hold. It is known that, in most practical scenarios, the maximum possible communication range of a node's transceiver is limited due to physical/manufacturing restrictions. Posing, though, such a constraint is beyond the scope of the current analysis, but will be revisited in chapter 5.

#### 2.3.4.1 Connectivity with current Delaunay neighbors

Considering communication issues, node  $i$  should be able to acquire information at step  $k$  from the nodes of the set  $\mathcal{F}_i^k$ , given the subset  $W_i^k \subset V_i^k$ , in order to be able to apply the coverage algorithm presented in the previous section. Ignoring the trivial case of receiving information

## 2. DIRECTIONAL-SEARCH APPROACH FOR AREA COVERAGE

---

from the node itself, as far as concerns the first part of the aforementioned union set (2.13), the node's transceiver should first have adequate communication range so that it can communicate with its current Delaunay neighbors  $\mathcal{N}_i^k$ .

Let us denote by  $R_i^k(I)$  and  $R_i^k(I)_{\text{wcs}}$  the minimum communication radius of node  $i$  at step  $k$  required in order to exchange information with a set of nodes  $I \subset I_n$ , from a centralized and decentralized point of view, respectively. It is easy to see that, from a centralized aspect, the minimum range required for guaranteeing connectivity of node  $i$  with  $\mathcal{N}_i^k$  at step  $k$  is equal to

$$R_i^k(\mathcal{N}_i^k) = 2 \max \left\{ d(x_i^k, \Delta_{ij}^k) : j \in \mathcal{N}_i^k \right\} = \max \left\{ \|x_i^k, x_j^k\| : j \in \mathcal{N}_i^k \right\}, \quad (2.19)$$

where  $\Delta_{ij}$  and  $d(x, M)$  are defined in (2.8) and (2.16), respectively. Although, expression (2.19) provides indeed the minimum range required, it cannot be used as a bound, from an independent point of view. In fact, node  $i$  needs to increase even more its communication range until it is ensured that its Voronoi cell will not be affected further, even if another node falls in range.

Considering algorithmic implementations of communication range adjustment, the main concept lays in gradual increase of the latter until sufficient information from neighbor nodes is obtained [16]. In fact, node  $i$  gradually increases its range and updates its Voronoi cell according to the nodes that fall in its range. The procedure ends when either  $S_i^k \supseteq \Omega$  or the node's range becomes twice the distance between the node and its farthest Voronoi cell vertex, i.e.

$$R_i^k(\mathcal{N}_i^k)_{\text{wcs}} = 2 \max \left\{ \|x_i^k - v_{i,j}^k\| : j \in I_{N(V_i^k)} \right\}, \quad (2.20)$$

since from that time on, any other node identified does not alter its Voronoi cell. The notation  $N(\cdot)$  stands for the number of the argument's vertices, as stated already in section 2.2.1. It should be noted that (2.20) seems to include some kind of recursiveness in its body; indeed, in order to compute the minimum communication range in order to exchange information with  $\mathcal{N}_i^k$ , one needs  $V_i^k$  (considering the second part), where  $\mathcal{N}_i^k$  is needed for its evaluation. However, (2.20) depicts  $R_i^k(\mathcal{N}_i^k)_{\text{wcs}}$  from an *analysis* point of view. The iterative algorithmic procedure for the latter's numerical evaluation is shown in Algorithm 2.1.

Note also that  $R_i^k(\mathcal{N}_i^k)_{\text{wcs}}$  is larger than the centralized bound, due to the distributed nature of the scheme. During the rest of the analysis that follows in this section, node  $i$  will be considered to obtain information from its current Delaunay neighbors  $\mathcal{N}_i^k$  via proper adjustment of its communication radius at  $R_i^k(\mathcal{N}_i^k)_{\text{wcs}}$ .



---

**Algorithm 2.1** Communication Range Adjustment for Connectivity with  $\mathcal{N}_i^k$ 


---

- 1:  $\diamond$  *Goal*: Identify current Delaunay neighbors and Voronoi cell
  - 2:  $R_i^k \leftarrow 0, S_i^k \leftarrow \emptyset$
  - 3:  $\hat{V}_i^k \leftarrow \Omega, \hat{\mathcal{N}}_i^k \leftarrow \emptyset$
  - 4: **while**  $R_i^k \leq 2 \max \left\{ \|x_i^k - \hat{v}_{i,j}^k\| : j \in I_N(\hat{V}_i^k) \right\}$  **and**  $S_i^k \subset \Omega$  **do**
  - 5:     increase  $R_i^k$
  - 6:     update  $S_i^k$
  - 7:     **if** node  $j$  detected **then**
  - 8:          $\hat{\mathcal{N}}_i^k \leftarrow \hat{\mathcal{N}}_i^k \cup j$
  - 9:         update  $\hat{V}_i^k$
  - 10:     **end if**
  - 11: **end while**
  - 12:  $V_i^k \leftarrow \hat{V}_i^k$
  - 13: isolate  $\mathcal{N}_i^k$  from the set  $\hat{\mathcal{N}}_i^k$
- 

**2.3.4.2 Guaranteeing connectivity with all possible future Delaunay neighbors**

Considering (2.12), what needs to be further ensured is connectivity of node  $i$  with the set  $\bigcup_{x_i^{k+1} \in W_i^k} \mathcal{N}_i^{k+1}$ , given  $W_i^k$ . Suppose an arbitrary point  $x_i^{k+1} \in W_i^k \subset V_i^k$ . The goal is to find the minimum communication radius of node  $i$  at step  $k$  in order to guarantee connectivity at that step with  $\mathcal{N}_i^{k+1}$ , from a decentralized point of view. At step  $k$ , node  $i$ , positioned at  $x_i^k$  with communication range  $R_i^k(\mathcal{N}_i^k)_{\text{wcs}}$ , has information about the coordinates of the nodes  $\mathcal{N}_i^k$  of the network. Thus, at that time, the first can evaluate its future Voronoi cell, supposing that its motion is to be performed at  $x_i^{k+1}$ , by taking into account only the nodes in  $\mathcal{N}_i^k$  and itself (i.e. ignoring the rest of the network, since it does not have knowledge of existence of the rest nodes, yet). Let us denote as  $V_i^{k+1} |_{\mathcal{N}_i^k}$  the aforementioned evaluated Voronoi cell. At this point, node  $i$  can be aware if a node  $j \in \mathcal{N}_i^k$  is about to leave the set of its Delaunay neighbors at the next step, supposing that its motion will be performed at  $x_i^{k+1}$ , via simple evaluation of  $V_i^{k+1} |_{\mathcal{N}_i^k}$ . What is unknown to the node-to-move yet are possible nodes of the network that may enter  $\mathcal{N}_i^{k+1}$ .

Let us consider again the worst case scenario. Suppose that  $m \in I_n$  is an extra node to possibly enter the set  $\mathcal{N}_i^{k+1}$  if motion is performed at  $x_i^{k+1}$ , where existence of  $m$  is unknown to node  $i$  yet. Considering (2.6), let  $h_{ij}$  stand for the line that equally divides the space into two

## 2. DIRECTIONAL-SEARCH APPROACH FOR AREA COVERAGE

halfplanes between two arbitrary nodes of the network, i.e.

$$h_{ij} = \{x \in \mathbb{R}^2: \|x - x_i\| = \|x - x_j\|\}, \quad i, j \in I_n, \quad i \neq j. \quad (2.21)$$

The critical case for node  $m$  to enter the set  $\mathcal{N}_i^{k+1}$  is when  $h_{im}^{k+1}$  marginally crosses the farthest vertex of  $V_i^{k+1} |_{\mathcal{N}_i^k}$ . Let  $v_{i,j^*}^{k+1} |_{\mathcal{N}_i^k}$  denote the farthest vertex of  $V_i^{k+1} |_{\mathcal{N}_i^k}$ , where the index  $j^*$  is given as

$$j^* = \arg \max \left\{ \left\| x_i^{k+1} - v_{i,j}^{k+1} |_{\mathcal{N}_i^k} \right\| : j \in I_{\mathcal{N}(V_i^{k+1} |_{\mathcal{N}_i^k})} \right\}. \quad (2.22)$$

It is well-known that, given two points  $a, b \in \mathbb{R}^2$  and a family of straight lines  $\mathcal{L}$ , where  $b \in \ell, \forall \ell \in \mathcal{L}$ , the farthest line from  $a$  (where  $d(a, \ell)$  is defined via (2.16)) is the one that is perpendicular to the line that connects  $a$  and  $b$ . Considering the above, one can conclude that the worst case scenario for the position of node  $m$  is when it lays along the line that connects  $x_i^{k+1}$  and  $v_{i,j^*}^{k+1} |_{\mathcal{N}_i^k}$ , at a distance from  $x_i^{k+1}$  equal to twice that of the aforementioned points. This case is depicted graphically in Fig. 2.5. The red dot represents  $x_i^{k+1}$ , while the blue line

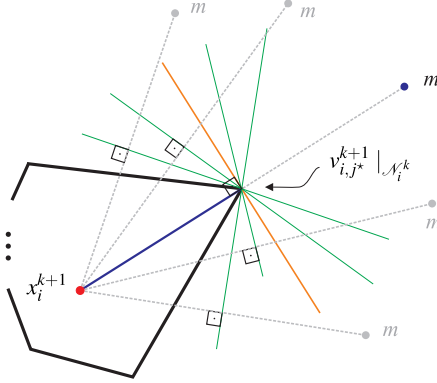


**Figure 2.5:** Worst case scenario for the existence of a node  $m$  that is to enter  $\mathcal{N}_i^{k+1}$ .

connects that node with the farthest vertex of its evaluated Voronoi cell  $V_i^{k+1} |_{\mathcal{N}_i^k}$ . The blue dot represents the worst case scenario (comparing to the other possible cases denoted by grey color) for the existence of node  $m$ . The rest of the nodes in the network are omitted for visualization purposes.

Considering Fig. 2.5, the worst-case for the position of node  $m$  is

$$x_m^{k+1} = x_i^{k+1} + 2 \left( v_{i,j^*}^{k+1} |_{\mathcal{N}_i^k} - x_i^{k+1} \right).$$

Thus, node  $i$  at  $x_i^k$  should have adequate communication range so that it can at least exchange information with that node,  $m$ , provided as

$$R_i^k \left( \mathcal{N}_i^{k+1} \right)_{\text{wcs}} = \left\| x_i^k - \left( x_i^{k+1} + 2 \left( v_{i,j^*}^{k+1} \mid_{\mathcal{N}_i^k} - x_i^{k+1} \right) \right) \right\| = \left\| \left( x_i^k + x_i^{k+1} \right) - 2v_{i,j^*}^{k+1} \mid_{\mathcal{N}_i^k} \right\|, \quad (2.23)$$

where the index  $j^*$  is defined in (2.22). It should be noted that  $x_i^k$  appears in the norm–argument of the upper part of (2.23), and not  $x_i^{k+1}$ , since we are interested in finding the appropriate communication range of node  $i$  at step  $k$  in order to communicate with node  $m$ . Furthermore, special attention should be given to the fact that the range defined in (2.23) is not the minimum required radius for guaranteeing connectivity with  $\mathcal{N}_i^{k+1}$  from a centralized point of view, since the first depicts the worst case scenario (wcs). However, it is considered as the optimum range from a decentralized point of view, considering that at that time, node  $i$  has knowledge of existence for the nodes  $\mathcal{N}_i^k$ .

The above become clearer via the following example. Consider the network depicted in Fig. 2.6(a). Node  $i$  is depicted with the red dot, while the time–step is considered as  $k$ . The

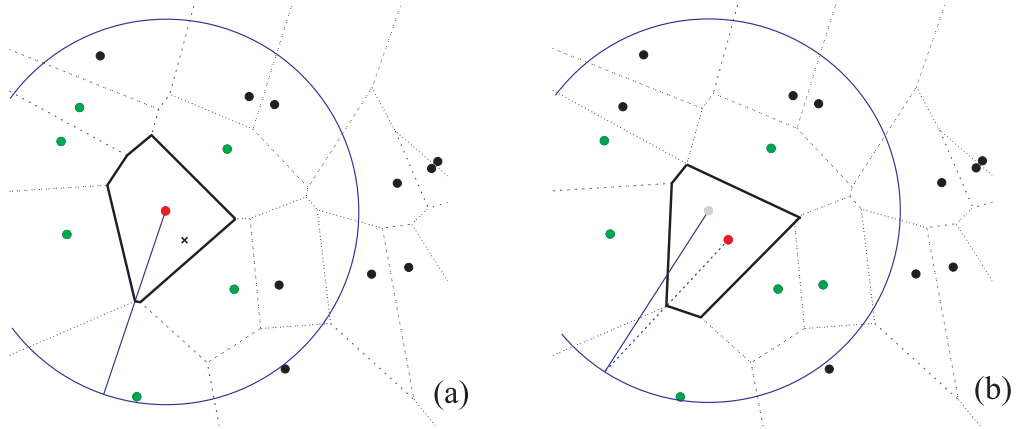


**Figure 2.6:** Communication radius of the node–to–move (red color) required in order to guarantee connectivity: (a) with  $\mathcal{N}_i^k$ , (b) with  $\mathcal{N}_i^{k+1}$ , for a given node’s motion (worst case scenario).

blue circle specifies the minimum communication radius of node  $i$  (from a decentralized point of view) required in order to communicate with  $\mathcal{N}_i^k$ , which are the green nodes of the figure. One can observe that the corresponding radius allows information exchange with some nodes of the network, other than the green ones.

Consider now that node  $i$  evaluates its future Voronoi cell, as if the network was consisted only of the nodes  $\mathcal{N}_i^k$ , i.e.  $V_i^{k+1} \mid_{\mathcal{N}_i^k}$ , as depicted in Fig. 2.6(b). The red dot denotes the possible destination of node  $i$  (depicted with the  $\times$  mark at Fig. 2.6(a)), while the grey one is its real

## 2. DIRECTIONAL-SEARCH APPROACH FOR AREA COVERAGE

position at step  $k$ . The farthest vertex of  $\hat{V}_i^{k+1} |_{\mathcal{N}_i^k}$  is needed to determine the worst-case for the position of a possible node  $m$ . In Fig. 2.6(b),  $x_i^{k+1}$  is connected with the imaginary  $x_m^{k+1}$  via the blue dashed line passing from  $v_{i,j^*}^{k+1} |_{\mathcal{N}_i^k}$ . One can see that no node lays in the worst-case position of node  $m$ . Thus, at this point  $R_i^k(\mathcal{N}_i^{k+1})_{\text{wcs}}$  can be computed via (2.23). It should be noted that the circle is centered at the grey sign (current node's position) and not at the red one (possible future node's position). Apart from that, the most right green node that will enter the set of Delaunay neighbors of node  $i$ , if the latter moves at  $x_i^{k+1}$ , is not taken into account into the computation of  $V_i^{k+1} |_{\mathcal{N}_i^k}$ , since that is the node to be identified. In fact, the only nodes in the network that play a role to its evaluation are the green nodes of Fig. 2.6(a). Finally, one can observe that  $R_i^k(\mathcal{N}_i^{k+1})_{\text{wcs}}$  in Fig. 2.6(b) is not the minimum radius required to exchange information with the green nodes of Fig. 2.6(b), since it corresponds to the worst case scenario.

Considering the above, the minimum communication radius of node  $i$  at step  $k$  required in order to exchange information with the nodes in the set  $\bigcup_{x_i^{k+1} \in W_i^k} \mathcal{N}_i^{k+1}$  is

$$R_i^k \left( \bigcup_{x_i^{k+1} \in W_i^k} \mathcal{N}_i^{k+1} \right)_{\text{wcs}} = \sup \left\{ R_i^k(\mathcal{N}_i^{k+1})_{\text{wcs}} : x_i^{k+1} \in W_i^k \right\}, \quad (2.24)$$

where  $R_i^k(\mathcal{N}_i^{k+1})_{\text{wcs}}$  is defined in (2.23). To summarize, the algorithm followed for evaluating  $R_i^k(\mathcal{F}_i^k)_{\text{wcs}}$  is provide in Algorithm 2.2. An issue of major importance is the fact that, after identification of  $\mathcal{N}_i^k$  via Algorithm 2.1, only evaluations are needed throughout the body of the algorithm procedure, and no communication range adjustment is demanded until  $R_i^k(\mathcal{F}_i^k)_{\text{wcs}}$  is defined.

**Corollary 2.1.** *The communication radius of node  $i$  at step  $k$  in order to guarantee connectivity with both current and all possible future Delaunay neighbors, should be at least*

$$R_i^k(\mathcal{F}_i^k)_{\text{wcs}} = \max \left\{ R_i^k(\mathcal{N}_i^k)_{\text{wcs}}, R_i^k \left( \bigcup_{x_i^{k+1} \in W_i^k} \mathcal{N}_i^{k+1} \right)_{\text{wcs}} \right\}, \quad (2.25)$$

where the corresponding radii are given by (2.20) and (2.24).

### 2.3.5 Simulation results

Simulation studies are presented in this section in order to show the efficacy of the proposed scheme. The region  $\Omega$  to be surveyed is a convex set in  $\mathbb{R}^2$ . During network evolution the covered area is increasing until it converges to an extremum solution, while the agents' kinematics

---

**Algorithm 2.2** Communication Range Adjustment Algorithm for Connectivity with  $\mathcal{F}_i^k$ 


---

- 1:  $\diamond$  *Goal*: Identify nodes whose Voronoi cells are possibly affected
  - 2:  $R_i^k \left( \bigcup_{x_i^{k+1} \in W_i^k} \mathcal{N}_i^{k+1} \right)_{\text{wcs}} \leftarrow 0$
  - 3: identify  $\mathcal{N}_i^k$  and  $V_i^k$  via Algorithm 2.1
  - 4: perform gridding on  $W_i^k$
  - 5: **for** each  $x_i^{k+1} \in W_i^k$  **do**
  - 6:     evaluate  $V_i^{k+1} |_{\mathcal{N}_i^k}$
  - 7:     evaluate  $v_{i,j^*}^{k+1} |_{\mathcal{N}_i^k}$
  - 8:     evaluate  $R_i^k \left( \mathcal{N}_i^{k+1} \right)_{\text{wcs}}$
  - 9:      $R_i^k \left( \bigcup_{x_i^{k+1} \in W_i^k} \mathcal{N}_i^{k+1} \right)_{\text{wcs}} \leftarrow \max \left\{ R_i^k \left( \bigcup_{x_i^{k+1} \in W_i^k} \mathcal{N}_i^{k+1} \right)_{\text{wcs}}, R_i^k \left( \mathcal{N}_i^{k+1} \right)_{\text{wcs}} \right\}$
  - 10: **end for**
  - 11:  $R_i^k \left( \mathcal{F}_i^k \right)_{\text{wcs}} \leftarrow \max \left\{ R_i^k \left( \mathcal{N}_i^k \right)_{\text{wcs}}, R_i^k \left( \bigcup_{x_i^{k+1} \in W_i^k} \mathcal{N}_i^{k+1} \right)_{\text{wcs}} \right\}$
  - 12: update  $S_i^k$
  - 13: identify  $\mathcal{F}_i^k$
- 

are described by (2.1). The control action is based on the coordination scheme proposed in section 2.3.3. Two series of simulations follow: one considering a sparse network and another considering a congested one. By the term sparse (congested), it is implied that there exists (does not exist) configuration such that  $\Omega$  is covered in the maximum possible ratio with no overlapping among the nodes' sensing patterns or with the boundary of  $\Omega$ .

The number of agents in the first case (sparse network) is set to  $n = 18$ , while in the second scenario the latter is set to  $n = 10$ . In both cases, the latter are deployed randomly in  $\Omega$ . The critical sensing radius of the agents' patterns is considered equal to  $r = 1.5\text{m}$  and  $r = 3\text{m}$ , respectively. The maximum theoretically (if possible) achievable sensing area,  $\sup \mathcal{A} \left( \bigcup_{i \in I_n} C_i \right) = n\pi r^2$ , corresponds to  $127.23\text{m}^2$  and  $282.74\text{m}^2$  in each case, while the area of the region of interest is  $\mathcal{A}(\Omega) = 226.37\text{m}^2$ . The convex area under surveillance is that presented in [15] and [21]. Ideally, if possible, the agents should be able to cover the region without any overlapping, and thus covering  $\frac{n\pi r^2}{\mathcal{A}(\Omega)} = 56.2\%$  and  $100\%$  of  $\Omega$ , respectively, where the latter maximum possible percentage ratio is trimmed at  $100\%$ . The value of  $\alpha$  in (2.15) was set to  $\alpha = 0.1$ . Simulation is stopped when all nodes' motions are unable to further increase coverage.

Considering the sparse-network case, the agents' initial positions, their evolution through time, along with the final network's state, when the control scheme presented in section 2.3.3

## 2. DIRECTIONAL-SEARCH APPROACH FOR AREA COVERAGE

is applied, are shown in the top part of Fig. 2.7, in this order. The black circles (blue dots) represent the nodes' final (initial) positions. As far as concerns the final nodes' state, it is

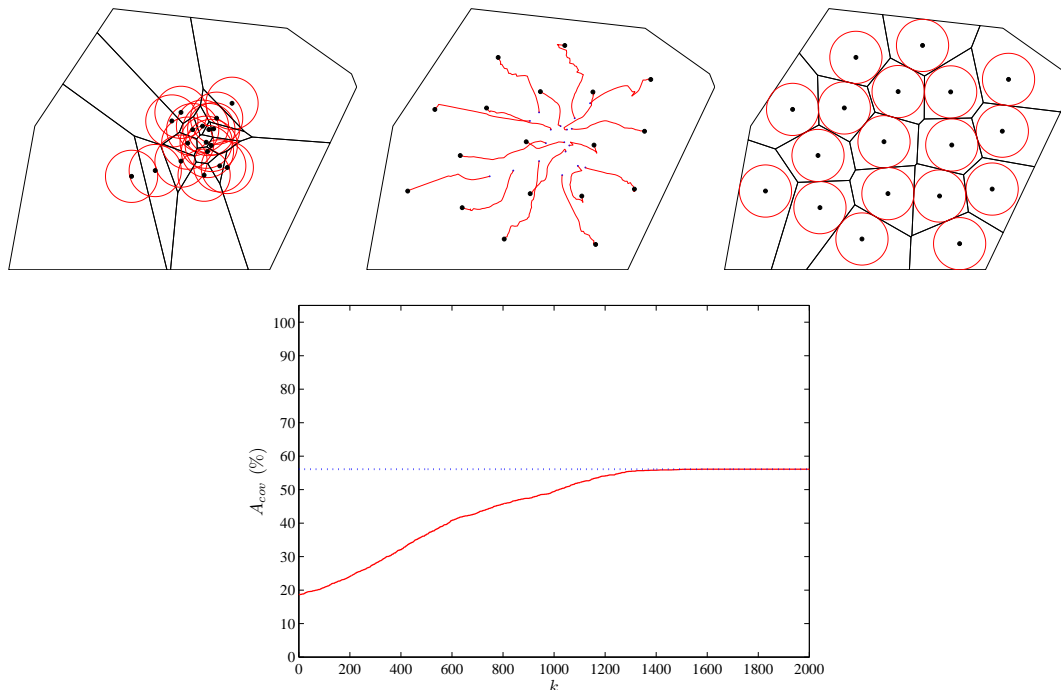


**Figure 2.7:** Sparse-network case study: [Left] Initial network configuration. [Middle] Network evolution through time. [Right] Final network optimum state. [Bottom] Percentage of covered area w.r.t. time.

obvious that the agents have self-positioned themselves in a way that there is no overlapping between their sensing patterns or the boundary of the region under surveillance, while attaining optimum coverage, i.e.  $\mathcal{H} = n\pi r^2$ .

The way in which the area of the covered region increases is shown in the bottom part of Fig. 2.7. The blue straight line represents the maximum possible coverage ratio, which in this case is 56.2%. The latter, starting from an initial value of 18.66% (dependent on the initial network configuration), increases as time passes by in a monotonic way, until it reaches its optimum value in less than 2000 steps.

Similarly, considering a congested network, the network's initial configuration, the nodes' evolution through time, along with their optimum configuration are shown in the top part of Fig. 2.8. It is apparent that in this case there exists overlapping among the nodes' sensory. Contrary to the previous case, the maximum possible coverage percentage of 100% is not reached

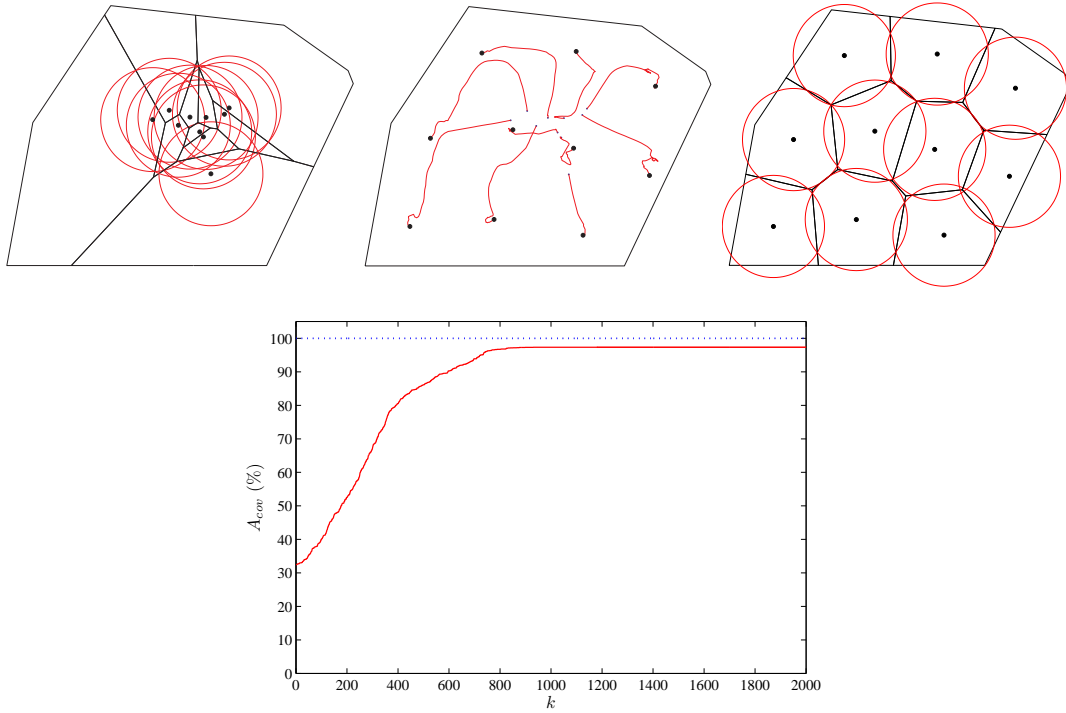


**Figure 2.8:** Congested-network case study: [Left] Initial network configuration. [Middle] Network evolution through time. [Right] Final network optimum state. [Bottom] Percentage of covered area w.r.t. time.

exactly, though approached at 97.33% in less than 1000 steps, starting from an initial value of 32.45%, as also seen by the bottom part of Fig. 2.8. In fact, the only way to guarantee existence of a configuration for complete coverage of  $\Omega$  is via global optimization techniques, something that is beyond the scope of this thesis. Either way, the state that the network converged to is an extremum of (2.12), while the coverage attained by the nodes is more than satisfactory.

Overall, one can see that the less the number of nodes in the network, the faster optimum coverage is reached. Indeed, since one node moves at a time and the nodes are selected in a random (or even in cyclic) manner, the less the number of nodes, the less possible is to come for a node that cannot contribute to coverage to move. Comparing this work to previous ones, it is seen that the network tries to optimize the total area covered by itself, while it does not base its action on CVT coordination schemes or nearest-neighbor rules [12, 13, 15, 22]. The fact that only one node moves at a time parts the main difference, while optimal area achievement is guaranteed in a monotonic manner by sufficient knowledge of a node's current and future Delaunay neighbors.

### 2.4 Conclusions

In this chapter a distributed control strategy for sensing coverage optimization by a group of mobile agents that consist a homogeneous sensor network was presented. The coordination scheme was based on Voronoi partitioning, where the nodes self-organize their action in a way that the total area covered by the network is an increasing function of time. Each node plans its current motion according to information obtained by its current and future Delaunay neighbors, which is guaranteed by proper communication range adjustment. Simulations confirmed the efficacy of the proposed scheme.



# 3

## Coverage by Heterogeneous Networks

### 3.1 Introduction

Voronoi tessellation forms the basis for decentralized self-decisioning schemes for the mobile members of the network, where a responsibility domain is assigned to each node [14]. Such a space-partitioning scheme greatly reduces the computational effort from a control point of view. Computational issues on its construction are discussed in [23, 24, 25].

This assignment is performed based on the spatial coordinates of the agents, ignoring any kind of heterogeneity. Hence, utilization of the latter implies that all nodes are homogeneous, which in coverage-based terms can be expressed as being characterized by identical sensing patterns. Weighted-Voronoi techniques have been developed [23, 26, 27], though, that take into consideration this unevenness and thus provide responsibility regions at each node, based not only on their spatial characteristics, but on their different power/range as well.

A major issue of additive/multiplicative weighted-Voronoi frameworks lays in their construction, since the modified Voronoi cells tend to consist of curved edges rather than straight lines (as in standard Euclidean Voronoi diagram) [27, 28], while the regions of responsibility assigned to the nodes are in some cases non-convex sets. This makes Centroidal Voronoi Tessellations (CVT) based coordination algorithms [13, 22, 29] even harder to be implemented in cases of mobile networks, since they tend to force the node to abandon its assigned region of responsibility (Voronoi cell).

Standard Voronoi tessellation for a set of static nodes imply that all nodes are homogeneous, in a general sense. Thus, it is assumed that they have identical sensing patterns and equal sensing range. Direct application of such schemes to heterogeneous networks, where the

### 3. COVERAGE BY HETEROGENEOUS NETWORKS

---

sensing radii of the nodes differ, results in unfair and incorrect region–assignment for the latter [19, 30]. Heterogeneous networks’ coordination is examined in [31] by tessellating the space via power diagrams [26] for the distortion case, coordinated via Centroidal Voronoi Tessellation (CVT) rules [16].

We provide an space–partitioning technique for heterogeneous networks that is by far less complex (from a computational effort point of view) comparing to weighted ones, while convexity of the cells is kept active. The proposed technique degenerates in the standard Voronoi diagram when dealing with homogeneous networks, while its application in heterogeneous ones provides the sufficient conditions for internal properties of Voronoi diagram to hold. Distributed control action for optimizing network’s coverage is based on the corresponding cells of the partitioning.

The main preliminaries concerning the network are presented initially, along with an introduction to Voronoi diagram, its properties and its application in decentralized control. The development of a space–partitioning scheme suitable for networks with uneven ranges in the sensing domains follows. Important remarks along with properties of this scheme are discussed, while a comparison with standard Voronoi partitioning follows. A distributed coordination framework for coverage optimization based on the modified space partitioning is developed in the sequel, along with connectivity issues concerning communication range adjustment of the nodes in order to self–deploy and evaluate their own coverage–contribution in a decentralized manner. Simulation studies are provided, in order to emphasize in the advantages of the proposed scheme when dealing with heterogeneous networks, contrary to existing algorithms based on standard partitioning.

## 3.2 Preliminaries — Motivation

### 3.2.1 Main Assumptions

A sensor network of  $n$  nodes is revisited in this chapter, similarly to Chapter 2. We will keep the same terminology throughout this thesis, and indicate wherever something is changed. Let us ignore mobility of the nodes at start in order to focus on the development of the partitioning of the space. Similarly to (2.2), the nodes’ are assumed to be able to sense omnidirectionally up to a maximum radius; however the latter differs among the nodes in this case. By denoting

these critical radii as  $r_i$ , the sensing region of each node  $i$  is

$$C_i = \{x \in \mathbb{R}^2: \|x - x_i\| \leq r_i\}, i \in I_n. \quad (3.1)$$

The fact that the maximum sensing radii of the nodes are not equal is the one that imposes network heterogeneity, and this is the reason for the repetition of the assumption.

Avoiding repeating the main preliminaries of Voronoi partitioning, the Voronoi and  $r$ -limited Voronoi cell of a node, along with its unexploited regions are defined in (2.6), (2.9), and (2.10), respectively. Apparently, these sets get affected by the network's heterogeneity, as of different sensing radii.

### 3.2.2 Properties of Voronoi diagram for homogeneous networks

As already mentioned, the Voronoi diagram for a set of nodes can be constructed only by knowing the spatial coordinates of them, as in (2.6). In fact, what is implied is that the nodes are all identical as far as concerns their capabilities (in a general sense). Thus, comparing two nodes, the common Voronoi edge is the line that is perpendicular on the middle of the line that connects the nodes themselves, providing so a fair equalized region-assignment. This fact results in two special properties of Voronoi diagrams presented in the sequel, which hold *only* for homogeneous networks.

In order to set them up, an alternative definition for the standard Voronoi cells  $V_i$  apart from that in (2.6) is given as

$$V_i = \Omega \cap \bigcap_{j \in I_n} H_{ij}, i \in I_n, \quad (3.2)$$

where  $H_{ij}$  are halfplanes in  $\mathbb{R}^2$  that specify responsibility regions for node  $i$  based on comparison with node  $j$  and are defined as

$$H_{ij} = \{x \in \mathbb{R}^2: \|x - x_i\| \leq \|x - x_j\|\}, i, j \in I_n. \quad (3.3)$$

By definition, it holds that  $H_{ii} = \mathbb{R}^2$ ,  $i \in I_n$ , and thus can be neglected, due to the presence of  $\Omega$  in (3.2). One can simply verify that definitions (2.6) and (3.2)–(3.3) are equivalent.

**Theorem 3.1.** *When all nodes in a network are identical and space-partitioning is performed by (2.6), if a point in the region under surveillance  $\Omega$  lays in the unexploited region of a node, then it lays in the sensing region of another node, i.e.*

$$\exists i \in I_n: x \in U_i \Rightarrow \exists j \in I_n, j \neq i: x \in C_j, \quad x \in \Omega.$$

### 3. COVERAGE BY HETEROGENEOUS NETWORKS

*Proof.* Let  $x \in \Omega \cap U_i$ . Then  $x \in \Omega \cap (C_i \setminus V_i)$  according to (2.10). Since  $x \in C_i$ , from (3.1) it follows that  $\|x - x_i\| \leq r$ . Since  $x \notin V_i$ , it holds from (3.2)–(3.3) that  $x \in \bigcup_{k \neq i} H_{ki} \Rightarrow \exists j, j \neq i: x \in H_{ji} \Rightarrow \|x - x_j\| \leq \|x - x_i\| \Rightarrow \|x - x_j\| \leq r \Rightarrow x \in C_j$ .  $\square$

**Theorem 3.2.** *When space-partitioning is performed based on (2.6), the total region surveyed by a network whose nodes are all identical can be written as*

$$\mathcal{C} = \Omega \cap \bigcup_{i \in I_n} C_i = \bigcup_{i \in I_n} V_i^r, \quad (3.4)$$

while its area is given by

$$\mathcal{A}(\mathcal{C}) = \sum_{i \in I_n} \mathcal{A}(V_i^r),$$

where the area-function is denoted by  $\mathcal{A}(\cdot)$ .

*Proof.* Based on (2.9) and (2.10), it is easy to verify that  $C_i = V_i^r \cup U_i$ ,  $i \in I_n$  (see Fig. 2.2); thus the total covered area can be written as

$$\begin{aligned} \mathcal{C} &= \Omega \cap \bigcup_{i \in I_n} C_i = \Omega \cap \bigcup_{i \in I_n} (V_i^r \cup U_i) = \bigcup_{i \in I_n} (\Omega \cap (V_i^r \cup U_i)) = \bigcup_{i \in I_n} ((\Omega \cap V_i^r) \cup (\Omega \cap U_i)) = \\ &= \bigcup_{i \in I_n} (V_i^r \cup (\Omega \cap U_i)) = \left( \bigcup_{i \in I_n} V_i^r \right) \cup \left( \bigcup_{i \in I_n} (\Omega \cap U_i) \right). \end{aligned}$$

What remains to be proven is that  $\bigcup_{i \in I_n} (\Omega \cap U_i) \subseteq \bigcup_{i \in I_n} V_i^r$ , since that will lead to the result of (3.4).

Let  $x \in \bigcup_{i \in I_n} (\Omega \cap U_i)$ . According to Theorem 3.1,  $\exists j: x \in C_j \Rightarrow x \in (V_j^r \cup U_j)$ ,  $U_j \subset V_i$ .

◇ If  $x \in V_j^r$ , then  $x \in \bigcup_{i \in I_n} V_i^r$  and the result is proven.

◇ If  $x \in U_j$ , then  $x \in V_i$ , since  $U_j \subset V_i$ . But, since  $x \in U_i$  it follows that  $x \in U_i \cap V_i = \emptyset \subseteq \bigcup_{i \in I_n} V_i^r$ .

Consequently,  $\bigcup_{i \in I_n} (\Omega \cap U_i) \subseteq \bigcup_{i \in I_n} V_i^r$ , resulting in (3.4).

Thus,  $\mathcal{A}(\mathcal{C}) = \mathcal{A}(\bigcup_{i \in I_n} V_i^r)$ , and since  $V_i^r \cap V_j^r = \emptyset$ ,  $\forall i, j \in I_n, i \neq j$ , it follows that  $\mathcal{A}(\mathcal{C}) = \sum_{i \in I_n} \mathcal{A}(V_i^r)$ .  $\square$

The aforementioned properties hold only when all nodes in a network are identical (while standard Voronoi tessellation is used for space-partitioning) and are the core for defining coverage performance of the network; hence, one can control either the sensing/transmission power of the nodes (in cases of power-efficient static networks) or the motion of the latter (in cases of mobile networks), accordingly.

For the sake of the development of a proper space-partitioning scheme, at this point let us define in a formal way the coverage performance of a sensor network via the ‘‘Area Coverage Percentage’’ (ACP) defined as the area of the sensed regions of  $\Omega$  divided by the area of the region of interest  $\Omega$ , i.e.

$$\text{ACP} = \frac{\mathcal{A}(\Omega \cap \bigcup_{i \in I_n} C_i)}{\mathcal{A}(\Omega)}. \quad (3.5)$$

In fact, this ratio expresses the coverage performance of the network as evaluated via the sensing regions  $C_i$ . Coverage performance of the network can moreover be evaluated via the independent  $r$ -limited Voronoi cells  $V_i^r$ , as of (2.9); let us define the “ $V^r$ -Estimated Area Coverage Percentage” ( $\hat{\text{ACP}}(V^r)$ ) as

$$\hat{\text{ACP}}(V^r) = \frac{\mathcal{A}(\bigcup_{i \in I_n} V_i^r)}{\mathcal{A}(\Omega)} = \frac{\sum_{i \in I_n} \mathcal{A}(V_i^r)}{\mathcal{A}(\Omega)}. \quad (3.6)$$

It is evident that, for a homogeneous network, it holds that  $\text{ACP} = \hat{\text{ACP}}(V^r)$ , as concluded by (3.5), (3.6) and Theorem 3.2.

### 3.2.3 Application in heterogeneous networks

The main disadvantage of the standard Voronoi tessellation scheme is that the space-partitioning is performed based only on the nodes positioning  $x_i$  in the plane and does not take into account the heterogeneity in the sensing patterns of the latter. If Voronoi diagram is used for region-assignment at the nodes and Theorem 3.2 holds, the nodes should try to optimize the area of their  $r$ -limited Voronoi cells (in a coverage-optimization scenario), resulting in optimum network sensing coverage. However, before optimizing the area of the nodes’  $r$ -limited Voronoi cells, it should first be ensured that any point sensed by a node, but does not lay inside its  $r$ -limited Voronoi (i.e. lays in the unexploited region of the node), is sensed by another “neighbor” node (Theorem 3.1). However, this does not hold true for heterogeneous networks, if standard Voronoi tessellation is applied for the region-assignment.

A graphical example is presented in Fig. 3.1 of a heterogeneous network where partitioning has been performed by standard Voronoi assignment. It is evident that there are large parts of the space assigned to nodes whose coverage performance is somehow limited, considering their relatively small maximum radii. On top of that, if someone examines the overall network’s coverage from an “ $r$ -limited Voronoi cells”-perspective, will conclude that some nodes will tend to move even if they already achieve optimum coverage (from an individual point of view). Consequently, what needs to be re-defined is a more suitable space-partitioning scheme for the case of heterogeneous networks, rather than a re-design of a coordination scheme.

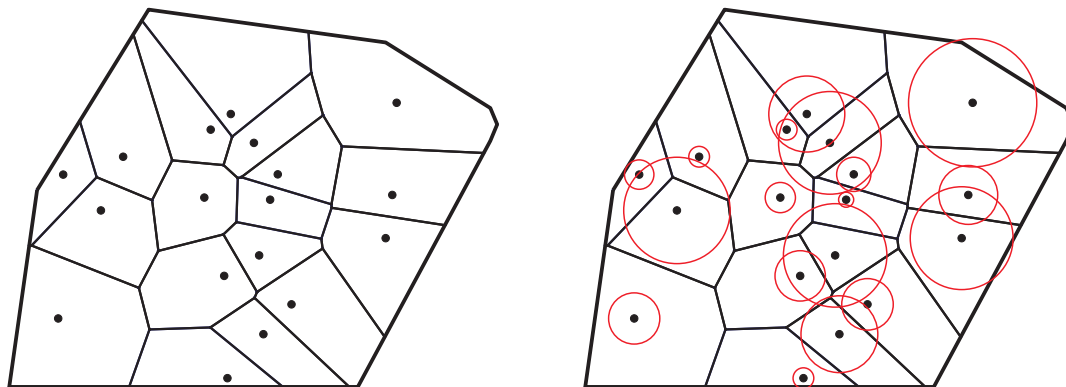


**Figure 3.1:** Inappropriateness of standard Voronoi tessellation when dealing with heterogeneous networks.

## 3.3 Proposed Partitioning of the Space

### 3.3.1 Basic concept

The example presented above shows that the assignment of the region of responsibility for each agent needs further attention when dealing with heterogeneous networks, and should be performed in a fairer way. Unlike other Voronoi tessellation techniques in the existing literature (also known as weighted or generalized Voronoi), the one that is proposed in this chapter keeps the *convexity* property of the assigned cells. This means that a Voronoi cell of a node will be a compact convex polygon in  $\mathbb{R}^2$  with no holes, allowing easier implementation of coverage control laws (compared to non-convex domains), from a computation point of view.

The scope of this chapter is to provide a modified Voronoi-originated definition for space-partitioning, suitable for cases where the nodes have different sensing capabilities. The goal of this scheme is to define each node's Voronoi cell in a way such that the unexploited regions in  $\Omega$  of a node will be surveyed by another (similarly to Theorem 3.1). Achieving that, coverage performance of the network can then be computed as the summation of the areas of the independent  $r$ -limited Voronoi cells (similarly to Theorem 3.2), leading in ease of implementation of distributed algorithms. Definitions along with the proofs of the corresponding properties will be provided in the sequel, after the development of the proposed scheme.

### 3.3.2 Development of the proposed space-partitioning technique

Using the alternative definition for a Voronoi cell in (3.2), the Voronoi cells via an arbitrary scheme can be defined as

$$\tilde{V}_i = \Omega \cap \bigcap_{j \in I_n} \tilde{H}_{ij}, \quad i \in I_n, \quad (3.7)$$

where repetition is important in order to avoid conflict of notations between standard and proposed region-assignment Voronoi techniques. In the sequel  $\tilde{H}_{ij}$ , instead of  $H_{ij}$ , will be used to denote the halfplanes defined by the proposed region-assignment scheme, and not by the standard one.

Such halfplanes  $\tilde{H}_{ij}$  result from comparing node  $i$  with the remaining  $n - 1$  nodes of the network. In order to complete the definition in (3.7), let us consider a network consisting of two nodes, as shown in Fig. 3.2. Suppose that the region under surveillance  $\Omega$  is the whole

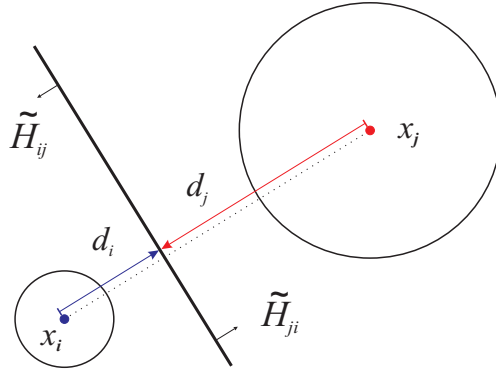


**Figure 3.2:** Notations for definition of  $\tilde{H}_{ij}$  halfplanes.

Euclidean configuration space. This will not affect anything in the sequel, since  $\Omega$  is already present in (3.7). In Fig. 3.2,  $d_i$  ( $d_j$ ) denotes the signed distance of node  $i$  ( $j$ ) from the line separating the two responsibility halfplanes,  $\tilde{H}_{ij}$  and  $\tilde{H}_{ji}$ . The distance between nodes  $i$  and  $j$  is denoted as  $w = \|x_i - x_j\|$ . It should be noted that  $d_i$  is measured from node  $i$  (whose Voronoi cell is to be defined), with positive direction towards node  $j$ , along the straight line that connects the nodes; thus, it can take both positive and negative values, depending on the topology of the nodes.

In order to build a closed-form definition for the aforementioned halfplanes, considering the above notations, let  $x$  lay on the common edge of the  $\tilde{H}_{ij}$  and  $\tilde{H}_{ji}$ . Then,  $\|x - x_i\|^2 = d_i^2 + (\|x - x_j\|^2 - d_j^2)$ . Expressing  $d_j$  in terms of  $d_i$ , the above expression is transformed into

### 3. COVERAGE BY HETEROGENEOUS NETWORKS

$\|x - x_i\|^2 = d_i^2 + \|x - x_j\|^2 - (w - d_i)^2 = \|x - x_j\|^2 - w^2 + 2d_iw$ . The latter is the equation of the common edge of the corresponding halfplanes; thus the  $\tilde{H}_{ij}$  halfplanes are defined as

$$\tilde{H}_{ij} = \{x \in \mathbb{R}^2: \|x - x_i\| \leq \|x - x_j\| + w(2d_i - w)\}, \quad i, j \in I_n, \quad (3.8)$$

which is the generalized expression of (3.3).

In the subsequent analysis, node  $i$  is supposed to be at a fixed position, while node  $j$  can slide along the straight line that connects them, in order to give a complete definition of  $\tilde{H}_{ij}$  (and consequently  $\tilde{H}_{ji}$ ) for all possible configurations of pairs of nodes. It is evident that  $w > 0$ , since  $w = 0$  implies that the two nodes coincide.

In the case where  $\Omega = \mathbb{R}^2$ , the Voronoi cells are unbounded sets; more specifically the whole space is separated into two halfplanes ( $\tilde{H}_{ij}$  and  $\tilde{H}_{ji}$ ), while the separating line is perpendicular to the line connecting the nodes. In standard Voronoi diagrams the value of  $d_i$  is equal to  $d_i = d_j = \frac{w}{2}$ , where  $d_j$  is the distance of node  $j$  from the halfplanes' separation-line, as measured from node  $j$  and towards node  $i$ . The maximum sensing radii of the nodes are denoted as  $r_i$  and  $r_j$ , respectively. Figure 3.3 shows the region-assignment to the nodes based on their radii and positioning. Hatched area corresponds to  $\tilde{H}_{ij}$  (region of responsibility assigned to

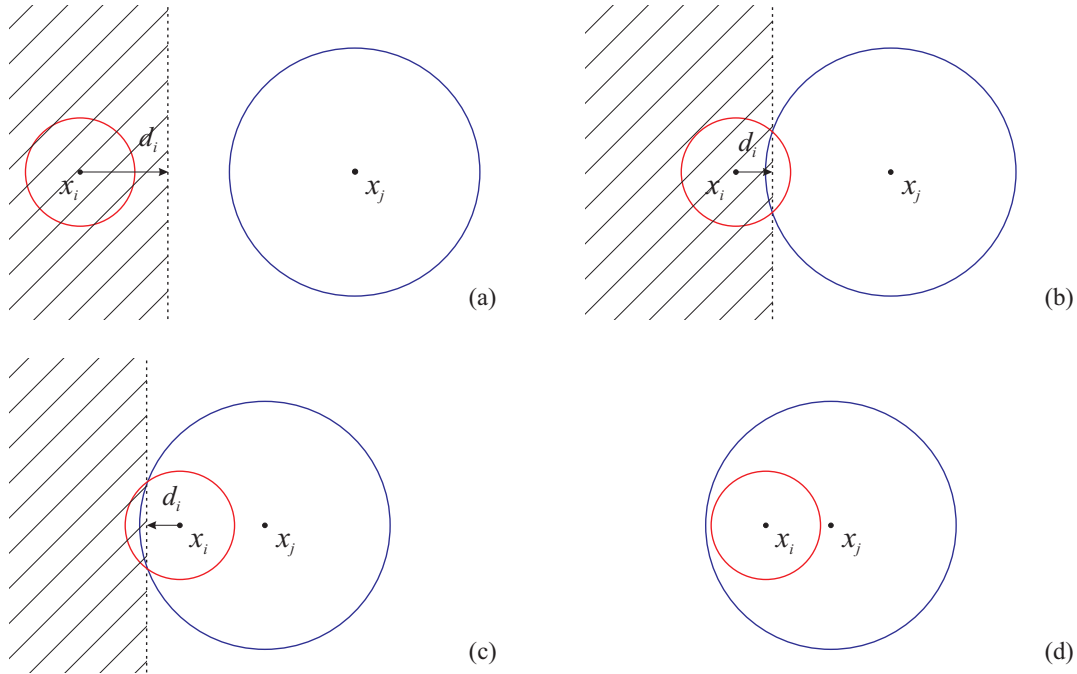


**Figure 3.3:** Space-partitioning based on the radii and relative positioning of a pair of nodes.



node  $i$  through comparison with node  $j$ ), while non-hatched is for  $\tilde{H}_{ji}$  (region of responsibility assigned to node  $j$  through comparison with node  $i$ ). Without loss of generality it is supposed that  $r_j > r_i$ ; this does not restrict the definition, since if one can define  $\tilde{H}_{ij}$ , then  $\tilde{H}_{ji}$  is also defined univocally (as shown from Figs. 3.3). Finally, it should be noted that  $d_i > 0$  holds in Figs. 3.3(a)–3.3(b), while in Fig. 3.3(c)  $d_i < 0$  holds, since  $d_i$  is measured from node  $i$  towards node  $j$ .

#### 3.3.2.1 Case I: The nodes' sensing regions do not overlap

The first case examined is when  $w \geq r_i + r_j$ , as shown in Fig. 3.3(a). This is the case where the sensing regions of the two nodes do not overlap, i.e  $C_i \cap C_j = \emptyset$ . In order the assignment to be fair, the separation of the regions of responsibility is chosen to be at

$$d_i = \frac{r_i}{r_i + r_j}w, \quad d_j = \frac{r_j}{r_i + r_j}w. \quad (r_i + r_j \leq w) \quad (3.9)$$

Practically, this is a weighted version of the standard Voronoi diagrams; the greater the sensing radius of a node is, the larger is the area it is responsible for, supposing that their sensing areas do not overlap. This proportionality incorporated in (3.9), is the one that makes the difference compared to the standard definition.

Equation (3.9) gives the distance at which the separation of the halfplanes takes place, as measured from nodes  $i$  and  $j$ , respectively. For a complete space-tessellation, examining Fig. 3.3(a),  $d_i + d_j = w$  holds, where both  $d_i, d_j$  are positive.

#### 3.3.2.2 Case II: The boundaries of the nodes' sensing regions intersect

Considering again Fig. 3.3, by sliding node  $j$  towards the node  $i$ , there will be an instance where  $\partial C_i \cap \partial C_j \neq \emptyset$ , where  $\partial C_k$  is the boundary of the set  $C_k$ ,  $k \in I_n$ , which corresponds to a circle. This condition holds as long as  $|r_i - r_j| \leq w \leq r_i + r_j$ . This corresponds to Figs. 3.3(b)–3.3(c). What is needed to be ensured is a property similar to that in Theorem 3.1. Unique solution to that is obtained iff  $d_i$  and  $d_j$  are chosen as the distances from the line that connects the points where the circles  $\partial C_i, \partial C_j$  intersect.

Let  $x_c$  be an intersection point of  $\partial C_i, \partial C_j$ . It follows then that  $\|x_c - x_i\|^2 = r_i^2$  and  $\|x_c - x_j\|^2 = r_j^2$ . Subtraction of the two latter equations results in  $\|x_c - x_i\|^2 - \|x_c - x_j\|^2 = r_i^2 - r_j^2 \Rightarrow (d_i^2 + \|x_c - x_j\|^2) - (d_j^2 + \|x_c - x_i\|^2) = r_i^2 - r_j^2 \Rightarrow d_i^2 - d_j^2 = r_i^2 - r_j^2$ . It should be noted that in this scenario,  $d_i$  can take both positive and negative values. However, the nodes' distance

### 3. COVERAGE BY HETEROGENEOUS NETWORKS

---

$w$  in either case is written as  $d_i + d_j$ ; indeed, examining Fig. 3.3(c), it is seen that  $d_i < 0$ , and thus  $w$  is written as  $d_i + d_j$ . Thus,  $d_i + d_j = w$  holds. Substitution of  $d_j$  in the previous equality results in  $d_i^2 - (w - d_i)^2 = r_i^2 - r_j^2 \Rightarrow -w^2 + 2d_i w = r_i^2 - r_j^2$ . Solving for  $d_i$ , and in the sequel computing  $d_j$  by  $d_i + d_j = w$ , the latter are given as

$$d_i = \frac{r_i^2 - r_j^2 + w^2}{2w}, \quad d_j = \frac{r_j^2 - r_i^2 + w^2}{2w}, \quad (|r_i - r_j| \leq w \leq r_i + r_j) \quad (3.10)$$

where  $d_i + d_j = w$  holds.

#### 3.3.2.3 Case III: A node's sensing region is subset of the other's pattern

The last case examined is when a node's sensing region is contained exclusively inside the other's, i.e.  $C_i \subseteq C_j$  or  $C_j \subseteq C_i$ . This case is depicted in Fig. 3.3(d). This is possible when  $0 < w \leq |r_i - r_j|$ . In such situation, considering contribution of the node in the network, node  $i$  is totally neglected, since its sensing coverage contribution is absolute zero. Thus,  $\tilde{H}_{ji} = \mathbb{R}^2$  and  $\tilde{H}_{ij} = \emptyset$  (resulting in  $\tilde{V}_i = \emptyset$ ).

What is important is the fact that this checking can be performed initially, and if a node's sensing region is found to be subset of another node's sensing region, then no region of responsibility is assigned to the first, which is neglected from the network. The space separation can follow among the remaining nodes, according to the given definition. Practically, this means that one can switch-off these redundant nodes in order to preserve consumed power of the network.

### 3.3.3 Properties of the proposed partitioning scheme

#### 3.3.3.1 Properties of proposed partitioning for heterogeneous and homogeneous networks

As already seen in section 3.2.3, when standard Voronoi tessellation technique is used for space-tessellation in homogeneous networks, results of Theorem 3.1 and Theorem 3.2 both hold. On the other hand, when dealing with heterogeneous ones, none of them hold. What will be proven in this section is that, application of the proposed Voronoi-partitioning scheme results in activeness of both properties when dealing with any kind of network (homogeneous or heterogeneous).

**Theorem 3.3.** *In a heterogeneous network, where the space-partitioning has been performed based on (3.7), if a point in the region under surveillance  $\Omega$  lays in the unexploited region of a node, then it lays in the sensing region of another node, i.e.*

$$\exists i \in I_n: x \in \tilde{U}_i \Rightarrow \exists j \in I_n, : x \in C_j, \quad x \in \Omega.$$

*Proof.* Consider a heterogeneous network of  $m$  nodes. Let  $\ell$  be the number of nodes whose coverage pattern is subset of another node's sensing region (Case III, section 3.3.2.3). Since for those nodes holds that  $\tilde{V} = \emptyset$ , ignoring them results in a network of  $n = m - \ell$  nodes.

Let  $x \in \Omega \cap \tilde{U}_i$ . By (2.10) it follows that  $x \in (C_i \setminus \tilde{V}_i)$ .

◇ Since  $x \in C_i$ , it holds that  $\|x - x_i\| \leq r_i$ .

◇ Since  $x \notin \tilde{V}_i$  it follows that  $x \in \bigcup_{k \neq i} \tilde{H}_{ki} \Rightarrow \exists j, j \neq i: x \in \tilde{H}_{ji}$ .

From (3.8) it holds that  $\|x - x_j\|^2 \leq \|x - x_i\|^2 + w(2d_j - w) \leq r_i^2 + w(2d_j - w)$ , where  $w = \|x_i - x_j\|$ .

◇ If  $|r_i - r_j| \leq w \leq r_i + r_j$  (Case II, section 3.3.2.2), then substitution of  $d_j$  by (3.10) results in  $\|x - x_j\|^2 \leq r_i^2 + w(2d_j - w) = r_i^2 + w \left( 2 \frac{r_j^2 - r_i^2 + w^2}{2w} - w \right) = r_i^2 + r_j^2 - r_i^2 + w^2 - w^2 = r_j^2 \Rightarrow x \in C_j$ , and the result is proven.

◇ If  $w > r_i + r_j$  holds  $\forall k \in I_n$ , then it will be shown that  $\tilde{U}_i = \emptyset$ . The necessary and sufficient condition for the existence of  $\tilde{U}_i \neq \emptyset$  is  $d_i < r_i$ , considering Fig. 3.3(a). By (3.9) it follows that  $d_i = \frac{r_i}{r_i + r_j} w > \frac{r_i}{r_i + r_j} (r_i + r_j) = r_i$ . Thus,  $\tilde{U}_i = \emptyset$  and the property holds.  $\square$

**Theorem 3.4.** *When space-partitioning has been performed based on (3.7), the total region surveyed by a heterogeneous network can be written as*

$$\mathcal{C} = \Omega \cap \bigcup_{i \in I_n} C_i = \bigcup_{i \in I_n} \tilde{V}_i^r, \quad (3.11)$$

where  $\tilde{V}_i^r$  is defined (equivalently to (2.9)) as

$$\tilde{V}_i^r = \tilde{V}_i \cap C_i, \quad i \in I_n. \quad (3.12)$$

Then, its area is given by

$$\mathcal{A}(\mathcal{C}) = \sum_{i \in I_n} \mathcal{A}(\tilde{V}_i^r).$$

*Proof.* The proof is identical to that of Theorem 3.2, where utilization of Theorem 3.3 is performed. The only difference lays in the  $\sim$ -notations.  $\square$

### 3. COVERAGE BY HETEROGENEOUS NETWORKS

---

At this point, the “ $\tilde{V}^r$ –Estimated Area Coverage Percentage” ( $\hat{\text{ACP}}(\tilde{V}^r)$ ), which stands for the network’s coverage performance as evaluated via the independent  $r$ –limited Voronoi cells (computed via the proposed technique), can be defined as

$$\hat{\text{ACP}}(\tilde{V}^r) = \frac{\mathcal{A}(\bigcup_{i \in I_n} \tilde{V}_i^r)}{\mathcal{A}(\Omega)} = \frac{\sum_{i \in I_n} \mathcal{A}(\tilde{V}_i^r)}{\mathcal{A}(\Omega)}. \quad (3.13)$$

**Remark 3.1.** *When dealing with a network whose nodes are all identical (i.e. homogeneous), the proposed space–partitioning degenerates into the standard one, as concluded by substituting  $r_i = r_j$  into (3.9)–(3.10). Thus, Theorems 3.1 and 3.2 still hold.*

**Proposition 3.1.** *By Theorem 3.4 and Remark 3.1 it follows that the estimated coverage performance via the  $r$ –limited Voronoi cells is for any network (homogeneous or heterogeneous) equal to the real coverage performance, when the region–assignment is performed based on the proposed scheme, i.e.  $\text{ACP} = \hat{\text{ACP}}(\tilde{V}^r)$ .*

#### 3.3.3.2 Discussion on physical properties of the proposed scheme

In section 3.3.1 two important properties of the proposed scheme were mentioned: fairness and convexity. Starting on how fair the algorithm is, one should examine more carefully Figs. 3.3. When the nodes are far away one from the other, then a wise choice is to assign to a weak node a small responsibility region, since due its very limited sensing capabilities, it has a low upper bound on its maximum coverage performance (considering its positioning in the plane along with the area it can cover). When the nodes’ sensing areas intersect, Theorem 3.3 provides a metric of fairness since each node asserts the region that is covered by itself only, while the part of the plane that is sensed by both of them is split correspondingly. Finally, when the sensing region of a “weak” node is subset of that of a “stronger” one, then the “weak” one is neglected, since its contribution to coverage is zero as long as it stays under the domination of the “stronger” one.

The second property mentioned is convexity of the nodes’ Voronoi cells. The motivation for imposing this property is because most coordination algorithms are based on Centroidal Voronoi Tessellations (CVT) [19, 22, 30]. It is well–known that the centroid of a convex polygon area lays in the interior of the latter; thus, moving a node towards the centroid of its Voronoi cell ensures that the node will not leave its own region of responsibility. This is a main advantage of the proposed scheme regarding weighted–Voronoi techniques that have been presented in the existing literature [27], where Voronoi cells are in general non–convex

sets. Regarding (3.7), since  $\Omega$  is convex and  $\Omega \cap \tilde{H}_{ij}$  are convex (since  $\tilde{H}_{ij}$  are open halfplanes in  $\mathbb{R}^2$ ), then each  $\tilde{V}_i$ ,  $i \in I_n$  is indeed convex, too.

Another interesting issue is the way in which the  $d_i, d_j$  change with respect to the nodes distance  $w$ , which can be assured by (3.9), (3.10) and Fig. 3.3. In fact, one can see that no discontinuity exists at the point where switching takes place, i.e. when  $w = R_i + R_j$ , as far as the distances  $d_i, d_j$  are concerned.

#### 3.3.3.3 Discussion on degenerate cases arising from the proposed scheme

It should be noted that the aforementioned properties also hold for homogeneous networks when standard Voronoi tessellation (2.6) is utilized for the partitioning of the space, and form the core for most Voronoi-based coordination algorithms. The main advantage of the proposed scheme regarding additive/multiplicative weighted-Voronoi techniques that have been presented in the existing literature [14, 27] is that the nodes' modified Voronoi cells are all convex sets (since they are the result of the intersection of convex sets), unlike the ones resulting from weighted-Voronoi techniques, which are in general concave sets. However, the proposed scheme is characterized as a “space partitioning” one, rather than a “tessellation”, as will be shown later.

This section is dedicated into highlighting some degenerate cases that arise from application of the proposed technique in heterogeneous sensor networks. Let us first examine a simple scenario: a network consisted of three nodes with different sensing radii, as shown in Fig. 3.4. In order to perform the proposed space-partitioning technique described in section 3.3.2 the nodes should be taken in pairs and the  $\tilde{H}_{ij}$  halfplanes should be defined according to their relative positioning and radii via Figs. 3.3. After the space-partitioning is completed, one can observe a small region denoted with red in Fig. 3.4.

Let us call these regions as sole cells since they do not lay (by definition) in any of the nodes' Voronoi cells of the network. Let  $\mathcal{O}$  denote the set of all sole cells in the plane. This part of the plane neither is it assigned uniquely at one node nor is it assigned to all of them simultaneously. If the network is homogeneous, then these cells disappear and shrink at a point which is the common vertex of the neighbor Voronoi cells. What should be noted is that due to the existence of sole cells, the Voronoi cells  $\tilde{V}_i$ ,  $i \in I_n$  computed by the proposed definition do not constitute a full tessellation of the space.

As seen, the reason that these cells exist is the insistence of keeping the convexity property of the Voronoi cells. Indeed, in order to avoid them, one should: (a) either use standard

### 3. COVERAGE BY HETEROGENEOUS NETWORKS

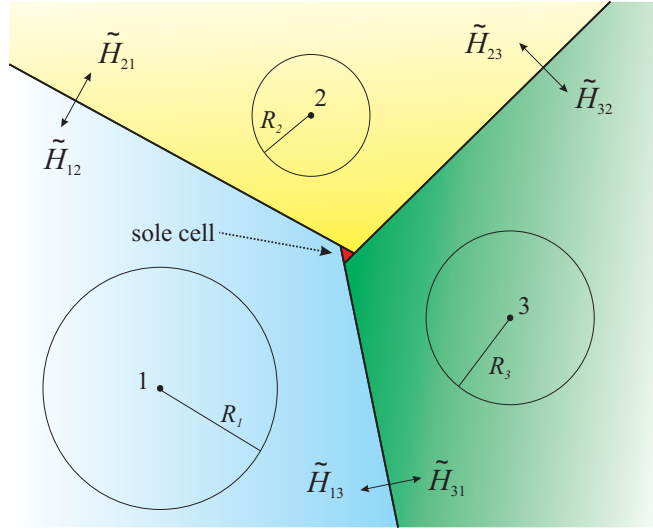


**Figure 3.4:** Space-partitioning via the proposed algorithm for a network consisting of three nodes in order to show the existence of sole cells.

weighted-Voronoi schemes which constitute a full tessellation of the configuration space, but the regions of responsibility in that case are in general concave sets, while their computation is by far more computationally intensive than the proposed one or, (b) use the standard Voronoi diagrams, whose inappropriateness in heterogeneous networks has already been shown in section 3.2.3. An important property concerning these cells follows.

**Theorem 3.5.** *When dealing with a heterogeneous network, where the space-partitioning has been performed via (3.7), no point in any sole cell belongs to the sensing pattern of any node, i.e.*

$$x \in \mathcal{O} \Rightarrow \nexists j: x \in C_j, \quad x \in \Omega$$

*Proof.* Let  $x \in \Omega \cap \mathcal{O}$ . Suppose that  $\exists j: x \in C_j$ . According to Theorem 3.4,  $\Omega \cap \bigcup_{i \in I_n} C_i = \bigcup_{i \in I_n} \tilde{V}_i^r$ ; thus  $\Omega \cap C_j \subseteq \bigcup_{i \in I_n} \tilde{V}_i^r$ . Consequently,  $\Omega \cap C_j \cap \mathcal{O} \subseteq \bigcup_{i \in I_n} \tilde{V}_i^r$ . Since  $x \in \Omega \cap C_j \cap \mathcal{O}$  and  $\bigcup_{i \in I_n} \tilde{V}_i^r \subseteq \bigcup_{i \in I_n} \tilde{V}_i$ , it follows that  $x \in \bigcup_{i \in I_n} \tilde{V}_i$ . But, since  $x \in \mathcal{O} \Rightarrow x \notin \bigcup_{i \in I_n} \tilde{V}_i$ . Consequently, the assumption that  $\exists j: x \in C_j$  is incorrect; thus, the result of the theorem holds.  $\square$

The last two cases examined have already been presented previously, but without any discussion. Referring to Fig. 3.3(c), it is easy to observe that in all cases node  $i$ , although owning a Voronoi cell, is outside of it. Figure 3.3(c) differs from Fig. 3.3(d) in the fact that in the first,

the  $r$ -limited Voronoi cell of the node is not empty; thus, the node does have the perception that its contribution to coverage is not zero at all (as happens in Fig. 3.3(d)).

**Remark 3.2.** *The set  $\emptyset \cup \bigcup_{i \in I_n} \tilde{V}_i$  consists a complete tessellation of  $\Omega$ .*

*Proof.* The proof is straightforward by definition of  $\emptyset$ . □

The cases discussed above are summarized and illustrated in Fig. 3.5, in order to provide an insight to the resulting space partitioning scheme.

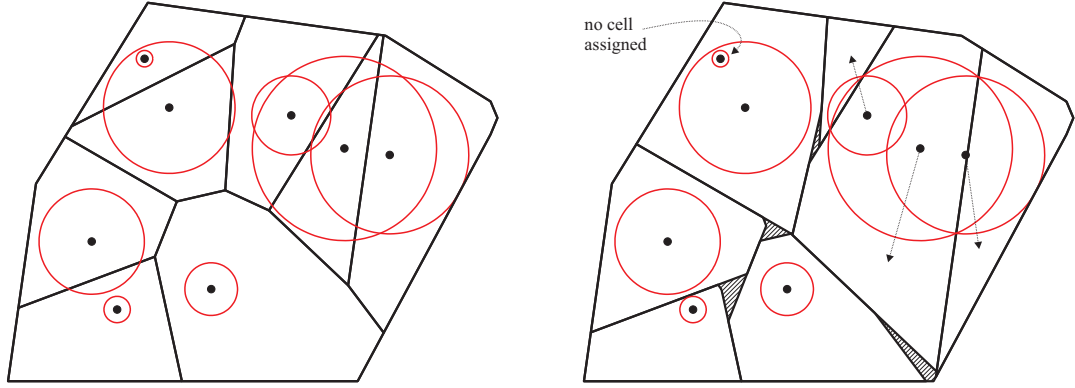


**Figure 3.5:** Voronoi partitioning via the standard [left] and modified [right] technique for a heterogeneous network to emphasize in the degenerate cases arisen.

Considering utilization of the aforementioned space partitioning scheme in swarm coordination applications, a smoothness analysis is essential. Observing Fig. 3.3, one can verify that the modified Voronoi cell of a node does not alter in a continuous manner (during the transition depicted in Figs. 3.3(c)–3.3(d)). However, considering coverage applications, the aforementioned analysis should be performed for the corresponding  $r$ -limited modified Voronoi cells of the nodes instead, which capture their sensing performance.

**Remark 3.3.** *The nodes'  $r$ -limited modified Voronoi cells are smooth (rectifiable) sets.*

*Proof.* Recalling (3.7), the  $r$ -limited modified Voronoi cell of a node  $i$  can be written as

$$\tilde{V}_i^r = \tilde{V}_i \cap C_i = \bigcap_{j \in I_n} \tilde{H}_{ij} \cap C_i \cap \Omega.$$

The discontinuity in  $\tilde{H}_{ij}$  halfspace during comparison of two arbitrary nodes lays during the transition depicted in Figs. 3.3(c)–3.3(d). However, during this transition it is apparent that the sets  $C_i \cap \tilde{H}_{ij}$  and  $C_j \cap \tilde{H}_{ji}$  vary smoothly; more specifically, the sets  $\tilde{V}_i^r$ ,  $\tilde{V}_j^r$  shrink at  $\emptyset$  (empty-set) and  $C_j$  (depending on the relation among their radii), respectively, in a continuous manner. Consequently,  $\tilde{V}_i^r$  is smooth, as the intersection of smooth sets. □

### 3. COVERAGE BY HETEROGENEOUS NETWORKS

#### 3.3.4 Numerical results

Numerical studies are carried out in this section, in order to show the efficacy of the proposed scheme. The region  $\Omega$  to be surveyed is a convex set in  $\mathbb{R}^2$ , the area of which is  $\mathcal{A}(\Omega) = 5.08 \text{ units}^2$ .

The nodes are deployed in the interior of  $\Omega$  in a random manner. At the first study, their number is  $n = 7$ , while their sensing radii are chosen as  $r_i = 0.08i$  units,  $i \in I_n$ , where the network's heterogeneity is evident.

The assigned regions of responsibility (Voronoi cells) for each node, via the standard Voronoi tessellation scheme is shown in Fig. 3.6(a). The nodes are numbered from 1 to 7 according to their sensing radius. At first, one sees that the whole region  $\Omega$  is partitioned into cells that are assigned to all of the nodes. The problem though is, that the assignment is not as fair as one should need. Indeed, considering nodes 1 and 7, it is apparent that, although node 1 is dominated by node 7, it is responsible for a large part of node's 7 pattern. Furthermore, the result of Theorem 3.1 does not hold at all, as expected. As a result, Theorem 3.2 does not hold, too, giving the nodes an illusionary perception of their coverage contribution. Computation of the network's coverage performance via the covered parts of all nodes' Voronoi cells ( $r$ -limited Voronoi cells) via (3.6) results in  $\hat{\text{ACP}}(V^r) = 38.20\%$ , while the real coverage performance is given by (3.5) as  $\text{ACP} = 50.01\%$ .

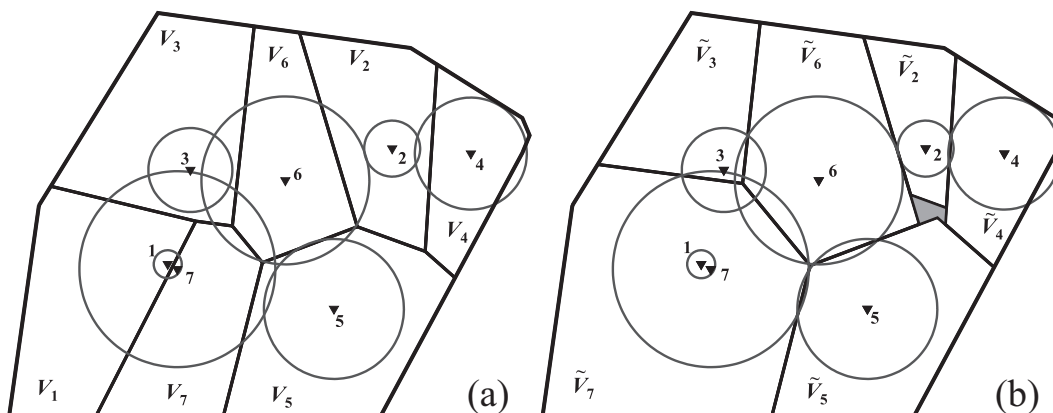


**Figure 3.6:** Voronoi partitioning via the standard [left] and proposed [right] technique for a heterogeneous network consisted of  $n = 7$  nodes (Case Study 1).

Figure 3.6(b) shows the region-assignment at the nodes, when the proposed technique is used. At first, one can notice the existence of sole-cells (denoted with gray), which were



described in section 3.3.3.3. However, important is the fact that, due to the way that the  $\tilde{V}_i$  definition was built, no point inside any sole-cell is sensed by any node (Theorem 3.5). Apart from that, one can see that no region of responsibility is assigned to node 1, since it is under the influence of node 7. As for Theorem 3.3, it holds for any part of the network, which is also seen clearly by the common Voronoi edge of any two nodes that their sensing patterns overlap. Finally, computation of the network's coverage performance via (3.13) results in  $\widehat{ACP}(\tilde{V}^r) = 50.01 = ACP\%$ , as expected due to Proposition 3.1. Thus, the nodes of the network are aware of their own contribution in coverage, as evaluated by the area of their  $r$ -limited Voronoi cells, while Theorem 3.4 holds.

In our second study, the nodes are not deployed randomly in  $\Omega$  as previously, but are positioned in a more "symmetric" manner. More specifically, the coordinates used are the final positions of the agents in Fig. 4.5 of [15]. The number of nodes is  $n = 16$ , while their radii  $r_i$  are set uniformly randomly between 0.15 and 0.6 units.

The assigned regions of responsibility (Voronoi cells) for each node, via the standard and proposed space-partitioning scheme are shown in Fig. 3.7(a) and 3.7(b), respectively. Unlike previously, the nodes in this case are not numbered to avoid unreadability of the resulting figures.

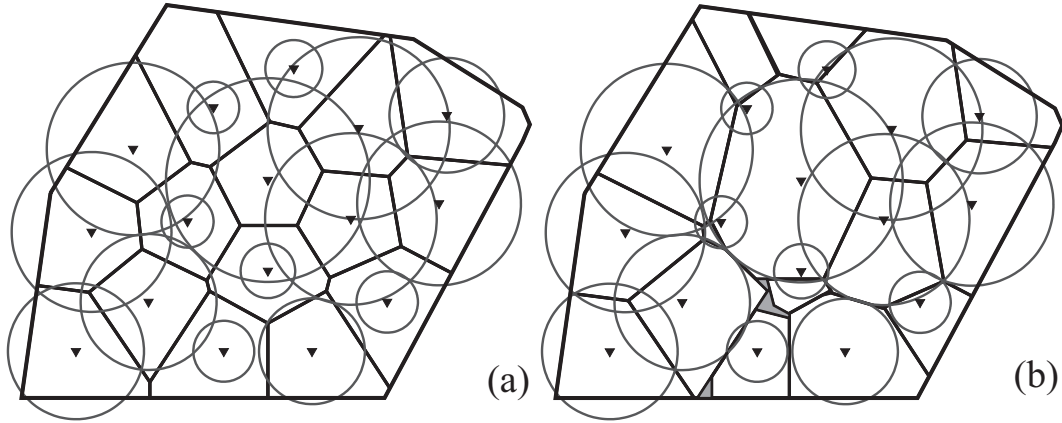


**Figure 3.7:** Voronoi partitioning via the standard [left] and proposed [right] technique for a heterogeneous network consisted of  $n = 16$  nodes (Example 2).

Considering Fig. 3.7(a), it is clear that the region-assignment among the nodes via (2.6) is not preferable, since the heterogeneity of the nodes' radii is not taken into account. On the other hand, Fig. 3.7(b) indicates that, although the space is not completely tessellated, the resulting region-assignment is the desired one, considering the heterogeneous nature of the network.

### 3. COVERAGE BY HETEROGENEOUS NETWORKS

---

As for the network's coverage performance (in the three ways defined by (3.6), (3.5) and (3.13)), it is computed as  $\widehat{\text{ACP}}(V^r) = 68.32\%$  and  $\text{ACP} = \widehat{\text{ACP}}(\tilde{V}^r) = 84.66\%$ . Furthermore, it should be noted that the result of Theorem 3.5 concerning the sole cells (gray regions) holds, as expected. Apart from that, it is seen that three of the nodes of the network (the ones with the three smallest radii), although owning a Voronoi cell, do not lay in its interior. However, they do contribute to its coverage, since  $\tilde{V}_i \cap C_i \neq \emptyset$ .

## 3.4 Proposed Algorithm for Optimum Area Coverage

### 3.4.1 Preliminaries

A space partitioning scheme suitable for heterogeneous networks has been developed and analyzed in previous section. The nodes are assumed to sense in an omnidirectional way, yet their maximum reliable sensing distance differs. The design of a distributed motion coordination scheme is to be developed in this section, based on the presented partitioning. Unlike the concept in Chapter 2, where the nodes were evolving in discrete time steps, continuous time motion of the latter is assumed in this chapter. Furthermore, let the density function  $\phi: \Omega \subset \mathbb{R}^2 \rightarrow \mathbb{R}_+$  describe the importance of any point  $x \in \Omega$  (considering surveillance purposes), representing the probability of an event to take place at  $x$ .

Each mobile node is assumed to move in  $\Omega$  via the control inputs  $u_i \in \mathbb{R}^2$ , while governed by simplified first-order kinodynamics, provided as

$$\dot{x}_i = u_i, \quad u_i \in \mathbb{R}^2, \quad x_i \in \Omega, \quad i \in I_n, \quad (3.14)$$

where the nodes's dimensions are assumed negligible. The sensing domain of the nodes in the network is that presented in (3.1). A node's performance function  $f_i: \Omega \subset \mathbb{R}^2 \rightarrow \mathbb{R}_+$  (representing the "amount" at which a point  $x$  is surveyed by node  $i$ ) can be described by the indicator function  $\mathbf{1}_{C_i \cap \Omega}$ , where  $\mathbf{1}_D(x) = 1$  if  $x \in D$  and 0 if  $x \notin D$ , for an arbitrary set  $D \subset \mathbb{R}^2$ .

In order for the members of the network to be able to exchange information among them (concerning their spatial coordinates and sensing radii), radio transceivers are assumed to be mounted on their platforms, where the latters' node-centered radiation patterns are assumed circular. All nodes that lay in the radiation pattern are assumed connected with the corresponding node, while (bidirectional) communication is supposed to be performed instantaneously.

Let the nodes be initially deployed randomly in  $\Omega$ ; the main objective is to design a decentralized coordination algorithm in a way that the nodes are able to self-position themselves at

certain spatial coordinates, such that an aggregate objective function  $\mathcal{H}$  is optimized. In this thesis, the area-related problem is examined, since it is often met in most practical scenarios on coordination of ground/aerial swarms [10, 32]. Considering (3.1) and the density  $\phi$  over  $\Omega$ , the total area of  $\Omega$  (weighted according to  $\phi$ ) surveyed by the network (i.e. the area of the set  $\Omega \cap \bigcup_{i \in I_n} C_i$ ) that needs to be (locally) maximized can be written as

$$\mathcal{H} = \int_{\Omega} \max_{i \in I_n} f_i(x) \phi(x) dx. \quad (3.15)$$

Note that (3.15) strays away from the numerical polygonal-based expressions presented in Chapter 2, but allows for far more efficient control designs due to its analytical form.

In a coverage optimization scenario, the agents should move in a way to try and cover the whole space  $\Omega$  (ideally, if possible), considering their limited sensing capabilities. Utilization of Voronoi tessellation in order to decompose the space and assign it among the nodes indicates that itself alone is not sufficient for the motion algorithm, since it is based only on the nodes' positioning, without having taken into consideration the sensing parts  $C_i$ . The main contribution of Voronoi diagrams in swarm coordination applications is the fact that their evaluation can be performed independently by the nodes themselves (without the need for a global coordinator) [16]; in fact, each node that needs to evaluate its Voronoi cell at an arbitrary time instance needs information only from its Delaunay neighbors, ignoring the status of the rest members of the network. The fact that only local information is required for the coordination algorithm is the one makes them applicable in real-time applications. Among the different objectives that can be assigned to a set of mobile nodes, in this thesis area-coverage maximization of a certain domain of interest is examined.

It is easily proven that for homogeneous networks and for  $f_i$  being the indicator function  $\mathbf{1}_{C_i \cap \Omega}$ , the criterion (3.15) can be written as [16]

$$\mathcal{H} = \sum_{i \in I_n} \int_{V_i} f_i(x) \phi(x) dx = \sum_{i \in I_n} \int_{V_i} \phi(x) dx = \sum_{i \in I_n} \mathcal{H}_i. \quad (3.16)$$

Practically, the above expression indicates that the total ( $\phi$ -weighted) area surveyed by the network ( $\mathcal{H}$ ) is decomposed as the summation of the areas surveyed by each node in the interior of their Voronoi cells ( $\mathcal{H}_i$ ). Unfortunately, the aforementioned property does not hold when the nodes' sensing radii differ. Hence, an issue of major importance is the partitioning scheme according to which the responsibility spaces are assigned, before one should proceed to the coordination algorithm design.

#### 3.4.2 Coordination Algorithm Development

As mentioned in the previous section, the main objective is to design a decentralized coordination algorithm, such that the total volume surveyed by the network, as provided in (3.15), is (locally) maximized along the nodes' trajectories. The problem has been treated in [21] and [13] in a more generalized manner (i.e. for different performance criteria); however, the nodes were considered homogeneous in regard to their sensing capabilities, while standard Voronoi partitioning of the space was used. Before proceeding to the main result, let us define some notations that will be used.

Let  $n_i$  be the outward unit normal at an arbitrary point  $x$  of  $\partial V_i^r$ , i.e.  $\|n_i(x)\| = 1$  and  $n_i(x) \perp \partial V_i^r|_x$ ,  $x \in S \subseteq \partial V_i^r$ , pointing towards the exterior of  $\partial V_i^r$ , where  $\partial S$  stands for the boundary of the compact set  $S$ . Then, taking into account the nodes' kinodynamics described in (3.14) and considering the network homogeneous (i.e.  $r_i = r > 0$ ,  $\forall i \in I_n$ ), the control law

$$u_i = \int_{\partial V_i^r \cap \partial C_i} n_i \phi \, dx, \quad i \in I_n, \quad (3.17)$$

leads in a network configuration where  $\mathcal{H}$  is maximum, as proposed in [21]. Apparently, in the previous expression, the set  $\partial V_i^r \cap \partial C_i$  represents the parts of the sphere  $\partial C_i$  that lay in the interior of  $V_i$ . It should be noted that since  $V_i^r$  are compact sets, then  $\partial V_i^r$  are closed and non-self-intersecting; thus, the exterior of the latter is always well-defined, considering the orientation of  $n_i(x)$ ,  $x \in \partial V_i^r \cap \partial C_i \subset \partial V_i^r$ .

Thus, intuitively, one can consider the parts of the sphere  $\partial C_i$  that lay on the boundary of the blind domains ( $\partial B_i$ ) as "attractors". The network topology at the converged (optimum) state is usually referred as area-centered configuration [21], due to the fact that, apart from  $\mathcal{H}$  being optimized, each integral  $\mathcal{H}_i = \int_{V_i^r} \phi \, dx$ ,  $i \in I_n$  of (3.16) is also locally optimum.

This section proposes utilization of that philosophy for the coordination of a network consisted of heterogeneous nodes. Unlike previous works which deal with mobile nodes of unequal or anisotropic sensing patterns [19, 29, 30, 33], partitioning of the configuration space is based on the modified Voronoi definition. Equivalently to the notations appearing in (3.17), let us denote as  $\tilde{n}_i$  the outward unit normal at an arbitrary point  $x$  of  $\partial \tilde{V}_i^r$ , in order to avoid conflicts in the notations.

**Theorem 3.6.** *Considering a mobile sensor network consisted of heterogeneous nodes with sensing domains as in (3.1), governed by (3.14), the coordination scheme*

$$u_i = \int_{\partial \tilde{V}_i^r \cap \partial C_i} \tilde{n}_i \phi \, dx, \quad i \in I_n \quad (3.18)$$

optimizes the performance criterion (3.15) along the nodes' trajectories, leading in a (modified) volume-centered configuration of the network.

*Proof.* Considering (3.15) and Remark 3.2 it holds that

$$\mathcal{H} = \int_{\Omega} \max_{i \in I_n} f_i \phi \, dx = \int_{\mathcal{O}} \max_{i \in I_n} f_i \phi \, dx + \sum_{i \in I_n} \int_{\tilde{V}_i} \max_{i \in I_n} f_i \phi \, dx.$$

By Theorem 3.5, since  $C_i \cap \mathcal{O} = \emptyset$ ,  $\forall i \in I_n$  it is concluded that  $f_i(x) = 0$ ,  $x \in \mathcal{O}$ ,  $\forall i \in I_n$ , and thus the first integral vanishes. Considering the second part, it holds by Theorem 3.3 that

$$\max_{j \in I_n} f_j(x) = f_i(x), \quad x \in \tilde{V}_i.$$

More specifically, if  $x \in \tilde{V}_i^r$  then  $\max_{j \in I_n} f_j(x) = 1 = f_i(x)$ . Alternatively, if  $x \in \tilde{B}_i$ , then  $f_i(x) = 0$  and  $f_j(x) = 0$ ,  $\forall j \in I_n \setminus \{i\}$ ; indeed, if we suppose that  $f_j(x) = 1$  for some  $j \in I_n$ , then  $x \in \tilde{U}_j$ . But then it should hold that  $x \in C_i$  by Theorem 3.3, which contradicts with the hypothesis that  $x \in \tilde{B}_i$ . Taking into account that  $\tilde{V}_i^r$  and  $\tilde{B}_i$  consist a tessellation of  $\tilde{V}_i$  leads to the result above.

Consequently,  $\mathcal{H}$  can be written as

$$\mathcal{H} = \sum_{i \in I_n} \int_{\tilde{V}_i} f_i \phi \, dx = \sum_{i \in I_n} \int_{\tilde{V}_i^r} \phi \, dx,$$

where  $f_i = \mathbf{1}_{C_i}$  was utilized. Taking the partial derivative of  $\mathcal{H}$  with respect to  $x_i$  we have

$$\frac{\partial \mathcal{H}}{\partial x_i} = \frac{\partial}{\partial x_i} \left( \int_{\tilde{V}_i^r} \phi \, dx \right) + \frac{\partial}{\partial x_i} \left( \sum_{j \neq i} \int_{\tilde{V}_j^r} \phi \, dx \right).$$

At this point, taking into account that  $\phi$  is independent of  $x_i$ , and the fact that infinitesimal motion of  $x_i$  may affect  $\tilde{V}_j^r$  iff  $\partial \tilde{V}_i^r \cap \partial \tilde{V}_j^r \neq \emptyset$ , the above expression can be rewritten via the generalized Leibniz integral rule [34] as

$$\frac{\partial \mathcal{H}}{\partial x_i} = \int_{\partial \tilde{V}_i^r} \tilde{v}_i^i \tilde{n}_i \phi \, dx + \sum_{j \neq i} \int_{\partial \tilde{V}_i^r \cap \partial \tilde{V}_j^r} \tilde{v}_j^i \tilde{n}_j \phi \, dx,$$

where  $\tilde{n}_i$  ( $\tilde{n}_j$ ) is the outward unit normal at  $\partial \tilde{V}_i^r$  ( $\partial \tilde{V}_j^r$ ) and  $\tilde{v}_i^i$ ,  $\tilde{v}_j^i$  stand for the Jacobian matrices with respect to  $x_i$  of the points  $x \in \partial \tilde{V}_i^r$ ,  $x \in \partial \tilde{V}_j^r$ , respectively, i.e.

$$\tilde{v}_j^i(x) \triangleq \frac{\partial x}{\partial x_i}, \quad x \in \partial \tilde{V}_j^r, \quad i, j \in I_n. \quad (3.19)$$

Considering the first integral, parts of  $\partial \tilde{V}_i^r$  may possibly lay either on  $\partial \Omega$ ,  $\partial C_i$ ,  $\partial \mathcal{O}$  (possible neighboring sole cells), or on the boundary of a neighboring modified  $r$ -limited Voronoi cell

### 3. COVERAGE BY HETEROGENEOUS NETWORKS

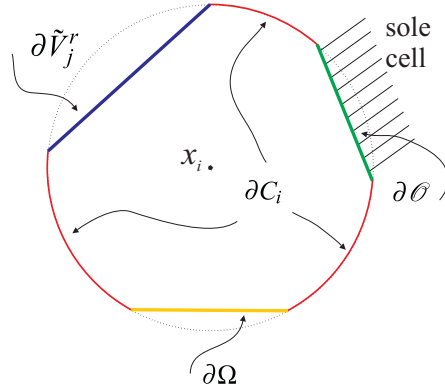


**Figure 3.8:** Decomposition of the set  $\partial\tilde{V}_i^r$  into mutually disjoint sets.

$(\bigcup_{j \neq i} \partial\tilde{V}_i^r \cap \partial\tilde{V}_j^r)$ , as shown for visualization purposes in Fig. 3.8. Consequently, the boundary  $\partial\tilde{V}_i^r$  can be decomposed as

$$\partial\tilde{V}_i^r = \{\partial\tilde{V}_i^r \cap \partial\Omega\} \cup \{\partial\tilde{V}_i^r \cap \partial C_i\} \cup \{\partial\tilde{V}_i^r \cap \partial\Theta\} \cup \left\{ \partial\tilde{V}_i^r \cap \bigcup_{j \neq i} \partial\tilde{V}_j^r \right\}.$$

But, since the above sets are disjoint,  $\frac{\partial\mathcal{H}}{\partial x_i}$  can be written as

$$\begin{aligned} \frac{\partial\mathcal{H}}{\partial x_i} = & \int_{\partial\tilde{V}_i^r \cap \partial\Omega} \tilde{v}_i^i \tilde{n}_i \phi \, dx + \int_{\partial\tilde{V}_i^r \cap \partial C_i} \tilde{v}_i^i \tilde{n}_i \phi \, dx + \int_{\partial\tilde{V}_i^r \cap \partial\Theta} \tilde{v}_i^i \tilde{n}_i \phi \, dx + \\ & \int_{\partial\tilde{V}_i^r \cap \bigcup_{j \neq i} \partial\tilde{V}_j^r} \tilde{v}_i^i \tilde{n}_i \phi \, dx + \sum_{j \neq i} \int_{\partial\tilde{V}_i^r \cap \partial\tilde{V}_j^r} \tilde{v}_j^i \tilde{n}_j \phi \, dx. \end{aligned}$$

Considering the third integral, if we assume that  $\tilde{V}_i^r \cap \Theta \neq \emptyset$ , then there exist parts of the ball  $C_i$  that lay in  $\Theta$ , which contradicts with Theorem 3.5. Thus,  $\partial\tilde{V}_i^r \cap \partial\Theta$  is a singleton or the empty-set, leading in vanishing the aforementioned integral term. As far as concerns the first integral, it is apparent that  $\tilde{v}_i^i = 0$  at  $x \in \partial\tilde{V}_i^r \cap \Omega$  since all  $x \in \partial\Omega$  remain unaltered by infinitesimal motions of  $x_i$ . Finally, simplifying the boundary set of the fourth integral as  $\partial\tilde{V}_i^r \cap \bigcup_{j \neq i} \partial\tilde{V}_j^r = \bigcup_{j \neq i} \partial\tilde{V}_i^r \cap \partial\tilde{V}_j^r$  leads in

$$\frac{\partial\mathcal{H}}{\partial x_i} = \int_{\partial\tilde{V}_i^r \cap \partial C_i} \tilde{v}_i^i \tilde{n}_i \phi \, dx + \sum_{j \neq i} \int_{\partial\tilde{V}_i^r \cap \partial\tilde{V}_j^r} (\tilde{v}_i^i \tilde{n}_i + \tilde{v}_j^i \tilde{n}_j) \phi \, dx.$$

With respect to the parts of the sphere that lay in  $\tilde{V}_i$ , i.e.  $\partial\tilde{V}_i^r \cap \partial C_i$ , any point  $x$  on that set moves along the direction of  $x_i$  with the same rate. Thus, it is apparent (considering pure translational motion of  $x_i$ ) that  $\tilde{v}_i^i(x) = I_N$ , where  $I_N$  stands for the  $N \times N$  identity matrix.

In order to complete the proof, one should examine that  $\tilde{v}_i^i(x) \tilde{n}_i(x) = -\tilde{v}_j^i(x) \tilde{n}_j(x)$  at  $x \in \partial\tilde{V}_i^r \cap \partial\tilde{V}_j^r$ . But,  $\tilde{v}_i^i(x) = \tilde{v}_j^i(x)$  on the set  $\partial\tilde{V}_i^r \cap \partial\tilde{V}_j^r$  by definition of the Jacobian matrices

$\tilde{v}$  provided in (3.19). Furthermore, it is clear by Figs. 3.3(b)–3.3(c) that  $\tilde{n}_i = -\tilde{n}_j$  at  $x \in \partial\tilde{V}_i^r \cap \partial\tilde{V}_j^r$ , since this is the common part of the line separating  $\tilde{V}_i, \tilde{V}_j$ . Indeed, even considering the degenerate case where a node lays in the exterior of its Voronoi cell (see Fig. 3.9), it can be seen that  $\tilde{V}_i^r$  and  $\tilde{V}_j^r$  lay on either side of the separating halfplane (degenerated in line in  $\mathbb{R}^2$ ), leading in the result at the common edge.

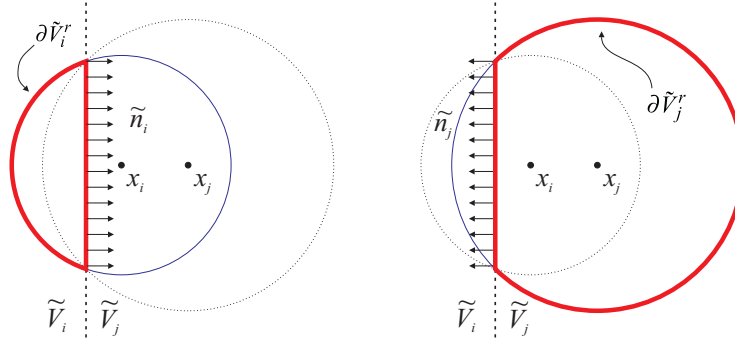


**Figure 3.9:** Graphical representation of  $\tilde{n}_i, \tilde{n}_j$  at the common boundary  $\partial\tilde{V}_i \cap \partial\tilde{V}_j$  for the degenerate case where  $x_i \notin \tilde{V}_i$ .

Considering the above,  $\frac{\partial \mathcal{H}}{\partial x_i}$  is simplified into (3.18), while recalling (3.14) it is concluded that (3.18) leads to a gradient flow of  $\mathcal{H}$  along the nodes trajectories.  $\square$

However, control law (3.18) assumes that each node is able to identify its own (modified)  $r$ -limited Voronoi cell. Thus, in order for the algorithm to be considered decentralized over a non-fully-connected graph of the network, the subset of nodes needed for its evaluation must be defined properly.

### 3.4.3 Connectivity Issues

Considering distributed approaches, each mobile node is assumed to be equipped with radio transceivers in order to be able to exchange information concerning its state with other members of the network. Let node  $i$  with sensing radius  $r_i$  be the arbitrary node for which the analysis will be performed. In a neighbor-identification scheme, the main concept lays in gradual increase of the communication radius from one step of the algorithm to another, until all nodes that can possibly affect the node's modified  $r$ -limited Voronoi cell are identified [16, 35, 36], considering (3.18). What needs to be determined properly is a critical communication radius  $R_i$  of node  $i$  which guarantees sufficient information from the neighboring nodes for evaluating  $\tilde{V}_i^r$ .

### 3. COVERAGE BY HETEROGENEOUS NETWORKS

---

Taking into account the heterogeneity of the network, it is apparent that the space partitioning presented in section 3.3 is based on the sensing radii of the nodes, apart from their spatial coordinates, and thus it is assumed that each node transmits its sensing radius along with its spatial coordinates during inter-communication. In this section, two scenarios are examined, considering knowledge of other members' sensing capabilities, as presented in the sequel.

#### 3.4.3.1 Case A: A-priori knowledge of the maximum sensing radius among all nodes of the network

Let us denote as  $\bar{r}$  the maximum sensing radius among all nodes of the network, i.e.

$$\bar{r} = \max \{r_i, i \in I_n\}. \quad (3.20)$$

In the first case examined, each node is assumed to have a-priori knowledge of  $\bar{r}$ . Discussing on the applicability of the aforementioned assumption, since the sensing radii of the nodes are fixed and do not alter during network evolution, it is not as conservative as it may seem. Apart from that, although  $\bar{r}$  is assumed to be a-priori known to the members of the network, the node to which that radius corresponds is not demanded to be known. At this point, a (conservative) lower bound on the communication radius  $R_i$  of node  $i$ , so that the control law (3.18) can be evaluated independently by each node, is stated in the following proposition.

**Proposition 3.2.** *For an arbitrary node  $i$ , the sufficient information for evaluation of  $\tilde{V}_i^r$  in a decentralized manner is obtained by the nodes that lay within range of  $r_i + \bar{r}$ .*

*Proof.* The main concept behind determining a low bound on the corresponding radius lays in gradual increase of the latter, until it is guaranteed that any other “unidentified” node of the network does not alter the node’s modified  $r$ -limited Voronoi cell (i.e. it does not affect the result of the control law). Taking into account the definition for the sets  $\tilde{V}_i^r$  (concluded straightforward by (3.7) and (2.9)), along with the generalized expression of the halfspaces  $\tilde{H}_{ij}$  provided in (3.8), one can express the aforementioned condition equivalently to  $\tilde{V}_i^r \subset \tilde{H}_{ij}$  for any other unidentified node  $j$  of the network.

However, examining Fig. 3.3(a), one can conclude that the critical case is when  $\|x_i - x_j\| = r_i + r_j$ . Considering the worst case scenario, the arbitrary node  $j$  can be assumed to be the node of the network at which  $\bar{r}$  corresponds (i.e.  $r_j = \bar{r}$ ). Existence of another node  $k$  in a distance from node  $i$  larger than  $r_i + \bar{r}$ , i.e.  $\|x_i - x_k\| \geq r_i + \bar{r}$ , does not affect the evaluated modified  $r$ -limited Voronoi cell; indeed, considering  $d_i$  the distance of node  $i$  from the halfplane separating



$\tilde{H}_{ik}$  and  $\tilde{H}_{ki}$  halfspaces (see Fig. 3.2), along with the expression of  $d_i$  that corresponds to Fig. 3.3(a) (i.e.  $\|x_i - x_k\| \geq r_i + r_k$ ) by equation (14) of [37], it holds that

$$d_i = \frac{r_i}{r_i + r_k} \|x_i - x_k\| \geq \frac{r_i}{r_i + r_k} (r_i + \bar{r}) \geq r_i.$$

Consequently,  $\tilde{H}_{ik} \supset C_i \supseteq \tilde{V}_i^r$ , and thus the result is proven.  $\square$

It should be noted that during network's evolution there is no need for adjustment of the nodes' communication radii  $R_i$ , assuming that the latter have been pre-set to the bound derived above, in order to guarantee inter-agent communication with the sufficient subset of nodes needed for  $\tilde{V}_i^r$  evaluation.

### 3.4.3.2 Case B: A-priori knowledge of the sensing-radii-set of the network

In this case-scenario, in order to derive a more strict bound on the communication radius  $R_i$  of the nodes, it is assumed that each node of the network has a-priori knowledge of the set  $\mathbf{r}$ , which contains the sensing radii of all members the network, i.e.

$$\mathbf{r} = \{r_j, j \in I_n\}, \tag{3.21}$$

whereas the bijection mapping from the set  $I_n$  onto the set  $\mathbf{r}$  is unknown to any node. It should be noted that in the case where two (or more) nodes have equal sensing radii (i.e.  $r_i = r_j$  for a pair of nodes  $i \neq j$ ), then their sensing radius is included twice (or more) in the set  $\mathbf{r}$ .

Let us denote with  $(\cdot)^{(k)}$  a variable as evaluated by node  $i$  at the  $k$ -th iteration of the radio-range adjustment scheme proposed. Let  $\mathbf{r}_{\text{rem}}^{(k)}$  stand for the set containing the radii of the remaining nodes that have not been identified until step  $k$ . An arbitrary node  $i$  gradually increases  $R_i$  until another neighbor node is identified in its range. By denoting this arbitrary neighbor node as  $m$ , the estimated modified  $r$ -limited Voronoi cell of node  $i$  at step  $k$  is then evaluated recursively as  $\tilde{V}_i^{r^{(k)}} = \tilde{V}_i^{r^{(k-1)}} \cap \tilde{H}_{im}$ . By the time that node  $m$  is identified, node  $i$  can update the radii-set of the *remaining* (i.e. unidentified yet) nodes of the network as  $\mathbf{r}_{\text{rem}}^{(k)} = \mathbf{r}_{\text{rem}}^{(k-1)} \setminus \{r_m\}$ . At this stage, a worst case scenario approach is followed. More specifically, an estimation is performed on the worst possible positioning and radius of any other node of the network, so that the modified  $r$ -limited Voronoi cell, as already evaluated, is marginally altered. Hence, a communication radius bound is computed to compensate for that (worst) case. The radio-range adjustment algorithm terminates when the current radius is greater or equal to that bound. It should be noted that the latter differs from one step of the algorithm to another.

### 3. COVERAGE BY HETEROGENEOUS NETWORKS

**Proposition 3.3.** *At the  $k$ -th step of the radio-adjustment-range scheme, the minimum required range of node  $i$ , in order to compensate for the worst case scenario (considering positioning and sensing range) for any unidentified node is*

$$R_i^{\text{wcs}(k)} = \left( 1 + \frac{\max \mathbf{r}_{\text{rem}}^{(k)}}{r_i} \right) \sup \left\{ \|x_i - x\|, x \in \partial \tilde{V}_i^{r(k)} \right\}.$$

*Proof.* Following the same concept as in the previous case-scenario considered, let us assume that the neighbor unidentified node  $m$  has sensing radius equal to  $r_m = \max \mathbf{r}_{\text{rem}}$ . The worst case scenario for the position of node  $m$  is to lay in such spatial coordinates where the halfplane that separates the halfspaces  $\tilde{H}_{im}, \tilde{H}_{mi}$  marginally crosses the farthest point of  $\partial \tilde{V}_i^r$ , as presented graphically in Fig. 3.10. Considering Fig. 3.2, this is the case where the distance of node  $i$

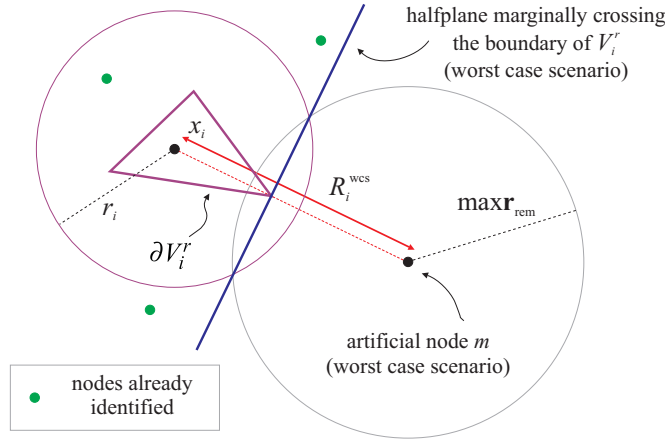


**Figure 3.10:** Graphical representation of the worst case scenario determination during the radio-range adjustment scheme.

from the aforementioned halfplane is

$$d_i = \sup \left\{ \|x - x_i\|, x \in \partial \tilde{V}_i^r \right\}.$$

Combining the aforementioned expression with the one provided in the proposed space partitioning definition [37], i.e.

$$d_i = \frac{r_i}{r_i + r_m} \|x_i - x_m\|,$$

and solving for  $\|x_i - x_m\|$ , results in

$$\|x_i - x_m\| = \left( 1 + \frac{r_m}{r_i} \right) \sup \left\{ \|x - x_i\|, x \in \partial \tilde{V}_i^r \right\}.$$

Considering the worst case scenario, i.e.  $r_m = \max \mathbf{r}_{\text{rem}}$ , along with setting  $R_i^{\text{wcs}}$  equal to  $\|x_i - x_m\|$  leads to the result.  $\square$

**Remark 3.4.** *The value for  $R_i$  resulting from Proposition 3.3 forms a tighter bound than the one presented in Proposition 3.2.*

*Proof.* The proof is straightforward by taking into account that  $\sup \left\{ \|x_i - x\|, x \in \partial \tilde{V}_i^{r(k)} \right\} \leq r_i$  (since  $\tilde{V}_i^r \subseteq C_i$ ) and  $\max \mathbf{r}_{\text{rem}}^{(k)} \leq \bar{r}$ . □

The radio–range adjustment scheme proposed, based on Proposition 3.3, is summarized in Algorithm 3.1.

---

**Algorithm 3.1** Distributed Radio–Range Adjustment Scheme for Heterogeneous Networks

---

```

1:  $\mathbf{r}_{\text{rem}} \leftarrow \mathbf{r} \setminus \{r_i\}$ 
2:  $R_i^{\text{wcs}} \leftarrow r_i + \max \mathbf{r}_{\text{rem}}$ 
3: while  $R_i < R_i^{\text{wcs}}$  &  $\mathbf{r}_{\text{rem}} \neq \emptyset$  do
4:   increase  $R_i$ 
5:   identify nodes in range
6:   if node  $m$  detected then
7:     update  $\tilde{V}_i^r$ 
8:     update  $\mathbf{r}_{\text{rem}}$ 
9:     update  $R_i^{\text{wcs}}$ 
10:  end if
11: end while

```

---

It should be noted that, although Proposition 3.2 provides a more conservative bound than Proposition 3.3, radio–range adjustment is not required in the first case, which might be desirable, depending on the application.

#### 3.4.4 Simulation Studies

Simulation studies are presented in this section in order to show the efficacy of the proposed scheme. The region  $\Omega$  to be surveyed is a convex set in  $\mathbb{R}^2$ , identical to that used in [15, 21]. The weighting function  $\phi$  was selected constant and equal to unity for visualization purposes, in both cases. In the first simulation study, the number of nodes is set to  $n = 10$ , while their kinematics are described by (3.14). The network heterogeneity is captured into their sensing radii, which were selected to vary between 0.18 and 0.5 units, resulting in a ratio between maximum and minimum sensing radius of the network around 2.5, while the standard deviation (std) of the set  $\{r_i, i \in I_n\}$  is evaluated as  $\sigma = 0.1$  units.

### 3. COVERAGE BY HETEROGENEOUS NETWORKS

Two series of simulations are performed for each study; at first, the control action is based on standard Voronoi tessellation via the control law (3.17), while in the sequel, the modified space partitioning scheme is utilized, while the control law is provided in this case by (3.18). The nodes are initially deployed randomly in  $\Omega$ , while the same initial configuration is used for both control laws considered. Considering the radii of the nodes, the maximum theoretically (if possible) achievable sensing area corresponds to  $\sum_{i \in I_n} \pi r_i^2 = 4.01 \text{ units}^2$ , while the area of the region of interest is given as  $\int_{\Omega} dx = 5.081 \text{ units}^2$ . In the case that the nodes can self-position themselves in a configuration where there is no overlapping among their sensing patterns or with the boundary of  $\Omega$ , they can cover  $\frac{\sum_{i \in I_n} \pi r_i^2}{\int_{\Omega} dx} = 78.9\%$  of  $\Omega$  (best case scenario).

Considering the standard Voronoi partitioning case, the nodes' initial configuration, their evolution through time, along with the final network's state, when the control scheme presented in (3.17) is applied, are shown in the top row of Fig. 3.11 (i.e. Figs. 3.11(a)–3.11(c)), in this order. As far as concerns the final nodes' state, it is apparent that the way they have self-

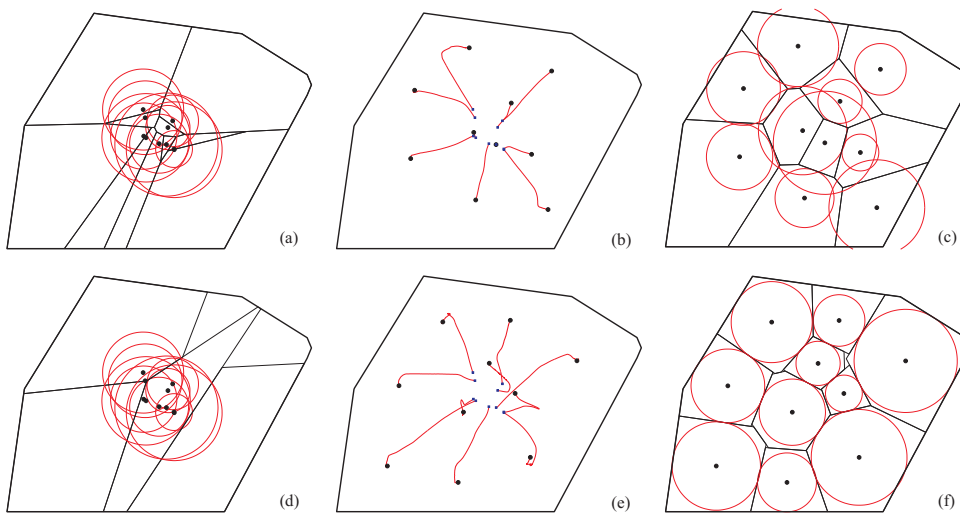


**Figure 3.11:** Case Study I — Coordination results derived via standard [top row] and modified [bottom row] Voronoi partitioning, respectively. [Left column] Initial network configuration. [Middle column] Network evolution through time. The black circles (blue squares) represent the nodes' final (initial) positions. [Right column] Final network state.

positioned themselves is not optimal at all, considering coverage criterion. The way in which the area of the covered region increases during network evolution is shown with the blue line in the left part of Fig. 3.12. The black dotted line represents the maximum possible coverage ratio, i.e. 78.9%. More specifically, the sensed area percentage, starting from an initial value

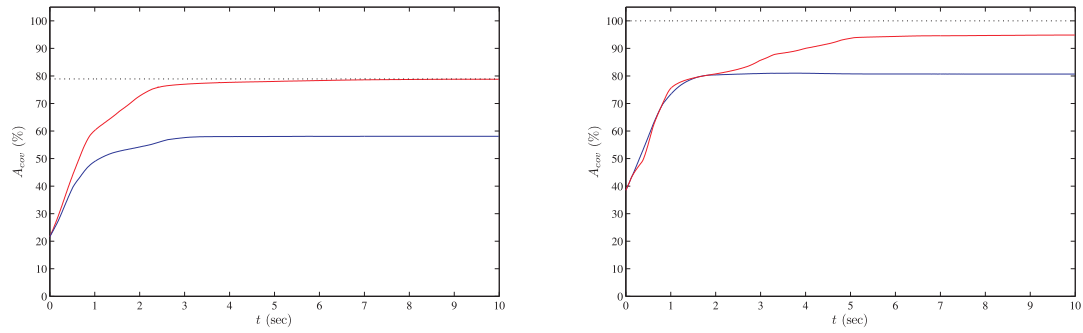


**Figure 3.12:** Percentage of covered area w.r.t. time for standard [blue line] and modified [red line] Voronoi partitioning utilization in the control law. Left (Right) part stands for Case Study I (II).

of 21.64% (dependent on the initial network configuration), increases as time passes, until it converges to 58.08% at around 4 secs.

In the sequel, the coordination algorithm proposed in this chapter—provided in (3.18)—is applied, which bases its action on the modified space partitioning presented in Section 3.3. In a similar manner, as in the previous case, the nodes’ initial configuration, their evolution through time, along with their final topological state are shown in Figs. 3.11(d)–3.11(f), respectively. Contrary to the previous case, the mobile network achieves coverage ratio equal to 78.81% in less than 10 secs, as indicated by the red line in the right part of Fig. 3.12. It should be noted that the total sensed area converges to the extremum in a monotonic manner, as proven in Section 3.4.2.

During the second simulation study, a network consisted of  $n = 7$  nodes is examined; however, in this case, there exists overlapping among the nodes’ sensing patterns in the converged state. Apart from that, the network’s heterogeneity is emphasized even more via higher std in the nodes’ radii ( $\sigma \approx 0.2$  units), while the maximum radius present in the network is about 3.5 times larger than the smallest one.

Similarly to the previous case–study examined above, the nodes’ initial configuration, their evolution through time, along with their final configuration are shown in Figs. 3.13(a)–3.13(c) for standard–Voronoi–based coordination, and Figs. 3.13(d)–3.13(f) when the modified partitioning scheme is utilized, respectively. One can observe that, although the maximum (ideally) coverage ratio is 100% in that case, none of the algorithms achieve it, while overlapping is present in the final (converged) network’s state. However, as shown in the right part of Fig. 3.12, the region of interest is covered/sensed by approximately 95% via the proposed scheme,

### 3. COVERAGE BY HETEROGENEOUS NETWORKS

---

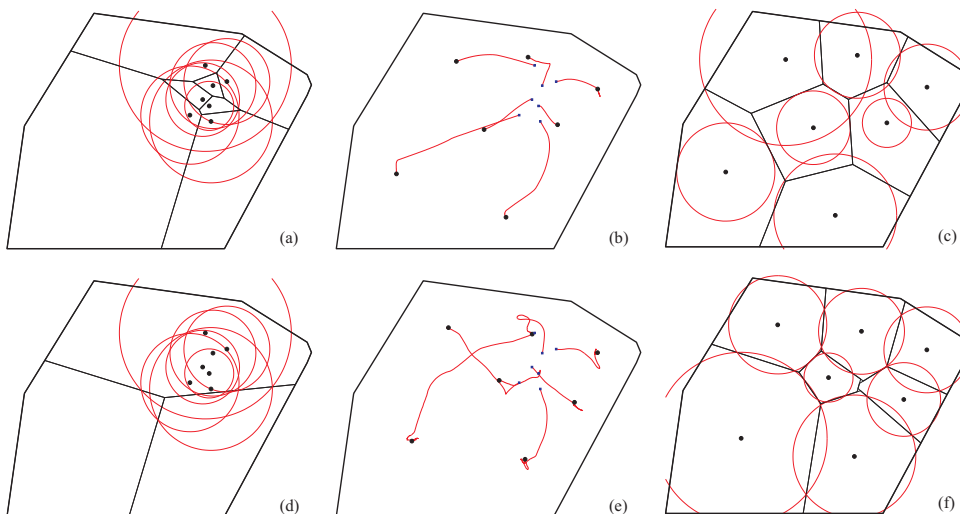


**Figure 3.13:** Case Study II — Coordination results derived via standard [top row] and modified [bottom row] Voronoi partitioning, respectively. [Left column] Initial network configuration. [Middle column] Network evolution through time. The black circles (blue squares) represent the nodes' final (initial) positions. [Right column] Final network state.

which is more than satisfactory, compared to the one provided via standard Voronoi partitioning, 80.5%.

It should be noted that, in both scenarios presented, convergence to the global optimum of  $\mathcal{H}$  is not the case; in fact, the only way to guarantee existence of a configuration for global coverage optimization of  $\Omega$  is via global optimization techniques, something that is beyond the scope of this thesis.

## 3.5 Conclusions

In this chapter a control scheme for motion coordination of the nodes in a heterogeneous sensor network has been proposed. The mobile agents are supposed to have circular sensing patterns whose radii differ, while the control approach is based on a space partitioning algorithm suitable for heterogeneous networks. The proposed technique leads in an area-coverage optimum configuration in a distributed manner. Results indicate the efficacy of the suggested control scheme when the modified Voronoi definition is utilized, compared to standard Voronoi-based ones.

# 4

## Area Coverage by Anisotropic Networks

### 4.1 Introduction

Assuming networks with homogeneous capabilities among their mobile nodes, distributed coordination algorithms have been developed in order to lead the nodes towards a desired topological configuration [38]. Cooperative action of agents via nearest neighbor rules for flocking purposes have been proposed in [39, 40], while several approaches base their action in geometric characteristics of the Voronoi–tessellation–based assigned spaces among the nodes [16, 21, 22].

The distributed nature of the previous approaches is either guaranteed via proper adjustment of the RF power of the nodes’ antennas [12], or via incorporation of extra constraints in the control design procedure [41, 42, 43]. Coordination of heterogeneous groups of agents considering their sensing abilities has been performed via utilization of alternate schemes for partitioning of the configuration space [26, 31, 37, 44, 45]. In these works the nodes’ sensing patterns were assumed circular of fixed radii, though the latter were allowed to be unequal among the members of the swarm.

Most of the works in the literature consider networks where the nodes’ sensing footprints are node–centered circular ones [16, 21]; however, in most applications this is rather unusual. This chapter examines the case where a node’s sensing region is approximated as any arbitrary convex set, while the node is not demanded to be centered at the pattern’s centroid (equivalently to the circle–scenarios). This provides a major advantage in the overall network’s coverage

## 4. AREA COVERAGE BY ANISOTROPIC NETWORKS

---

performance, although increasing the control law complexity. The nodes' pattern is assumed to be identical for all nodes of the network, both in orientation and scaling terms.

It should be stated that coordination schemes have been developed in the case where the nodes have wedge-shaped sensing patterns [19, 30], while allowing rotation of the pattern during the nodes' motion. In this work, we develop a control law that relies on certain Helly-type theorems concerning homothets of planar convex curves [46, 47], allowing no rotation. However, the nodes' sensing domains are not restricted to wedge-shaped ones, but are considered as *any* strictly convex compact planar set, instead.

In section 4.2 the main assumptions concerning the network are defined, while the area-coverage objective by a set of mobile agents is introduced, in the case where the footprints are governed by a high degree of anisotropy. Considering non-radial sensor patterns, the tessellation of the space into subsets assigned at the nodes is defined in the sequel, based on properties for homothets of planar convex curves. The proposed coordination algorithm is developed in Section 4.3.2, the distributed nature of which is analyzed, assuming omnidirectional antennas. Illustrative examples are provided that emphasize in the advantages of the proposed law over approximating the sensing domain of the nodes as node-centered circular ones.

The coverage problem is revisited in section 4.4 in order to allow for rotating footprints of the nodes. The proposed innovative generalized partitioning is utilized in the control framework design in order to properly regulate both the nodes' translation and rotation during their convergence towards optimum topology. Its supremacy over existing techniques is further indicated by simulations, amending for almost any arbitrary sensing pattern.

### 4.2 Preliminaries — Motivation

#### 4.2.1 Main Assumptions and Definitions

Consider  $n$  available mobile nodes responsible for the sensing coverage of a convex compact region  $\Omega \subset \mathbb{R}^2$ . Let the density function  $\phi : \Omega \subset \mathbb{R}^2 \rightarrow \mathbb{R}_+$  describe the importance of any point  $x \in \Omega$ , considering sensing coverage purposes (e.g. representing the probability of an event to take place at  $x$ ). Let the set  $I_a$  contain all natural numbers up to  $a$ , i.e.  $I_a = \{k \in \mathbb{N} \mid k \leq a\}$ . The nodes positions are denoted by  $x_i$ ,  $i \in I_n$ .

Each node's motion is assumed to be governed by simplified kinodynamics as

$$\dot{x}_i = u_i, \quad x_i \in \Omega, \quad u_i \in \mathbb{R}^2, \quad i \in I_n. \quad (4.1)$$



Each mobile agent is equipped with an on-board sensor, where its sensing domain,  $C(x_i)$ , is assumed to be identical for all nodes. The role of the argument in the aforementioned notation is to characterize the point at which the predefined pattern  $C$  is translated at. In this chapter, the sensing pattern is not necessarily demanded to be circular and/or node-centered. Thus, the sensed domain of the network, denoted as  $\mathbf{C}$ , can be expressed as  $\mathbf{C} := \Omega \cap \bigcup_{i \in I_n} C(x_i)$ .

Considering sensing coverage (i.e. fire surveillance [10], intruder [11], or survivor detection [48]) of the planar domain  $\Omega$ , the nodes should move in such spatial coordinates, so that an area-based criterion is optimized. Let the nodes' coverage performance indicator be  $\mathbf{1}_{C(x_i)}(x) = 1$  (0) if  $x \in (\notin) C(x_i)$ ,  $i \in I_n$ , for the sensing domain  $C(x_i)$ . The selected performance criterion under optimization is the total area sensed by the robotic network (i.e. area of the union of the nodes' footprints), corresponding to

$$\mathcal{H} = \int_{\Omega} \max_{i \in I_n} \mathbf{1}_{C(x_i)}(x) \phi(x) dx = \int_{\mathbf{C}} \phi(x) dx. \quad (4.2)$$

The main objective from here on is the design of a spatially distributed coordination algorithm that leads the robotic swarm in obtaining an  $\phi$ -weighted area-optimal topology.

### 4.2.2 On Non-Uniform Sensing Patterns

In this chapter, the sensing region of the node is assumed any arbitrary convex compact set. In some cases, though, the sensors' footprints are by nature concave (non-convex) sets (i.e. directional microphones [2]).

In other cases, where RF nodes [1] play the role of the sensing devices (i.e. communication coverage scenarios), the issues become more complicated, since the footprints are time-varying (battery life-time dependent), or even environment-dependent in the presence of obstacles, while their identification is unreliable. In this chapter it is assumed that omnidirectional antennas are embedded on the mobile nodes, responsible for inter-agent information exchange, while anisotropy is supposed to be encapsulated in the nodes' sensing footprints.

The standard approach for utilization of previously developed distributed coordination schemes [12, 16, 21] is to define the largest node-centered disk inscribed in the pattern, and use this set as the node's sensing domain  $C(x_i)$  in the sequel (see Fig. 4.1). In this chapter, though, the demand for node-symmetric regions is relaxed, and larger (area-wise) subsets as the nodes' sensing domains can be used, as shown in Fig. 4.1, resulting in a more efficient network's optimal state. Algorithms for extracting the maximal-area convex subset inscribed

## 4. AREA COVERAGE BY ANISOTROPIC NETWORKS

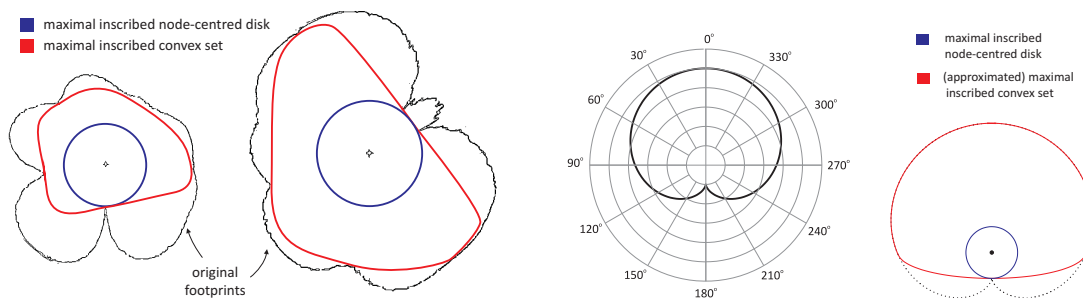


**Figure 4.1:** Graphical example to indicate the benefits arisen by allowing non-node-centered sensing domains in coverage applications. [Left] The node’s patterns are the antenna’s radiation pattern in T-mote Sky platforms as provided in [1]. [Right] The node’s pattern is a typical cardioid footprint of directional microphones as provided in [2].

in planar sets (*aka* potato-peeling problem) have been proposed in [49, 50, 51], while their analysis does not lie within the scopes of this thesis.

It should be noted, that approximating the nodes’ pattern with a convex inscribed set does not imply that the original footprint is assumed convex, too. The main motivation arises from the fact that approximating the first (non-convex, in the general case) as a larger set than a node-centered disc one encapsulates the network’s sensing performance more efficiently. The demand for convexity though arises from utilization of certain Helly-type properties for planar curves [47] in the coordination algorithm development stage; however, even this does not reduce its supremacy over the node-centered inscribed disc approximation.

### 4.3 Optimum Coverage in Anisotropic Networks

#### 4.3.1 Space Partitioning

Voronoi diagrams [14], weighted-Voronoi diagrams and power diagrams [26] are efficient tools for space partitioning, utilized in most control schemes concerning cooperative robotics. For homogeneous networks, the main philosophy is that the space under consideration is partitioned into  $n$  convex Voronoi cells,  $\{V_i, i \in I_n\}$ , as already defined in (2.6), assigned to the mobile agents responsible for coverage of  $\Omega$ . For networks where the nodes have circular sensing footprints, coordination for area-coverage purposes is based on the parts of the Voronoi cells that are sensed by the nodes [21, 45], also known as  $r$ -limited Voronoi cells, where  $r$  is the common radius of the sensing disks.

It is apparent that, since the sensing regions of the nodes are arbitrary in our case, an alternative way for space partitioning is sought. This need arises from the fact that distance-based tessellations are formed strictly on the nodes coordinates, while the coverage performance indices  $\mathbf{1}_{C(x_i)}$  in (4.2) are not node-symmetric in our case. Before proceeding to the design of the partitioning scheme, the following preliminaries on Helly-type properties for planar strictly convex curves are needed.

**Definition 4.1.** [46] *A planar convex curve  $\mathcal{C}$  is defined as the boundary of a proper convex subset  $D \subset \mathbb{R}^2$ , i.e.  $\mathcal{C} := \partial D$ . A strictly convex curve is a convex curve containing no line segment.*

**Definition 4.2.** *Given a set  $D \subset \mathbb{R}^2$ , any set of the form  $\lambda D + \mathbf{v}$ ,  $\lambda > 0$ ,  $\mathbf{v} \in \mathbb{R}^2$  is a homothet of  $D$ . Specifically, for  $\lambda = 1$ , the above family defines the translates of  $D$ . Equivalently are defined the homothets/translates of a curve  $\mathcal{C}$ .*

**Lemma 4.1.** [46, 47] *Any two distinct homothets of a planar strictly convex curve  $\mathcal{C}$  have at most two intersection points.*

Unlike the majority of previous works, that perform space partitioning based on the nodes' spatial coordinates, in this chapter, due to the anisotropy of the sensing patterns, the partitioning is based on the footprints of the nodes, rather than their positions, resulting in a pattern-based approach of the partitioning problem.

**Remark 4.1.** *In the case where the boundaries of the nodes' sensing domains are polygons instead of strictly convex curves, Bezier-curves [52] under-approximation can be used in order to provide the necessary conditions for utilization of Lemma 4.1, with a trade-off of a slight area reduction in the approximated sensing domain.*

Let  $\mathcal{W} = \emptyset \cup \{W_i, i \in I_n\}$  be a tessellation of the sensed space  $\mathbf{C}$ , where the sets  $W_i$  are parts of  $\mathbf{C}$  assigned to node  $i$ , while  $\emptyset$  are possibly existing regions in  $\mathbf{C}$  which are not assigned to any node. Similarly to the concept of chapter 3, each cell  $W_i$  is defined as

$$W_i = \bigcap_{j \in I_n} W_{ij}, \quad (4.3)$$

where the sets  $W_{ij}$  are convex compact subsets of  $\mathbf{C}$  introduced in Definition 4.3.

**Definition 4.3.** *Given two arbitrary nodes  $i, j$ , let  $\partial C(x_i), \partial C(x_j)$  be the boundary strictly convex curves enclosing their sensing domains. By denoting as  $|\cdot|$  the cardinality of the set-argument, the sets  $W_{ij}$  are defined as follows:*

#### 4. AREA COVERAGE BY ANISOTROPIC NETWORKS

- If  $|\partial C(x_i) \cap \partial C(x_j)| \leq 1$ , then  $W_{ij} := C(x_i) \cap \Omega$ .
- Otherwise, i.e.  $|\partial C(x_i) \cap \partial C(x_j)| = 2$  (Lemma 4.1), let  $x_{ij}^{(1)}, x_{ij}^{(2)}$  be the intersection points of the curves. The latter define a separating line, that tessellates  $C(x_i) \cup C(x_j)$  into two disjoint compact subsets,  $C_{ij}^{(1)}, C_{ij}^{(2)}$ , respectively. Then

$$W_{ij} := C_{ij}^{(\ell)} \cap \Omega, \text{ where } \ell \in \{1, 2\} : C_{ij}^{(\ell)} \subseteq C(x_i). \quad (4.4)$$

Apparently, the domain  $W_{ji}$  is then defined univocally as  $W_{ji} := \Omega \cap \{C(x_i) \cup C(x_j)\} \setminus W_{ij}$ .

Figure 4.2 depicts graphically the way that the sensed space of a network consisted of six nodes is partitioned. At first, one can verify that if an arbitrary node  $i$  (take for example

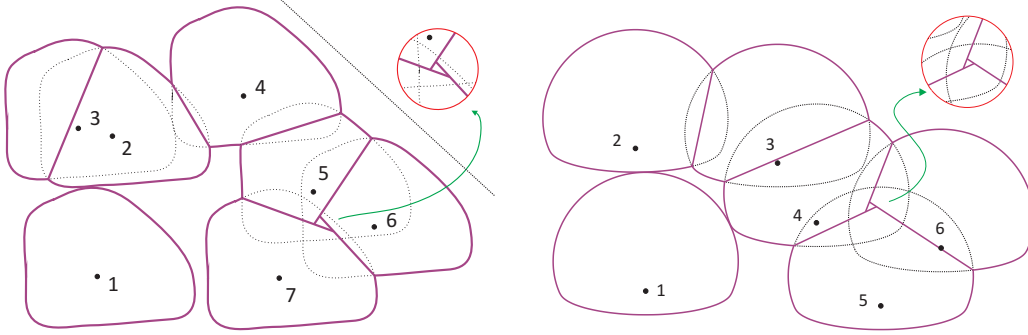


**Figure 4.2:** Illustrative examples of the partitioning of the sensed domain of a network via Definition 4.3 for RF (left) and acoustic (right) devices, based on their approximation as of Figure 4.1.

node 1 in both scenarios) is compared with any other node  $j$  for which  $|\partial C(x_i) \cap \partial C(x_j)| \leq 1$  holds, then this comparison does not affect  $W_i$ , considering (4.3) and Definition 4.3. In order to provide the reader with an insight on what equation (4.4) represents, pairs 2–3 (right) or 2–4 (left) for example can be examined, where the nodes' sensing domain is split correspondingly, via the line that connects the two points where their boundaries intersect.

Furthermore, by observing the region among the nodes 4–5–6 (right), one can verify that  $\{W_i, i \in I_n\}$  is not a tessellation of the sensed space  $\mathbf{C}$ , since there exists a part of the plane that is sensed by the nodes, although it is not assigned to any of them. Let us call the set of these regions as *sole cells*, denoted as  $\mathcal{O}$ , previously. Apparently, since  $\mathcal{O} = \mathbf{C} \setminus \{W_i, i \in I_n\}$ , then  $\mathcal{W} = \mathcal{O} \cup \{W_i, i \in I_n\}$  consists a tessellation of  $\mathbf{C}$ .

### 4.3.2 Spatially Distributed Coordination Algorithm

The core objective of this section is the design of a distributed coordination law that leads the network in a covered–area–optimum spatial topology. More specifically, the nodes’ control actions  $u_i$  are determined so that the nodes’ trajectories represent a gradient ascending flow of the criterion under optimization,  $\mathcal{H}$ , while only local information is required, i.e. spatial information from a subset of neighboring nodes.

It should be stated that distributed gradient ascent laws in swarm robotics guarantee convergence to a locally optimum state, rather than the global optimum one. In fact, global optimization techniques require supervisory knowledge of the network’s state by all the members–nodes, which cast them impractical to be implemented in real–time applications. Hybrid or heuristic laws can be applied after convergence in order to try reach a “better” state in area–wise terms [53], though such scenarios are not examined in this chapter. At this stage, let us state the main result of the section in the following Theorem.

**Theorem 4.1.** *Considering a mobile sensor network consisted of nodes with arbitrarily strictly convex sensing patterns, governed by the kinodynamics described in (4.1), the coordination scheme*

$$u_i = \alpha_i \int_{\partial W_i \cap \partial C(x_i)} n_i \phi \, dx, \quad \alpha_i > 0, \quad i \in I_n, \quad (4.5)$$

where  $n_i$  is the outward unit normal on  $\partial W_i$ , maximizes the performance criterion (4.2) along the nodes’ trajectories in a monotonic manner, leading in a locally area–optimal configuration of the network.

*Proof.* Considering (4.2) and taking into account that the sets  $W_i$ ,  $i \in I_n$  are mutually disjoint, the partial derivative of  $\mathcal{H}$  with respect to  $x_i$  is written as

$$\frac{\partial \mathcal{H}}{\partial x_i} = \frac{\partial}{\partial x_i} \int_{\mathcal{O}} \phi + \frac{\partial}{\partial x_i} \int_{W_i} \phi + \sum_{j \neq i} \frac{\partial}{\partial x_i} \int_{W_j} \phi,$$

where integration variables were omitted for notation simplicity. At this point, the former expression can be written via the generalized Leibniz integral rule [34] (by converting surface integrals to line ones) as

$$\frac{\partial \mathcal{H}}{\partial x_i} = \int_{\partial W_i \cap \partial \mathcal{O}} v_0^i n_0 \phi + \int_{\partial W_i} v_i^i n_i \phi + \sum_{j \neq i} \int_{\partial W_i \cap \partial W_j} v_j^i n_j \phi,$$

where  $v_i^i, v_j^i$  stand for the Jacobian matrices with respect to  $x_i$  of the points  $x \in \partial W_i$ ,  $x \in \partial W_j$ , respectively. In a similar manner,  $v_0^i$  is defined as  $v_0^i(x) := \frac{\partial x}{\partial x_i}$ ,  $x \in \partial \mathcal{O}$ ,  $i \in I_n$ , while  $n_0$  stands for the outward unit normal at  $\partial \mathcal{O}$ .

## 4. AREA COVERAGE BY ANISOTROPIC NETWORKS

---

Since parts of  $\partial W_i$  may possibly lie either on  $\partial\Omega$ ,  $\partial C(x_i)$ ,  $\partial\mathcal{O}$  (possible neighboring sole cells), or on the boundary of neighboring sensed assigned cells, the expression  $\frac{\partial\mathcal{H}}{\partial x_i}$  can be written as

$$\begin{aligned} \frac{\partial\mathcal{H}}{\partial x_i} = & \int_{\partial W_i \cap \partial\mathcal{O}} v_0^i n_0 \phi + \int_{\partial W_i \cap \partial\Omega} v_i^i n_i \phi + \int_{\partial W_i \cap \partial C(x_i)} v_i^i n_i \phi + \\ & \int_{\partial W_i \cap \partial\mathcal{O}} v_i^i n_i \phi + \sum_{j \neq i} \int_{\partial W_i \cap \partial W_j} v_i^i n_i \phi + \sum_{j \neq i} \int_{\partial W_i \cap \partial W_j} v_j^i n_j \phi. \end{aligned}$$

Equivalently to [21], the term concerning the static boundary  $\Omega$ , along with the integrals on the common part of the lines separating  $W_i, \mathcal{O}$  and  $W_i, W_j$ , respectively, are nullified, resulting in

$$\frac{\partial\mathcal{H}}{\partial x_i} = \int_{\partial W_i \cap \partial C(x_i)} n_i \phi.$$

Hence, the proposed control law (4.5) leads to a gradient flow of  $\mathcal{H}$  along the nodes trajectories, while  $\mathcal{H}$  increases monotonically, since

$$\frac{d\mathcal{H}}{dt} = \sum_{i \in \mathcal{I}_n} \frac{\partial\mathcal{H}}{\partial x_i} \cdot \dot{x}_i = \sum_{i \in \mathcal{I}_n} \alpha_i \left\| \int_{\partial W_i \cap \partial C(x_i)} n_i \phi \right\|^2 \geq 0.$$

□

### 4.3.3 Distributedness Issues

The main concept in the coordination scheme is that the network should organize its action in a distributed manner; thus, an arbitrary node  $i$  should be able to identify the nodes in its neighbourhood and evaluate the part of the sensed region that is assigned to it, i.e.  $W_i$ , without requiring to acquire knowledge of the state/configuration of the whole network.

Power control techniques have been proposed in the existing literature for adaptively adjusting the communication radius of a node, for the purpose of identifying its neighbours or establishing valid routing paths [16, 35, 54]. However, these techniques assume networks whose sensing patterns are node-centered circular ones. The scope of the ensuing analysis is to determine a worst case scenario topology, such that information from any other node is redundant for evaluation of the proposed control law.

Let the radiation pattern of the RF devices correspond to a disc (i.e. omnidirectional antennas). Assuming no adaptation of the latter's radius, a worst case scenario approach is followed in order to determine a critical value for the nodes' radii, so that any other unidentified node (i.e. does not lie in-range) is redundant for evaluating  $u_i$  via (4.5). In fact, even in the case where the pattern is allowed to alter through time (online communication radius adaptation),

the power control scheme presented by the authors in [16] can be utilized, via modification of that critical radius. The aforementioned bound is defined via the following Lemma.

**Lemma 4.2.** (*Conservative bound*) *The subset of nodes required for distributed evaluation of  $W_i$  are the ones in range of*

$$\sup\{\|x_i - x_j\| \mid |\partial C(x_i) \cap \partial C(x_j)| = 1\}.$$

*Proof.* Examining the proposed control law (4.5), one can verify that if a node can distributively evaluate  $W_i$ , then the former is spatially distributed, too. However, according to Definition 4.3, it is apparent that only the nodes for which  $|\partial C(x_i) \cap \partial C(x_j)| \in \{1, 2\}$  holds, alter the set  $W_i$ . Note that the case where the boundaries intersect at exactly one point is included as the marginal case. Considering the worst case scenario (in terms of distance among two nodes), an arbitrary node  $i$  should ensure that it is able to acquire information from the nodes that may lie in such coordinates so that  $|\partial C(x_i) \cap \partial C(x_j)| = 1$ .  $\square$

A graphical interpretation of the computation of that conservative bound is provided in Fig. 4.3. The red line denotes the geometric locus of the center of an arbitrary node so that

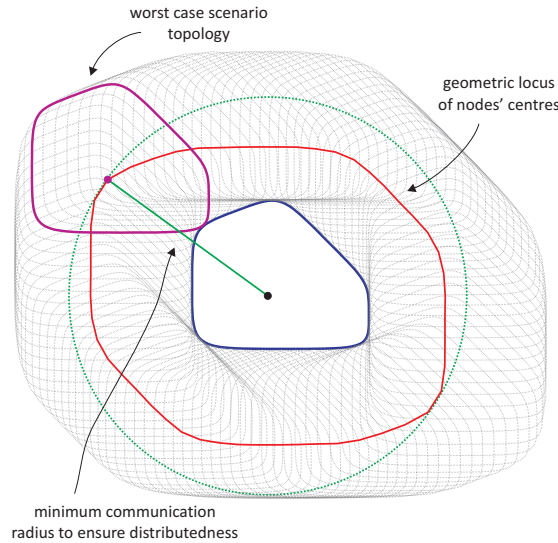


**Figure 4.3:** Graphical example of defining the topological worst case scenario among two arbitrary nodes in order to determine the communication radius bound.

the boundaries of the two nodes intersect at a singleton. Along this curve there is a point that represents the center of the worst case scenario topology [purple line] among the two

## 4. AREA COVERAGE BY ANISOTROPIC NETWORKS

---

nodes, while the communication radius bound of Lemma 4.2 that ensures distributedness of the partitioning scheme (and consequently the proposed control law) is defined as the distance among the two nodes (at this worst case scenario topology) [green line].

**Remark 4.2.** *The bound provided in Lemma 4.2 is common for all nodes, since  $i, j$  nodes are arbitrary. Furthermore, if a communication link among two nodes  $i, j$  exists, then it is bidirectional, since the radiation footprints are determined via the radius of Lemma 4.2 (worst case scenario; see Fig. 4.3).*

**Remark 4.3.** *The bound on the communication radii of the nodes can be determined a-priori and not during the coordination stage, since it is only dependent on the common nodes' sensing pattern.*

### 4.3.4 Numerical studies

The control scheme proposed in this section is verified via simulation studies. The nodes in the networks under consideration are initially deployed randomly in a convex compact planar region. The latter is selected identical to that used in [21] for consistency, while the importance function  $\phi$  is set equal to unity for visualization purposes. As far as the sensing pattern of the nodes is concerned, a non-trivial arbitrary convex one is selected. More specifically the latter is chosen as the (approximated) maximal convex set inscribed in the interior of T-mote Sky footprints [1], as depicted graphically initially in the left part of Fig. 4.1. A short discussion is following on their determination in order to provide ease of re-productivity of the results presented in the sequel.

Let  $v_j, j \in I_5$  be a set of planar points normalized so that  $\|v_j\|_\infty \leq 1$ , selected as

$$v_j: (0,0), (1,0), (1, 3/8), (1/2, 7/8), (0, 11/16).$$

Let  $m_j, j \in I_5$  stand for the middle points of the line segments connecting  $v_j, v_{j+1}$ . By convention, it holds that  $v_6 \equiv v_1$  and  $m_6 \equiv m_1$ . The boundary of the sensors' pattern selected for the simulations following is consisted of the union of five Bézier curves of 3<sup>rd</sup> order, i.e.  $\partial C_i = \bigcup_{j \in I_5} B_j$ ,

$$B_j = (1 - \tau)^3 P_{j,0} + (1 - \tau)^2 \tau P_{j,1} + (1 - \tau) \tau^2 P_{j,2} + \tau^3 P_{j,3},$$

where  $\tau \in [0, 1]$ , while the control points  $P_{j,k}, k = 0, \dots, 3$  are selected as

$$P_{j,0} = m_j, P_{j,1} = P_{j,2} = v_{j+1}, P_{j,3} = m_{j+1}, j \in I_5.$$



The above are summarized graphically in Fig. 4.4, while the arbitrary node is selected in the interior of the normalized pattern at  $(3/7, 3/10)$ , in order to keep consistency with Fig. 4.1.

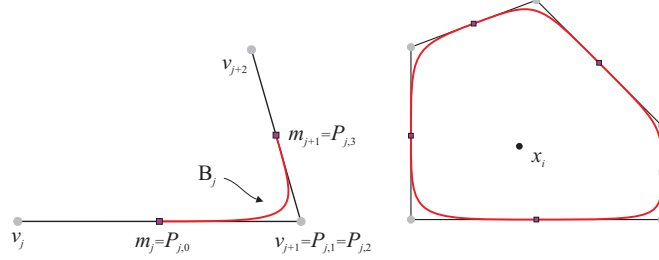


**Figure 4.4:** Sensing pattern of the nodes utilized in the simulations, defined as the union of sequential Bézier curves.

As already discussed, most control techniques in the existing literature consider networks with circular node-centered sensing footprints. However, in cases where the sensors are anisotropic, a standard approach is to approximate their patterns with the maximal node-centered disk inscribed in the sensor footprint. In this chapter, the control scheme proposed in section 4.3.2 is compared via simulations to the one proposed by the authors in [21], i.e.

$$\tilde{u}_i = \alpha_i \int_{\partial B_i^r \cap \partial V_i^r} n_i \phi, \quad \alpha_i > 0, \quad i \in I_n, \quad (4.6)$$

where the  $\sim$ -sign is used in order to distinguish between the control laws, while  $\alpha_i$  are strictly positive scalars, equivalently to (4.5). In the former expression,  $B_i^r := \{x \mid \|x - x_i\| \leq r\}$  represents a disc of radius  $r$  around  $x_i$ , while  $V_i^r := V_i \cap B_i^r$  ( $r$ -limited Voronoi cell) is the intersection of the aforementioned disc with the assigned Voronoi cell, as defined in (2.6).

It should be stated clearly that the coordination scheme (4.6) is proven to lead to area-optimal network configuration when the nodes sensing patterns are circular. The scope of the comparison that follows between the two control schemes is to show the benefits of the proposed law when dealing with anisotropic sensors. In fact, when  $C(x_i) \equiv B_i^r$ , the coordination scheme defined in (4.5) degenerates in (4.6), while the partitioning  $\mathcal{W}$  is the standard Voronoi tessellation,  $\mathcal{V}$ .

*Case Study I.* In the first scenario examined, the network is consisted of  $n = 12$  nodes, initially deployed randomly in a region on the top-right part of  $\Omega$ . Their sensing patterns were selected as described above, scaled via a factor of  $\lambda = 0.6$  around the node. Taking into account the area of  $\Omega$ ,  $\int_{\Omega} \phi = 5.0809$  units<sup>2</sup>, along with that of an arbitrary sensor footprint, i.e.  $\int_{C_i} \phi = 0.2443$  units<sup>2</sup>, the nodes can achieve coverage ratio, in a best case scenario, equal

#### 4. AREA COVERAGE BY ANISOTROPIC NETWORKS

to 57.6952%. This case is when the nodes can self-position themselves (if possible) in a way where there is no overlapping among their patterns or with the boundary  $\Omega$ .

In the case where control law (4.6) is to be applied, the sensing domains of the nodes are firstly approximated as node-centered discs of radius equal to  $r = 0.18$  units (maximal inscribed node-centered ones). In this case, the nodes' initial configuration, their evolution through time, along with the final network's state, are shown in the top row of Fig. 4.5, in this order, where the scalars  $\alpha_i$  was selected as  $\alpha_i = \alpha = 3$ ,  $i \in I_n$ .

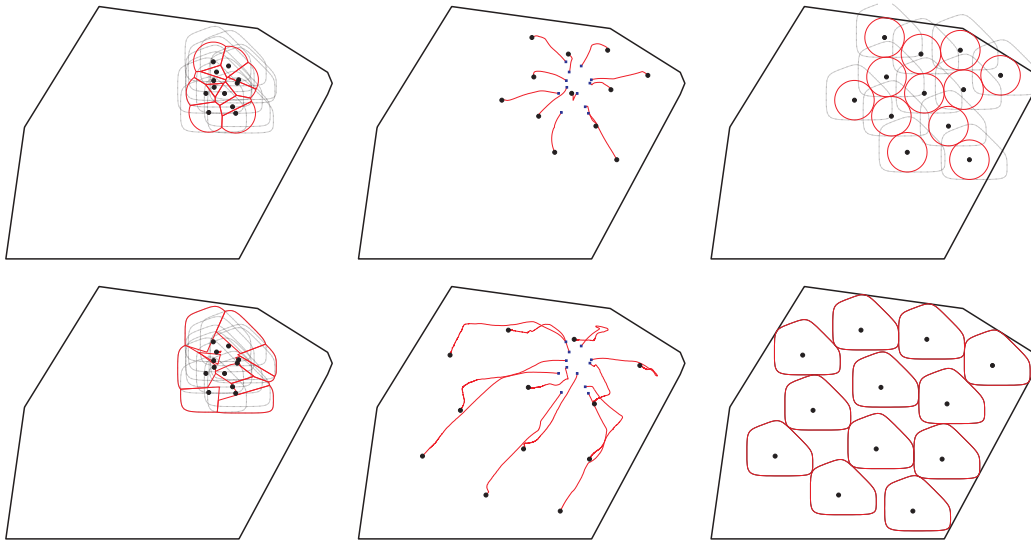


**Figure 4.5:** Case Study I — Coordination results derived via control schemes (4.6) [top row] and (4.5) [bottom row], respectively. [Left column] Initial network configuration. [Middle column] Network evolution through time. The black circles (blue squares) represent the nodes' final (initial) positions. [Right column] Final network state.

It is apparent that the nodes have positioned themselves in a way that the discs do not overlap among them or with the boundary of  $\Omega$ . However, although the coordination scheme assumes uniform omnidirectional coverage performance, one can verify that the (real) coverage performance of the network via the patterns  $C_i$  can be increased even more. Figure 4.6 [left part] depicts the evolution the network's coverage ratio, i.e.  $\mathcal{H}/\int_{\Omega}\phi$  w.r.t. time when coordination scheme (4.6) is applied [blue solid line]. It is apparent that, although the network's performance increases from 14.0857% to 36.3818% of  $\Omega$ , this percentage is not satisfactory considering the maximum possible coverage ratio 57.6952% (best case scenario). It should be noted, however, that this deficiency is due to the approximation of the sensing patterns as discs and not due to the control law.

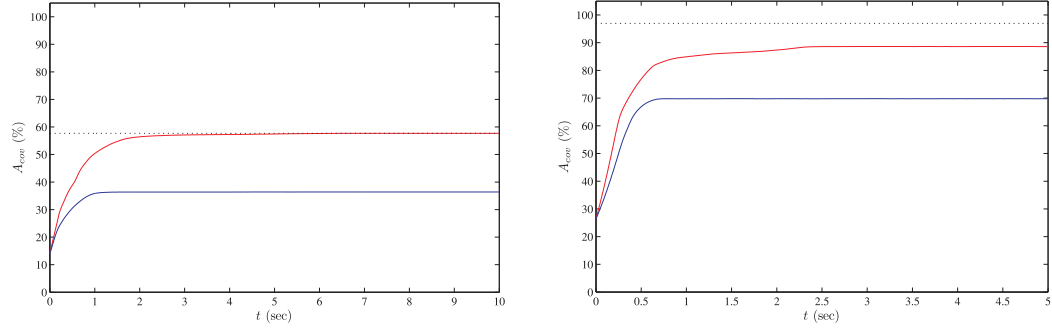


**Figure 4.6:** Percentage of sensed area w.r.t. time for Case Study I [left] and II [right], when control schemes (4.6) [blue line] and (4.5) [red line] are applied, respectively. The black dotted line represents the maximum possible coverage ratio in each case.

On the other hand, applying the control scheme (4.5)—without the need for “altering” (approximating) the nodes’ patterns—one can observe the behavior of the network in the bottom row of Fig. 4.5. Comparing the figures in the middle column (i.e. network evolution w.r.t. time via the two control laws), one can verify that the nodes tend to “spread” more uniformly in this case, since they (indirectly) try to avoid overlapping among their patterns. The red solid line in Fig. 4.6 depicts the way that the coverage ratio of the network increases to its optimal value, which in this case is equal to the maximum possible one, i.e. 57.6952%, while monotonic increase of the latter is guaranteed.

*Case Study II.* In this study, the number of nodes is selected as  $n = 6$ , while their pattern is the original one (presented at the beginning of the section) scaled by a factor of  $\lambda = 1.1$ . The latter have area equal to  $\int_{C_i} \phi = 0.8211$  units<sup>2</sup>, while the network can cover ideally (if possible)  $n \int_{C_i} \phi = 96.9600\% \int_{\Omega} \phi$ . The nodes are initially deployed around the centroid of  $\Omega$ , covering 26.4291% of  $\Omega$ . Applying the coordination scheme (4.6) with  $\alpha_i = \alpha = 2$ , the network’s evolution is depicted in the top row of Fig. 4.7, equivalently to Case Study I.

One can observe that, although the nodes have moved away from each other so that the discs (of radius  $r = 0.33$  units) do not overlap, there is still space that can be covered, taking into consideration the patterns  $C_i$ . This is also verified by examining the total covered area increase w.r.t. time, as depicted in the right part of Fig. 4.6 with the blue solid line, where the area covered at the final configuration is equal to 69.7661%.

Alternatively, when the proposed control action (4.5) is applied, as one can observe from the bottom row of Fig. 4.7 and the red solid line in the right part of Fig. 4.6, the network achieves coverage ratio equal to 88.6032% monotonically, while the nodes’ performance is

#### 4. AREA COVERAGE BY ANISOTROPIC NETWORKS

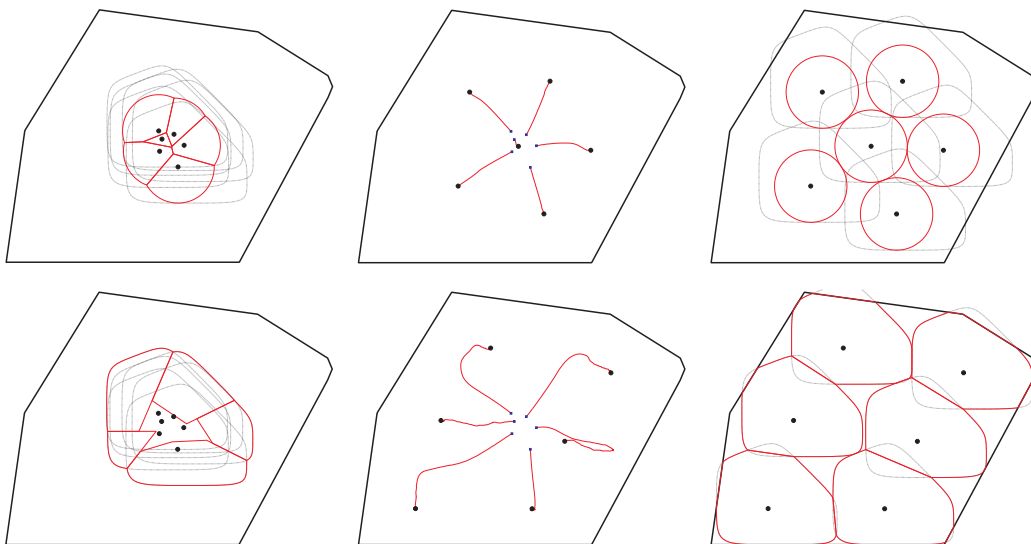


**Figure 4.7:** Case Study II — Coordination results derived via control schemes (4.6) [top row] and (4.5) [bottom row], respectively. [Left column] Initial network configuration. [Middle column] Network evolution through time. The black circles (blue squares) represent the nodes' final (initial) positions. [Right column] Final network state.

quite satisfactory.

*Case Study III.* A third simulation has been conducted with a different pattern than the one in the two first. More specifically the latter is chosen as a strictly-convex approximation (see Remark 4.1) of the maximal convex set inscribed in the interior of directional microphones cardioid footprint [2], as depicted graphically initially in the left part of Fig. 4.1.

In the scenario following, the network is consisted of  $n = 10$  nodes, initially deployed randomly in a region on the top-right part of  $\Omega$ . In a best case scenario, the nodes can achieve coverage ratio equal to 100%, as the case when the nodes can self-position themselves (if possible) in a way where there is no overlapping among their patterns or with the boundary  $\Omega$ .

In the case where control law (4.6) is to be applied, the sensing domains of the nodes are firstly approximated as node-centered discs (maximal inscribed node-centered ones). In this case, the nodes' initial configuration, their evolution through time, along with the final network's state, are shown in the top row of Fig. 4.8, in this order.

Even though there are no overlapping parts in the final configuration, it can be observed that the (real) coverage performance of the network via the patterns  $C(x_i)$  can be further increased. Figure 4.9 depicts the evolution the network's coverage ratio, i.e.  $\mathcal{J}^c / \int_{\Omega} \phi$  w.r.t. time when coordination scheme (4.6) is applied [blue solid line]. It is apparent that, although there is an

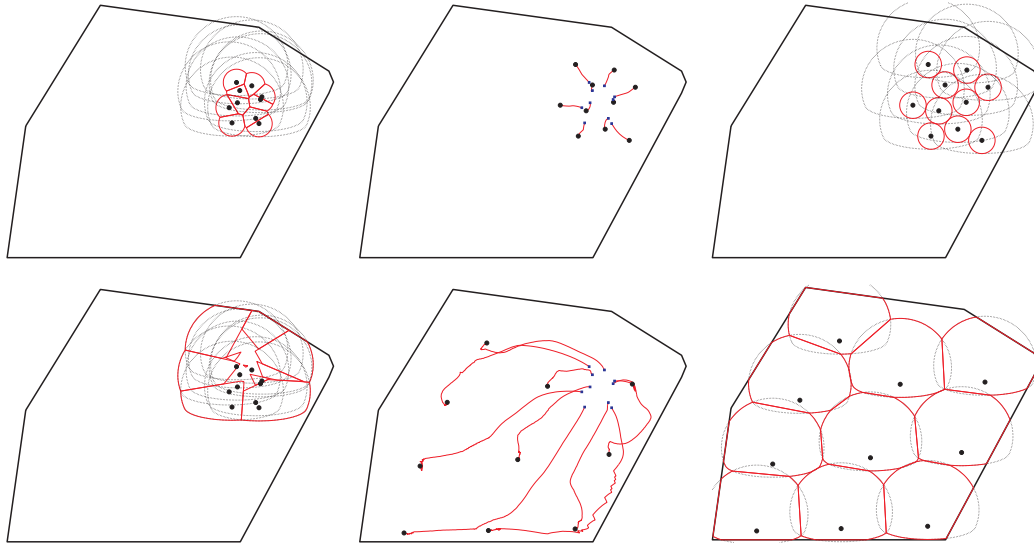


**Figure 4.8:** Case Study III — Coordination results derived via control schemes (4.6) [top row] and (4.5) [bottom row], respectively. [Left column] Initial network configuration. [Middle column] Network evolution through time. The black circles (blue squares) represent the nodes’ final (initial) positions. [Right column] Final network state.

increase in the coverage performance, it is not satisfactory considering the maximum possible coverage ratio, which is mainly due to the approximation of the original patterns.

On the other hand, applying the control scheme (4.5), the evolution of the the network is depicted in the bottom row of Fig. 4.5. The figures indicate that the nodes are placed in a more appropriate way in space, while the monotonicity property of coverage is verified also by Fig. 4.6.

## 4.4 Extensions via Allowing Rotation of the Footprints

### 4.4.1 Motivation

Standard uniform radial models are mainly assumed in the majority of the sensing applications due to its ease of manipulation when related to control design. Although these models have the major advantages of avoiding issues that arise from nodes’ rotation (due to the sensor model being rotation-invariant), they suffer from encapsulating scenarios such as visual inspection of areas (via wedge-shaped cameras [55]), intruder detection missions via utilization of directional microphones [2], or even communication-coverage applications [5], where the antennas play dual role, both “sensing” and information exchange [1]. The majority of these

#### 4. AREA COVERAGE BY ANISOTROPIC NETWORKS

---

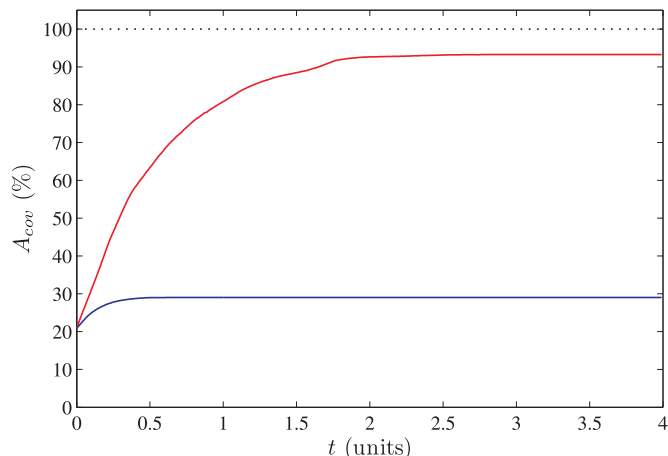


**Figure 4.9:** Percentage of sensed area w.r.t. time for Case Study III, when control schemes (4.6) [blue line] and (4.5) [red line] are applied, respectively.

applications require development of control schemes that go beyond the assumption of radial uniform sensing pattern, since they are either characterized by wedge-shaped ones or even arbitrary (non)/convex ones. The usual way to overcome this restriction is to under-approximate the sensor model via the largest node-centered inscribed circular one and apply the already existing schemes.

This was overcome in the previous section, by developing a control strategy for anisotropic sensors. However, in that case the sensors were considered to have common orientation, while no rotation of the sensing domain was taken into account. Apart from that the sensory of the nodes, although arbitrary, was assumed to be a compact convex set, derived as the maximal inscribed convex set in the original footprint (in case of non-convex domains). The reason for that demand was the utilization of specific Helly-type theorems for planar convex curves [46, 47], during the development of the space partitioning.

This section is an extension of that work, by allowing the rotation of the patterns, thus dropping the conservative demand for common orientation. Furthermore, the sensing footprint for the nodes is not required to be a convex set (since the homothetic requirement [46] is dropped), while heterogeneity in the network lies in the scaling factor of the (common) pattern among the nodes. The proposed control scheme is based on an appropriate partitioning of the sensed space, while in the sequel account for both translational and rotational motion of the nodes in order to reach an area-optimum topological state.

### 4.4.2 Problem Statement

We examine the problem for a team of nodes responsible for coverage of a domain of interest. Let each node be equipped with a sensing device appropriate for the current swarm-objective. In contrast to the majority of the works in coverage control, the sensing patterns considered in this work are not required to be node-centered circular ones (standard disc model). In regard to the extensions provided in comparison with the previous section, in this one:

- The approach of under-approximating the original pattern (non-convex in the general case) with the maximal-area inscribed node-centered disc (Fig. 4.10a) or convex set (Fig. 4.10b) is extended by taking into account the original footprints in the coordination scheme (convex or not).
- The demand for common orientation among the nodes' convex approximated footprints (Fig. 4.10b) is dropped, allowing for different ones, not only during the initial configuration, but throughout the network evolution, by adding extra control inputs for orientation control.
- Although all nodes are assumed to be equipped with the same kind of sensor (i.e. same sensing pattern), the latter is allowed to be scaled among the nodes (Fig. 4.10c), incorporating the network's heterogeneity.

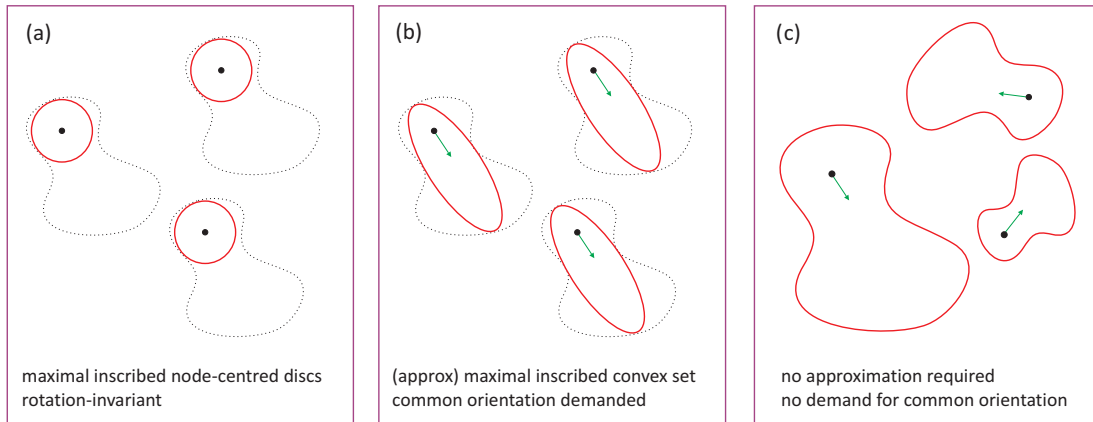


**Figure 4.10:** Graphical representation of the evolution of suggested techniques for non-uniform sensor footprints.

Let  $C^\circ$  be the common pattern of the nodes, the pinch-point (base-node) of which is assumed, without loss of generality, at the origin. The sensing pattern of the node  $i$  is determined

## 4. AREA COVERAGE BY ANISOTROPIC NETWORKS

---

by the base-pattern  $C^\circ$ , translated at the node's position, while rotated and scaled accordingly. That is

$$C_i := x_i + \mathbf{R}(\theta_i) \lambda_i C^\circ, \quad (4.7)$$

where  $x_i$  are node's- $i$  spatial coordinates,  $\theta_i$ ,  $\lambda_i$  its orientation and scaling compared to the base-pattern, while  $\mathbf{R}(\cdot)$  is the rotation matrix corresponding to the angle argument, that is

$$\mathbf{R}(\cdot) = \begin{bmatrix} \cos(\cdot) & -\sin(\cdot) \\ \sin(\cdot) & \cos(\cdot) \end{bmatrix}.$$

Although different orientations are allowed among the nodes in this work, they are assumed to be controlled via an extra control input at each nodes' kinodynamics, that is

$$\dot{x}_i = u_i, \quad x_i \in D \subset \mathbb{R}^2, \quad u_i \in \mathbb{R}^2, \quad (4.8)$$

$$\dot{\theta}_i = \omega_i, \quad \theta_i, \omega_i \in \mathbb{R}, \quad (4.9)$$

where (4.8) represents the node's translation-part and (4.9) the part concerning the pattern's rotation.

Having defined the nodes' footprints, one can formally associate the network's performance with them as of (3.15). It should be noted that although the indicator function  $f_i$  is parametrized/dependent on  $x_i$  in previous works, i.e.  $f_i(x; x_i)$ , in this work is also dependent on the non-common orientation and scaling among the nodes,  $f_i(x; x_i, \theta_i, \lambda_i)$ .

The decision for the motion is taken based on own self-localization information along with that acquired from the neighbouring nodes. In regard to the need for information exchange, it is assumed that:

**Assumption 4.1.** *Each node has sufficient transceiver RF-range so that it can exchange information at any time with any node that it shares sensed parts with.*

### 4.4.3 Proposed Pattern-based Partitioning

Having in mind the need for distributed coordination scheme towards the optimization of the overall coverage performance of the network, a region of responsibility is assigned at each node in a local manner, assisting in lowering the computational complexity in the optimization problem via proper space decomposition.



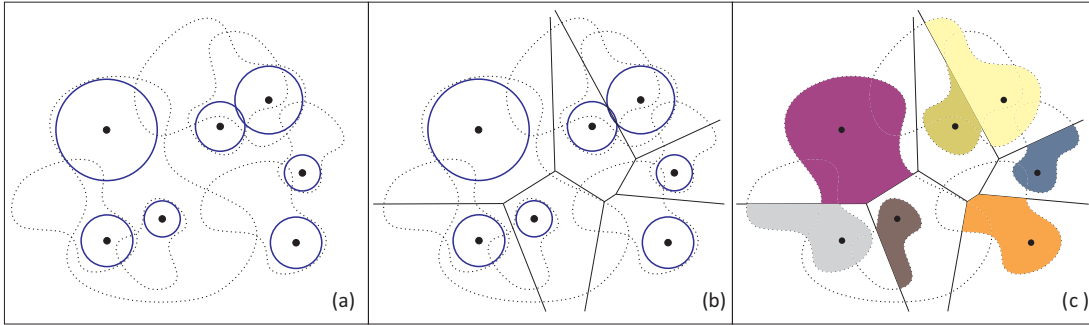


**Figure 4.11:** Graphical representation of the need for alternate partitioning in non-uniform sensor networks. (a) Anisotropic heterogeneous network approximated with disc-model. (b) Corresponding power diagram based on the approximation of node-centered maximal inscribed circles. (c) Real network's coverage via the original non-uniform patterns, as evaluated through the simultaneously sensed and assigned cells.

#### 4.4.3.1 Related Approaches

The most common approach followed in swarm coordination for defining the way that the configuration space is tessellated among the nodes is the well-known Voronoi partitioning [14]. More specifically, each node is set responsible for the parts of the area under consideration that are closer to that node compared to any other in the network. The resulting Voronoi diagram is proven to be the optimal way of tessellating the space in the Euclidean metric in a distance-based manner, based only on the nodes' coordinates, while suitably resolves the standard case of swarms with disc-patterns. Alternatively, considering heterogeneity among the members of the network via unequal disc-radii, the power diagram can be utilized for the space partitioning purpose, which can be considered as the Voronoi diagram in the Laguerrean metric [37, 56].

The main issue with the previous approach lies mainly in the disc-model approximation rather than the partitioning method itself. Although almost any sensing pattern can be approximated with its maximal inscribed node-centered disc, resulting in rotation-invariant schemes, the approximation cost is in some cases extremely conservative, comparing the real and approximated coverage performances of the network (see Fig. 4.11a).

Figure 4.11 depicts graphically a non-uniform network, along with its approximation via the disc model. Due to the heterogeneity in the unequal radii, the space is tessellated via the power diagram, as shown in Fig. 4.11b. Although the latter provides a fair way for assigning the parts of the space at the nodes, considering their radial approximated performance, it appears to be unsuitable if someone examines the original patterns via the corresponding sensed assigned

## 4. AREA COVERAGE BY ANISOTROPIC NETWORKS

---

cells (Fig. 4.11c).

An extension to this issue has been proposed in previous section, bypassing the standard uniform model. However, the demand for common orientation of the sensors' footprints, arising from utilization of particular Helly-type theorems [46], imposes a hard constraint from an application point of view. We consider the case where the nodes have non-uniform, not necessarily convex, unequally scaled sensing footprints, allowing for different pattern-orientations as well. The partitioning is performed in the network's sensed space, rather than the whole region of interest.

### 4.4.3.2 Proposed Partitioning

Let  $C_i$ ,  $i \in I_n$  be the sensing patterns of the  $n$  nodes of a network, which are assumed: a) non-uniform and non-convex (in the general case), b) same in shape, though unequally scaled, c) non-commonly oriented (in the general case). These features have been graphically summarized in Fig. 4.10c. Each footprint is characterized by a pinch-point, which is the node itself; its positioning is denoted as  $x_i$ , while  $\theta_i$  stands for the orientation of the pattern/sensing-node.

Unlike distance-based tessellation schemes that are based on the nodes' positioning alone and uniform disc sensing models, the approach presented in this section relies solely on the footprints. Let  $W_i$  be the region of responsibility of node  $i$ , restricted in the domain of interest  $\Omega$ . The former is defined via comparison of that node's footprint with the pattern of any other neighbouring node, as the part of the sensed space that is sensed by that node only, that is

$$W_i: = \Omega \cap C_i \setminus \bigcup_{j \neq i} C_j, \quad i \in I_n. \quad (4.10)$$

Apparently, the set-family  $\{W_i, i \in I_n\}$  does not consist a complete tessellation of the sensed space, since the common parts of the sensing domains are not yet characterized. Let us denote them as  $W_c$ , that is

$$W_c: = \bigcup_{i \neq j} C_i \cap C_j \cap \Omega, \quad (4.11)$$

which are not assigned at any node by definition.

**Remark 4.4.** *The set  $W_c$  in (4.11) can alternatively be defined via the sets  $W_i$  as  $W_c = \bigcup_{i \in I_n} C_i \setminus \bigcup_{i \in I_n} W_i$ . In a straightforward manner, the set  $\{W_1, W_2, \dots, W_n, W_c\}$ , consisted of mutually disjoint sets, tessellates completely the sensed space.*

**Remark 4.5.** Unlike the cells resulting from distance-based partitioning techniques [14] or certain pattern-based ones [57], the sets defined in (4.3) are, in the generic case, non-compact.

**Remark 4.6.** In the case where a node's pattern is completely included in the union of the footprints of the rest of the network, that is  $C_i \subset \bigcup_{j \neq i} C_j$ , no region of responsibility is assigned at it ( $W_i = \emptyset$ ), as derived directly from definition.

In order to provide a visual aspect of the proposed partitioning scheme, the network initially presented in Fig. 4.11 is revisited. Figure 4.12 presents visually the way that the sensed space is partitioned and assigned among the nodes via the proposed scheme. The non-coloured parts

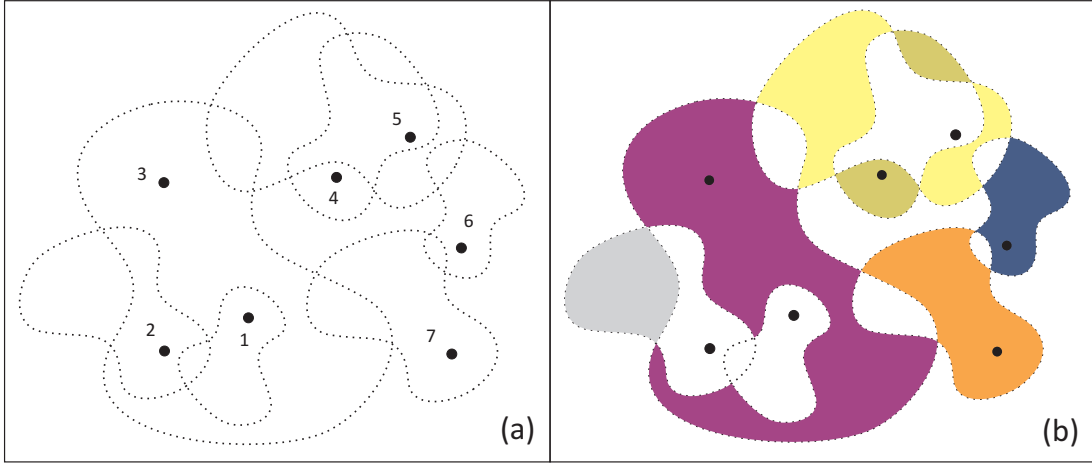


**Figure 4.12:** Illustrative example indicating the partitioning of the sensed space via the proposed technique.

of the sensed domain belong to the set  $W_c$  and correspond to the parts of the network that are sensed by more than one node at the same time. It should be noted that the sensed domain of the bottom small node (node 1) belongs to that set since it lies exclusively in the sensing region of a “larger” node (in terms of pattern-scale; purple-coloured) (Remark 4.6). As defined in (4.10), one can verify that the assigned parts are the ones that are sensed exclusively by one node, while the issue stated in Remark 4.5 can be examined via the nodes 4–5, indicating the (possibly) disjoint nature of the resulting cells.

Utilizing the formerly defined partitioning scheme, the network's coverage performance index  $\mathcal{H}$  can be decomposed as

$$\mathcal{H} = \sum_{i \in I_n} \int_{W_i} \phi + \int_{W_c} \phi, \quad (4.12)$$

## 4. AREA COVERAGE BY ANISOTROPIC NETWORKS

---

resulting directly from Remark 4.4. Note that  $W_i, W_c$  are already defined as subsets of the domain  $\Omega$ .

### 4.4.4 Distributed Motion Coordination

Unlike the majority of works presented in the existing literature on the field of distributed swarm coordination, this work incorporates rotation of the sensing pattern, thus allowing an extra degree of freedom, and demanding an extended control design. The need for rotation arises from the fact of a non-radial anisotropic sensing performance assumption, providing however the ability to achieve far better optimal topological configurations.

Let us further introduce some notations at this point. For any set  $S$  with well-defined exterior, let  $n(x)$  stand for the outward unit normal vector pointing towards the exterior of  $S$  for any  $x \in \partial S$ , where  $\partial S$  is the boundary of the set. For the sake of notations' simplicity, the former definition is extended in the case where the set  $S$  is non-compact, too, as long as the exterior of every sub-part of it is well-defined. These properties hold for both  $W_i$  and  $W_c$ , as defined in (4.10)–(4.11), presented also visually in Fig. 4.12. We will refer to  $n(x)$ ,  $x \in \partial W_i$  and  $n(x)$ ,  $x \in \partial W_c$  simply as  $n_i$  and  $n_c$ , respectively. At this point let us state the main result.

**Theorem 4.2.** *In a mobile sensor network governed by (4.8)–(4.9) with arbitrary non-radial nodes' sensing performance, the control law*

$$u_i = \alpha_{i,u} \int_{\partial W_i \cap \partial C_i} n_i \phi, \quad (4.13)$$

$$\omega_i = \alpha_{i,\omega} \int_{\partial W_i \cap \partial C_i} \mathbf{R}(90^\circ)(x - x_i) \cdot n_i \phi, \quad (4.14)$$

where  $\alpha_{i,u}, \alpha_{i,\omega} > 0$ , leads the network monotonically towards a locally area-optimal configuration.

*Proof.* We start by evaluating the time derivative of the criterion under optimization  $\mathcal{H}$  as

$$\frac{d\mathcal{H}}{dt} = \sum_{i \in I_n} \left\{ \frac{\partial \mathcal{H}}{\partial x_i} \cdot \dot{x}_i + \frac{\partial \mathcal{H}}{\partial \theta_i} \dot{\theta}_i \right\}.$$

Interested in the design of gradient-based control action, that is

$$u_i = \alpha_{i,u} \frac{\partial \mathcal{H}}{\partial x_i}, \quad \omega_i = \alpha_{i,\omega} \frac{\partial \mathcal{H}}{\partial \theta_i},$$

we begin with the translational part of the proposed law,  $u_i$ , by evaluating the partial derivative of the decomposed performance index w.r.t.  $x_i$ , followed by the corresponding rotational part,  $\omega_i$ .

Falling along the lines of [21, 45], utilization of the Leibniz integral rule [34] in (4.12) results in

$$\begin{aligned}\frac{\partial \mathcal{H}}{\partial x_i} &= \sum_{j \in I_n} \int_{\partial W_j} \frac{\partial x}{\partial x_i} n_j \phi + \int_{\partial W_c} \frac{\partial x}{\partial x_i} n_c \phi \\ &= \sum_{j \neq i} \int_{\partial W_j} \frac{\partial x}{\partial x_i} n_j \phi + \int_{\partial W_i} \frac{\partial x}{\partial x_i} n_i \phi + \int_{\partial W_c} \frac{\partial x}{\partial x_i} n_c \phi.\end{aligned}$$

Considering the second integral, the boundary  $\partial W_i$  can be decomposed into a) parts that lay on the border of the area of interest,  $\partial W_i \cap \partial \Omega$ , b) parts that are shared by  $\partial W_c$ ,  $\partial W_i \cap \partial W_c$ , and c) parts that orient towards the uncovered space,  $\partial W_i \cap \partial C_i$ . This decomposition is depicted graphically in Fig. 4.13 [upper part].

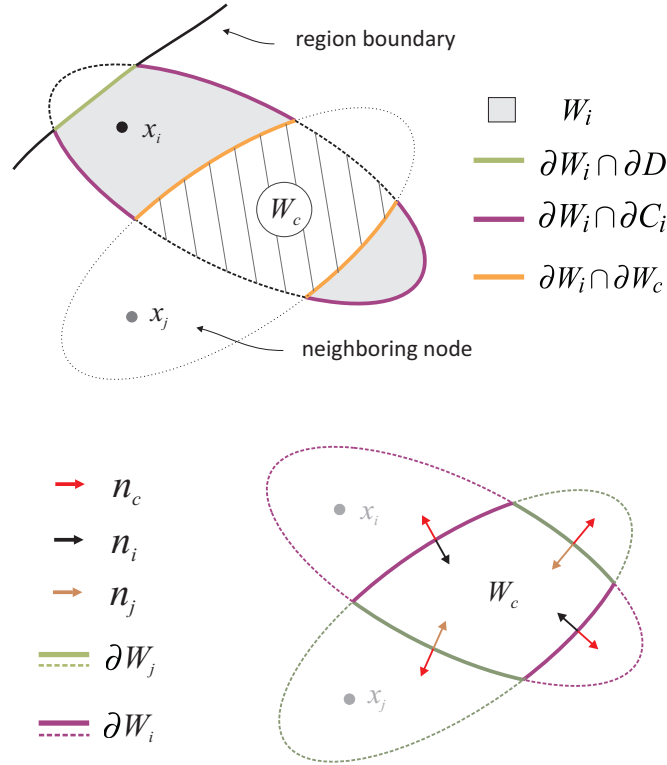


**Figure 4.13:** Decomposition of  $\partial W_i$  into mutually disjoint sets.

However, at  $x \in \partial \Omega$  it holds that  $\frac{\partial x}{\partial x_i} = \mathbf{0}$ , since we assume a static surveillance domain. In addition, since at the common boundaries it holds that  $\frac{\partial x}{\partial x_i} n_j = -\frac{\partial x}{\partial x_i} n_c, j \in I_n$  (see Fig. 4.13 [bottom part]), the former expression simplifies into

$$\frac{\partial \mathcal{H}}{\partial x_i} = \int_{\partial W_i \cap \partial C_i} \frac{\partial x}{\partial x_i} n_i \phi. \quad (4.15)$$

#### 4. AREA COVERAGE BY ANISOTROPIC NETWORKS

Exactly the same concept is repeated for the rotational part, by evaluating the partial derivative of  $\mathcal{H}$  w.r.t.  $\theta_i$  as

$$\frac{\partial \mathcal{H}}{\partial \theta_i} = \int_{\partial W_i \cap \partial C_i} \frac{\partial x}{\partial \theta_i} \cdot n_i \phi. \quad (4.16)$$

What remains is the evaluation of the partial derivatives  $\frac{\partial x}{\partial x_i}, \frac{\partial x}{\partial \theta_i}$  at  $x \in \partial W_i \cap \partial C_i$ . However, each point lying on the boundary of the a node's sensing domain can be expressed as

$$x = x_i + \rho(x) \begin{bmatrix} \cos(\xi(x) + \theta_i) \\ \sin(\xi(x) + \theta_i) \end{bmatrix}, \quad (4.17)$$

as also depicted graphically in Fig. 4.14, where it is evident that the parameters  $\rho, \xi$  for each

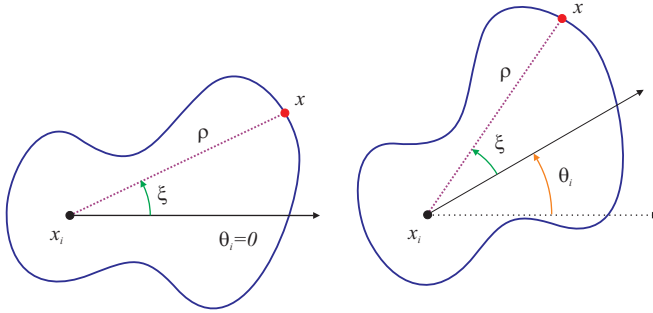


**Figure 4.14:** Notations concerning the proof of the main theorem.

$x$  are not dependent on the configuration of the sensor, i.e.  $x_i, \theta_i$ , but exclusively on the pattern itself.

Consequently,  $\frac{\partial x}{\partial x_i} = \mathbb{I}_2$  as the identity matrix, resulting directly from (4.17), simplifying the control action via (4.15) into (4.13). Similarly,

$$\frac{\partial x}{\partial \theta_i} = \rho(x) \begin{bmatrix} -\sin(\xi(x) + \theta_i) \\ \cos(\xi(x) + \theta_i) \end{bmatrix}.$$

Utilizing the rotation matrix notation and substituting back the trigonometric terms via (4.17) results in

$$\frac{\partial x}{\partial \theta_i} = \rho(x) \begin{bmatrix} 0 & -1 \\ 1 & 0 \end{bmatrix} \begin{bmatrix} \cos(\xi(x) + \theta_i) \\ \sin(\xi(x) + \theta_i) \end{bmatrix} = \mathbf{R}(90^\circ)(x - x_i),$$

leading the gradient-based rotational control into (4.14).

Updating the time derivative of the sensed area via the proposed control law results in

$$\frac{d\mathcal{H}}{dt} = \sum_{i \in I_n} \left\{ \alpha_{i,u} \left\| \frac{\partial \mathcal{H}}{\partial x_i} \right\|^2 + \alpha_{i,\omega} \left| \frac{\partial \mathcal{H}}{\partial \theta_i} \right|^2 \right\} \geq 0,$$

for  $\alpha_{i,u}, \alpha_{i,\omega} > 0$ , guaranteeing monotonic convergence of the network towards the optimum state. This completes the proof.  $\square$

**Remark 4.7.** *The proposed control scheme degenerates into the one presented in chapter 3, when the sensing domains are assumed circular node-centered ones, providing so an extension for arbitrarily non-radial patterns. Evidently, in the former case, due to the rotation-invariance of the disc-model, the rotational part of the control action is not taken into account.*

It should be noted that the proposed control law does not require global knowledge of the network's state, but instead only by those within an a-priori bounded range, as stated in the following lemma.

**Lemma 4.3.** *Assumption 4.1 serves as a conservative bound on the range required for the control law (4.13)–(4.14) to be spatially distributed.*

*Proof.* Examining (4.13)–(4.14), one can verify that the distributed nature of the control law is directly inherited by that of the partitioning scheme proposed in section 4.4.3. Therefore, if a node is able to evaluate its own region of responsibility  $W_i$  via local interaction, then this information is adequate in order to evaluate the control. However, according to (4.10), one can see that only the nodes that share common sensing parts are required (Assumption 4.1) or even marginally the ones that their boundaries intersect at a singleton. Following a worst case topology approach, a conservative upper-bound on the required range is provided as

$$\sup \{ \|x_i - x_j\| : |\partial C_i \cap \partial C_j| = 1 \},$$

where  $|\cdot|$  stands for the cardinality number of the set-argument. Although the aforementioned bound may seem of high complexity, it has the advantage of being dependent only of the nodes base patterns and therefore can be evaluated a-priori.  $\square$

### 4.4.5 Simulation Studies

Numerical results derived from simulations studies conducted are presented in this section. Two illustrative series of simulations follow for two kinds of sensing patterns. In both studies the domain under surveillance is the same, identical to the one used in [21] for consistency purposes. The proposed control law (4.13)–(4.14) based on the partitioning scheme (4.10) is compared for evaluation purposes with the control proposed in [21], appropriate for disc-modelled networks, as of (4.6).

*Case-Study 1.* In the first simulation presented, a homogeneous network of 8 nodes is examined. Their sensing footprints are assumed ellipsoidal ones with their axes-parameters set as  $a = 0.5$  units,  $b = 0.3$  units, while the relative position of the node to the footprint is set

#### 4. AREA COVERAGE BY ANISOTROPIC NETWORKS

at half-way along the long axis, as shown in the left part of Fig. 4.15. All nodes are initially randomly placed in a small region of the interior of  $\Omega$ , with random patterns' orientations.

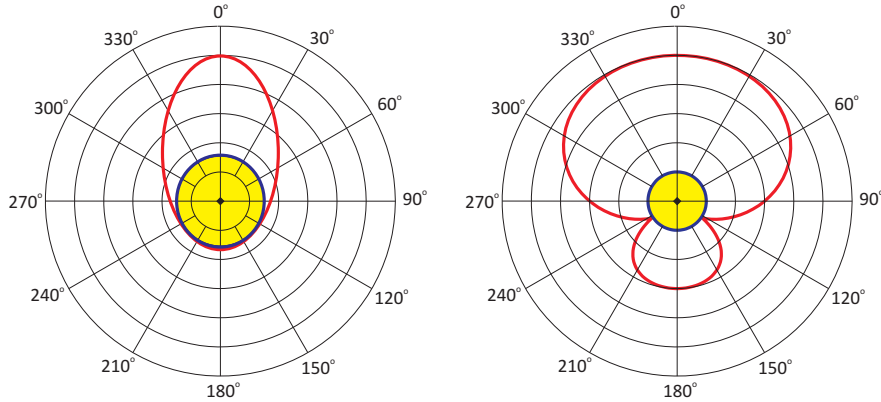


**Figure 4.15:** Normalized patterns used in the first [left] and second [right] simulation study, respectively, along with their maximal inscribed node-centered discs.

Initially, the control scheme (4.6) is applied in order to control the nodes' motion. The ellipsoidal model is approximated as the maximal inscribed node-centered disc, while standard Voronoi partitioning is utilized during the coordination stage in order to perform region-assignment and evaluate the control action. The nodes' initial configuration, their paths followed during transition, along with the final network's configuration are presented from left to right in the top row of Fig. 4.16, in this order.

Judging from the end-configuration one can observe at first that the nodes have indeed positioned themselves in an area-optimal topology, considering the disc models, as expected. Apparently, due to the rotation-invariance of the disc model, there is no control to amend for orientation-regulation of the original footprints. Examining, though, the real network's performance evaluated via the original ellipsoidal patterns, it is evident that the network can achieve far better sensing coverage ratio of the space under consideration. More specifically, the network starting from an initial coverage percentage of  $\Omega$  equal to 35.26% converges to 52.05%, as shown with the blue line in the left part of Fig. 4.17, which is the optimal network's performance if someone takes into account only the approximated discs. As before, this poor performance is due to the demand for disc approximation of the original patterns, so that the existing control strategies can be applied for network coordination.

On the other hand, utilizing the proposed control scheme for the nodes' motion coordination, that takes into account both the patterns' anisotropy and the need for their orientation



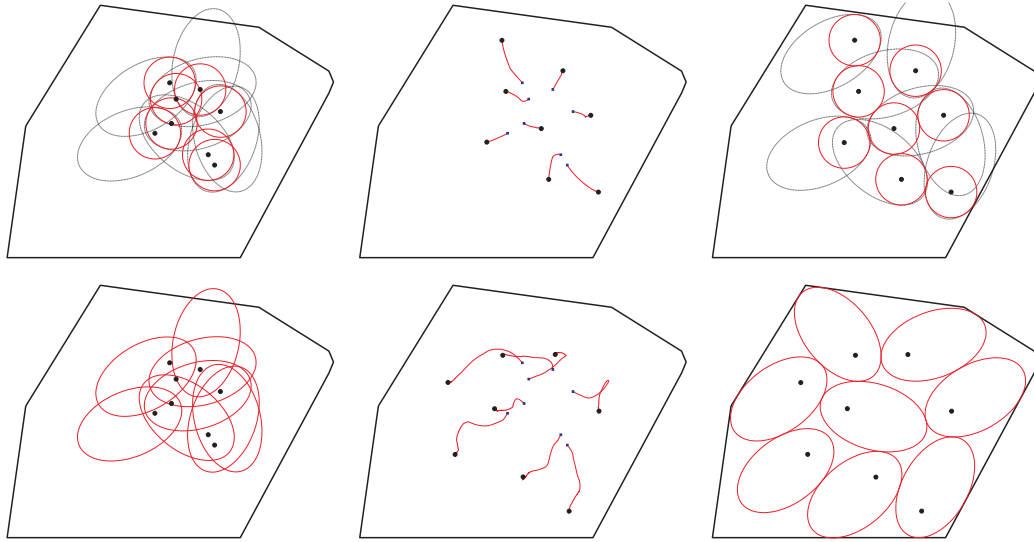


**Figure 4.16:** [Case–Study 1]: Coordination results derived via control schemes (4.6) [top row] and (4.13)–(4.14) [bottom row], respectively. [Left column] Initial network configuration. [Middle column] Network evolution through time. The black circles (blue squares) represent the nodes’ final (initial) positions. [Right column] Final network state.

regulation, produces the results depicted in the bottom row of Fig. 4.16. It is apparent that the nodes have been organized in a way that optimum coverage is attained, equal to 74.16% (red line in left part of Fig. 4.17), while their orientation is controlled properly via (4.14), as also seen in the right part of Fig. 4.17.

*Case–Study 2.* In the second scenario studied, a more application–oriented sensing pattern has been selected in order to emphasize in the advantages of the scheme proposed in this section. More specifically, the hypercardioid footprint is selected representing that of directional microphones [2], suitable for application where specific sound needs to be captured even in loud/noisy environments (i.e. environmental sensing, security applications). The normalized pattern is depicted in the right part of Fig. 4.15.

In addition, the scaling of the pattern of each node differs, imposing heterogeneity in the network’s nature, while the network’s maximum achievable coverage performance is quite larger than that of case–study 1. When coordination is performed based on the disc–model approximation of the pattern, the power diagram [14] is utilized for partitioning the space, since the resulting circles are of unequal radii. The results in this case are depicted in the top row of Fig. 4.18, where one can observe that the nodes have not spread much, even if optimum disc–coverage has been achieved at the final configuration equal to 38.65% starting from an

## 4. AREA COVERAGE BY ANISOTROPIC NETWORKS

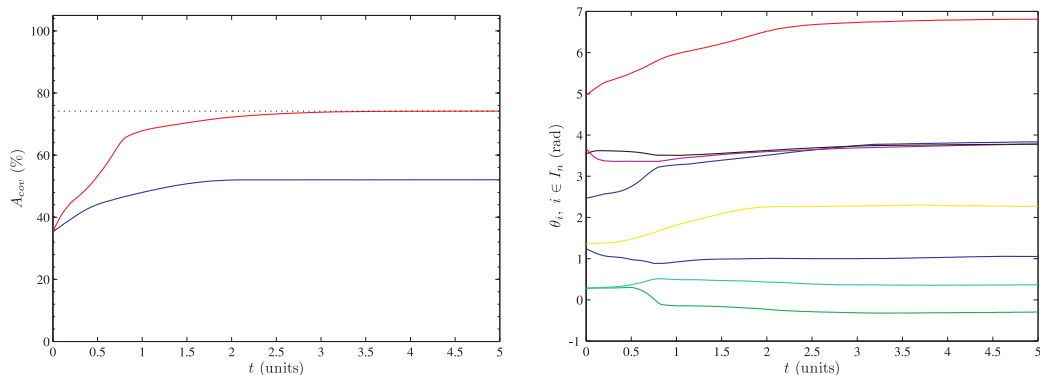


**Figure 4.17:** [Case-Study 1]: [Left] Evolution of covered area percentage w.r.t. time evaluated via the non-uniform original patterns. Blue (Red) line corresponds to top (bottom) row of Fig. 4.16. [Right] Evolution of nodes' orientation w.r.t. time corresponding to the bottom row of Fig. 4.16.

initial value of 35.05%.

Simulation results derived by applying the proposed control scheme in this section are presented in the bottom row of Fig. 4.18. Observing the nodes' paths it is evident that the latter have deployed themselves in  $\Omega$  trying to cover as much space as possible taking into account their original non-convex domains, rather than approximating them (disc or convex-set approximation). The percentage of area covered during network's transition, evolving monotonically towards the optimum value, is depicted in the left part of Fig. 4.19 [red line], where its performance efficiency (97.91%) in comparison to the disc-model case [blue case] is apparent, relying on proper regulation of both positioning and orientation (Fig. 4.19) of the patterns.

It should be noted that the proposed scheme has increased complexity in its evaluation when dealing with arbitrary non-convex sensing domains, especially when compared with approaches that are based on disc models. Particularly, the demand arises from the difficulty in parametrizing complex boundary curves, when compared to evaluations that are based on circle-arcs. In fact, even if numerical approaches are utilized in order to avoid complex curves' descriptions, extra computational demand is needed at evaluating the corresponding boundary-parts appearing in the proposed control law. However, the overall network's performance in our case is by far superior to that of disc-approximating techniques, arising so a trade-off to balance: complexity vs. performance.

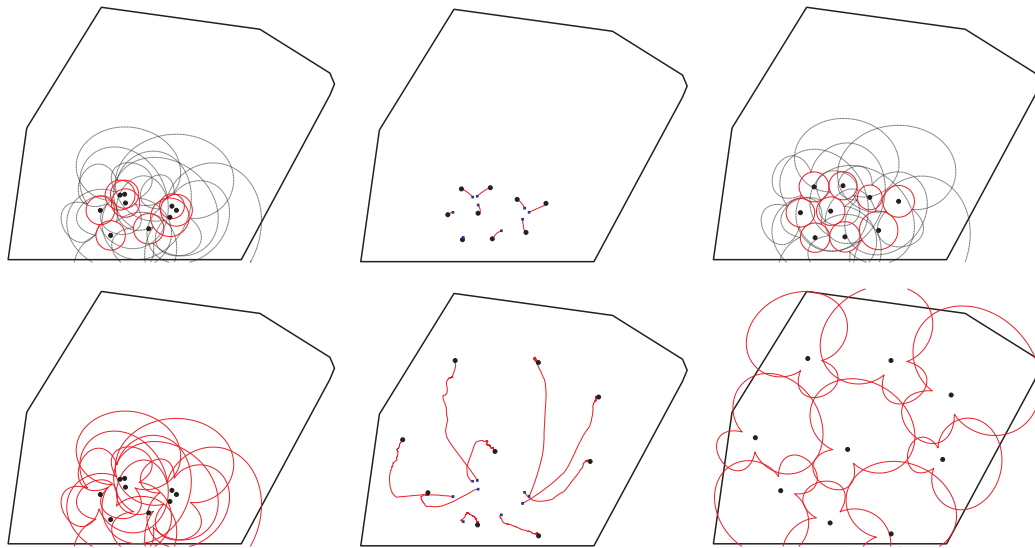


**Figure 4.18:** [Case–Study 2]: Coordination results derived via control schemes (4.6) [top row] and (4.13)–(4.14) [bottom row], respectively. [Left column] Initial network configuration. [Middle column] Network evolution through time. The black circles (blue squares) represent the nodes’ final (initial) positions. [Right column] Final network state.

## 4.5 Conclusions

In this chapter, a distributed algorithm was proposed for area coverage optimization in mobile sensor networks with arbitrary strictly convex sensing patterns. Unlike the majority of previous works, the sensing domain of the nodes is not circular or node–centered, but is assumed to be any general convex set in the plane. Distributed coordination is performed based on a space partitioning scheme, developed via the footprints of the nodes. In order to confirm efficiency of the proposed scheme, simulation results are provided, where typical directional microphones’ cardioid footprints were utilized, along with RF radiation patterns.

Results are extended to amend for non–common headings of the nodes’ footprints. The network is considered anisotropic (arbitrary patterns) and heterogeneous (in terms of scaling), allowing for almost any arbitrary sensory, highly differentiating from standard circular–case assumptions appearing in the existing literature. Efficient partitioning of the sensed domain is proposed in order for the nodes to distributively evaluate the corresponding parts that should determine their motion for coverage–increase. The presented scheme was proven to guarantee monotonic increase of the area sensed by the network while accounts not only for the nodes’ positioning, but sensor orientation as well, further evaluated via simulation studies.

## 4. AREA COVERAGE BY ANISOTROPIC NETWORKS

---

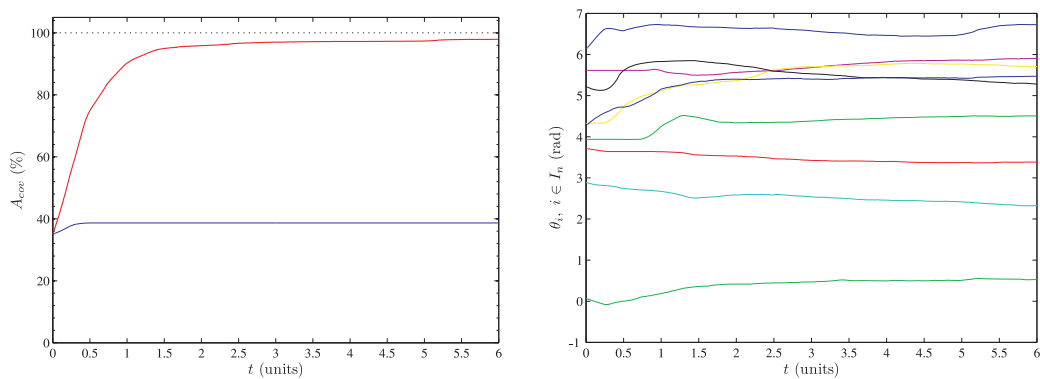


**Figure 4.19:** [Case–Study 2]: [Left] Evolution of covered area percentage w.r.t. time evaluated via the non–uniform original patterns. Blue (Red) line corresponds to top (bottom) row of Fig. 4.18. [Right] Evolution of nodes’ orientation w.r.t. time corresponding to the bottom row of Fig. 4.18.

# 5

## Coverage with Constraints in the Communication Range

### 5.1 Introduction

In optimization scenarios by mobile robotic swarms, the agents plan their actions in a distributed way, while an aggregate team objective function is to be optimized. Henceforth, ensuring valid paths for information flow among the nodes is crucial throughout the evolution of network in order to guarantee distributed data transmission [58].

However, it is evident that demand for connectivity preservation and area coverage optimality cannot be achieved simultaneously, and thus there is trade-off to be balanced [40, 59, 60]. Distributed coordination of mobile networks for achieving consensus based on nearest neighbor rules has been proposed by the authors in [39], while connectivity control of networks has been examined in [41, 61]. A trade-off between area coverage and communication costs, related with the power consumption needed for delivering information to a base station, is addressed in [62].

In the majority of works presented in the existing literature, the communication range of the nodes' antennas is assumed either variable and bounded (in terms of upper limit) [35], or fixed and bounded but greater than twice the sensing range [16, 21]. This dependence of the radio range on the sensing one, although not encountered in practice, remarkably surpasses any network connectivity issues, and subsequently concentrates on optimization of the covered area.

In this chapter the distributed area coverage control problem is addressed in mobile robotic

## 5. COVERAGE WITH CONSTRAINTS IN THE COMMUNICATION RANGE

---

networks under communication constraints. The standard case of correlating the nodes' radio range with the sensing one is extended, allowing the first to take any value, and not necessarily twice or larger of the sensing range. The members of the network are allowed to exchange information among them in a number of hops, via internal broadcasting/forwarding messages between consecutive motion steps. The proposed control framework is based on proper categorization of the nodes, according to the existence of arcs in their individual assigned cells or their contact with the boundary of the region of interest. Their motion is performed in order to increase the network's coverage performance, while maintaining connectivity among neighboring nodes at same time. Simulation results indicate that the control plan achieves respectable coverage performance in the case of RF-constrained networks.

### 5.2 Problem Setup — Preliminaries on Connectivity

#### 5.2.1 Coverage Problem Formulation

Let us revisit the coverage setup of chapter 2, where the nodes' motion is governed by the discrete time model as of (2.1), while their sensing footprint is the uniform radial one in (2.2), allowing  $r$  to be a range-threshold beyond which sensing results are considered unreliable. Let the area-related criterion in (3.15) be the optimization cost to be maximized throughout the network's evolution.

Coordination schemes that are to be developed for a mobile sensor network should be characterized by distributed nature. This means that each node should plan its motion according to information acquired only from its "neighboring" nodes, while global knowledge of the network should not be demanded, since it is never available in practice. For this purpose, each mobile robot vehicle is assumed to be equipped with a radio transceiver, able to transmit information radially (omnidirectionally) around the corresponding node's position up to a range equal to  $R$ . Equivalently, each node receives messages from any neighboring node that transmits in that range.

From an application perspective, the aforementioned radio-range,  $R$ , is somehow uncorrelated to the sensing one,  $r$ , since it is dependent on the antenna's characteristics (i.e. transmission power, antenna gain etc). This is exactly the case examined in this chapter; that is, the antennas' radius is permitted to take any arbitrary value independent of the sensing range, contrary to the majority of works in the literature. Thus, communication range can even be less

than twice the sensing one (i.e. the trivial case), while this value is assumed to be fixed and common for all nodes.

Considering the above, the communication graph of the network can be defined, denoted as  $G_c$ . In this graph, an edge exists between two nodes if  $\|x_i - x_j\| \leq R$ , entailing that, in this case, a bidirectional communication link exists among nodes  $i, j$  for information flow. It should be mentioned that the communication graph is independent of the nodes' sensing range, but depends only on nodes' positions and their communication capabilities. The following definitions are provided in order to determine neighboring relationships in the communication graph.

**Definition 5.1.** *For a given sensor network communication graph  $G_c$ , a routing path of length  $\ell$  among two nodes  $i, j$  is a sequence of  $\ell + 1$  nodes  $i, k_1, k_2, \dots, k_{\ell-1}, j$  such that  $i \longleftrightarrow k_1 \longleftrightarrow k_2 \dots \longleftrightarrow k_{\ell-1} \longleftrightarrow j$ , where notation  $\longleftrightarrow$  implies direct RF connectivity among two nodes. A network is considered fully (end-to-end) connected if there exists an RF routing path among any two nodes of it.*

The main objective in an RF-aware coverage scenario that this chapter deals with can be formulated as a proper design of distributed control action of the nodes, so that performance criterion (3.15) is maximized, while network maintains end-to-end RF-connectivity, given that initially the network is fully connected.

Utilizing Voronoi partitioning defined in (2.6), one can determine neighboring relationships between nodes via utilization of the Voronoi cells. Two nodes are considered as Delaunay neighbors if they share an edge of their Voronoi cells, as of (2.7). In a similar way, the  $2r$ -limited Delaunay neighbors can be defined as the pairs of nodes the share an edge of their  $r$ -limited Voronoi cells, that is

$$\mathcal{N}_i^{2r} = \{j \in I_n : V_i^r \cap V_j^r \neq \emptyset \text{ (non singleton)}, j \neq i\}, i \in I_n. \quad (5.1)$$

Based on these relationships one can define the corresponding graphs. A graph  $G = \{V, E\}$  consists of a set of vertices (nodes)  $V$ , along with a set of edges  $E$  containing the relationship links among the nodes. The Delaunay graph  $G_d$  of a network is based on neighboring described in (2.7), while the corresponding  $2r$ -limited Delaunay graph,  $G_d^{2r}$ , on (5.1), respectively. One can easily verify that  $G_d^{2r} \subseteq G_d$ . The reader is encouraged to refer to [63] for additional details on graph preliminaries.

Figure 5.1 shows the Voronoi and the  $r$ -limited Voronoi partitioning, along with the neighboring relationships, for an arbitrary group of nodes. It should be noted that if two nodes are

## 5. COVERAGE WITH CONSTRAINTS IN THE COMMUNICATION RANGE

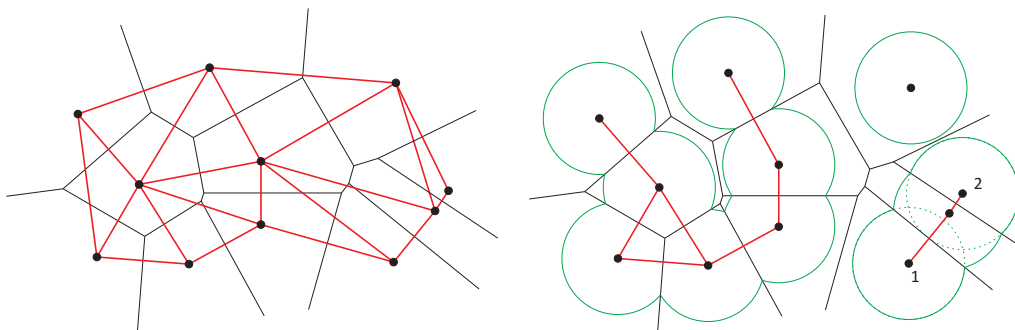


**Figure 5.1:** Graphical representation of the Delaunay [left] and  $2r$ -limited Delaunay [right] neighbors in a sensor network.

neighbors in  $G_d^{2r}$  graph, then their distance is less than  $2r$ ; however, the reverse does not always hold, as seen by the numbered bottom-right nodes of Fig. 5.1. Although the circles of these nodes intersect (dashed line), this does not hold for their  $r$ -limited Voronoi cells.

Considering the criterion  $\mathcal{H}$  in (3.15) along with Voronoi partitioning, the total area sensed by the network can be expressed as the summation of the areas of the  $r$ -limited Voronoi cells of the nodes as of (3.16). Figure 5.2 shows a simple scenario of an area-optimum network configuration in the open space. Red links indicate the neighboring relationships among the  $2r$ -limited Delaunay neighbors. It is evident that if  $R \geq 2r$ , the latter are trivially RF-connected. Consequently, since any information required during the coordination stage is guaranteed, the agents can plan their motion in order to maximize the network's aggregate objective (3.15), or equivalently minimize the area of their possible overlapping sensing parts. More specifically,

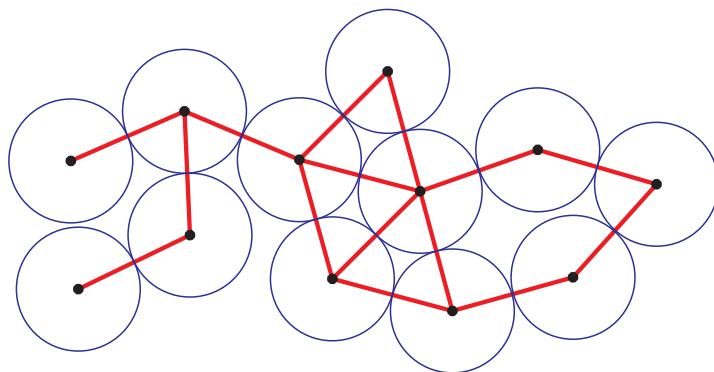


**Figure 5.2:** Example of area-optimal configurations achieved via (4.6) for an arbitrary sensor network.

such configurations can be achieved if the nodes' control action is selected as in (4.6), as



proposed in [21], To associate (4.6) with Fig. 5.2, the nodes are pushed to move towards the “arcs” of their corresponding  $r$ -limited Voronoi cells, heading thus towards the uncovered space and increasing the overall network’s coverage performance.

### 5.2.2 Radio Connectivity Issues

According to the example presented above, along with (4.6), in order for the nodes to be able to contribute in network’s coverage performance increase, they need information from their current  $2r$ -limited Delaunay neighbors, which is trivially guaranteed if  $R \geq 2r$ . In this chapter this trivial assumption is ignored and by uncorrelating the aforementioned radii. At this point let us introduce some definitions on multi-hopping interaction.

**Definition 5.2.** *Two nodes  $i, j$  in  $G_c$  are defined as  $N$ -hops connected, denoted as  $i \overset{N}{\longleftrightarrow} j$ , if the minimum-length path among them has length  $N$ . For the trivial case of direct RF connectivity, that is  $N = 1$ , we will simply refer as connected, i.e.  $i \longleftrightarrow j$ .*

**Definition 5.3.** *For any node  $i$ , the set  $\mathcal{D}_i^N$  is defined as the set of nodes that node  $i$  is at most  $N$ -hops connected, that is*

$$\mathcal{D}_i^N = \left\{ j \in I_n : i \overset{\ell}{\longleftrightarrow} j, \ell \leq N, j \neq i \right\}, \quad i \in I_n. \quad (5.2)$$

**Assumption 5.1.** *Initially, at time-step  $k = 0$ , each node is connected via at most  $N$ -hops with all its  $2r$ -limited Delaunay neighbors, for an a-priori given  $N \in I_{n-1}$ , that is*

$$j \in \mathcal{N}_i^{2r} \Rightarrow j \in \mathcal{D}_i^N, \quad i \in I_n.$$

*Practically, the assumption indicates that if two nodes share parts of their sensing domains, then there exists an at-most  $N$ -hops routing path connecting them, initially.*

The main motivation to introduce the aforementioned assumption that demands at most  $N$ -hops connectivity among  $2r$ -limited Delaunay neighbors is the fact that, each node in order to plan its motion appropriately, has to evaluate its  $r$ -limited Voronoi cell (see (4.6)), while that set,  $\mathcal{N}_i^{2r}$ , is sufficient for  $V_i^r$  evaluation. It should be noted, though, that proper design of an alternate distributed control scheme is necessary in order to amend not only for network’s coverage performance, but to *maintain* that  $N$ -hops connectivity among neighboring nodes throughout the deployment stage.

## 5. COVERAGE WITH CONSTRAINTS IN THE COMMUNICATION RANGE

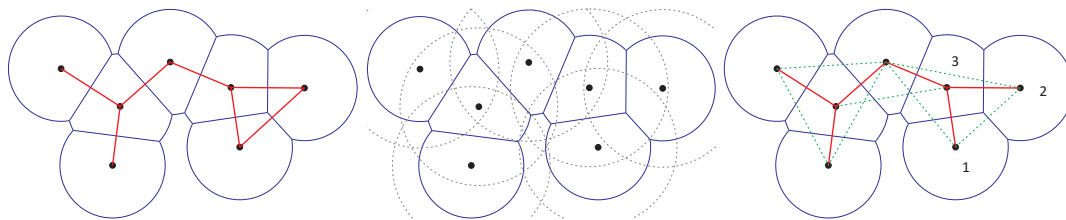


**Figure 5.3:** Graphical representation of the need for multi-hopping in order to acquire sufficient information for distributed  $V_i^r$  evaluation.

These issues are also presented visually in Fig. 5.3, depicting a simple network of seven nodes with  $R = 1.5r$ . Neighboring relationships via the  $r$ -limited Voronoi sets is depicted in the Figure’s left part, while the network’s communication graph is shown in solid line at the right part, given the fixed RF-radii [middle part] (uncorrelated with the sensing performance of the team). It should be observed that nodes 1 and 2, even though they are not directly connected, they can exchange information via node 3, and hence considered 2-hops connected, that is  $1 \overset{2}{\longleftrightarrow} 2$ , depicted with dashed line in the Figure. That multi-hopping connectivity nature of the network can be proven to be crucial concerning optimization issues, since the aforementioned nodes should have perception of existence of each other in order to properly evaluate their corresponding cells and apply their corresponding coverage control in the sequel [see left part].

From an application point of view, the concept of multi-hopping can be considered as sequential TX/RX services at each step of the motion-loop, in order to ensure sufficient information exchange among members that share common parts in their sensing domains. An algorithmic sketch of that procedure is described in Algorithm 5.1. It is apparent that the TX/RX loop and the motion-loop do not run in parallel, but in a somehow nested manner. It should be noted that, since the  $2r$ -limited Delaunay neighbors are initially  $N$ -hops connected, it is up to the control design to ensure further connectivity maintenance in order to benefit from its optimality-oriented nature.

Compared to the standard case —where at each iteration a node broadcasts its position, receives the positions of its neighbors and determines its motion in the sequel, based on that data,— in the case of  $N$ -hops each node repeats  $N$  times the broadcasting-reception procedure, in order to fully identify its neighbors that are  $N$ -hops afar, in each step. The iterative identification process of  $\mathcal{D}_i^N$  for  $N = 3$  hops is depicted graphically in Fig. 5.4 for an arbitrary network. Although, the broadcasting-reception iteration is executed  $N$  times at each “motion”-time-step, and thus overweights the links’ load, it allows for guaranteeing monotonic increase

---

**Algorithm 5.1** Identification of  $\mathcal{N}_i^{2r}$  neighbors via multi-hopping for fixed RF range

---

```

1: loop
2:   add self in PositionList
3:   for  $m = 1: N$  do
4:     broadcast PositionList
5:     receive messages from nodes in range
6:     add information received in PositionList
7:   end for
8:   ...
9:   (control scheme)
10:  ...
11: end loop

```

---

in the network’s coverage performance, as it will be shown in the sequel, assuming proper control design.

The main problem though with connectivity preservation in mobile networks lies in the fact that usually local information is insufficient to guarantee global results. A quite instructive example is presented in Fig.4 of [41], where it is shown that if 2 pairs of nodes decide, independently of each other, to drop the communication link among them, then global end-to-end connectivity is violated, although the nodes assume that it is preserved from a decentralized aspect.

In this chapter, in order to account for increase in coverage performance of the network in time, only one node is allowed to move at each step  $k$  [35]. This can be performed by cyclic operation of the nodes in a periodic mode. Although this demands some initial synchronization of the network, it does not require any central supervision during operation. Consequently, at an arbitrary time step, a node is able to identify if it is its turn to move or not, in a time-based manner, similarly to the concept of chapter 2. It should be noted though, that the current assumptions/approach do not account for packet losses or reception delays, unlike probabilistic models. However, decision on motion is taken at the end of each time step (Fig. 5.4, at the end of the  $T$ -interval), regardless of the information acquired, allowing for proper synchronization of the network.

In fact, the demand for motion of one node at each step arises mainly from the need for connectivity maintenance with the set  $\mathcal{N}_i^{2r}$  in order to evaluate properly in the sequel the corre-

## 5. COVERAGE WITH CONSTRAINTS IN THE COMMUNICATION RANGE

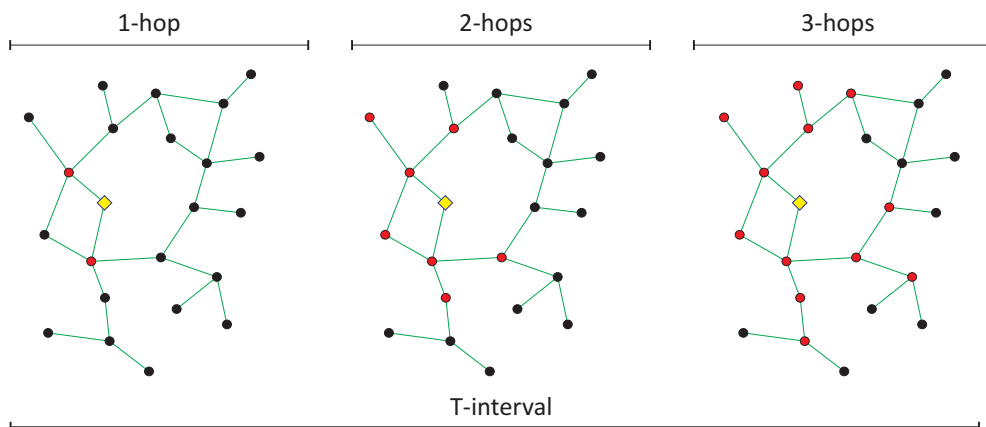


**Figure 5.4:** Evolution of  $\mathcal{D}_i^N$ -set identification during a time-step interval  $T$ . The 3-hops neighbors of the yellow diamond-shaped node are identified sequentially (red ones) via chained neighbors-transmission. The repeated RX/TX process takes place during the time-step interval  $T$ .

sponding coverage optimization law. Figure 5.5, depicts a simple network of two nodes, which share parts in their sensing domains. In the case both nodes are allowed to move, in order to *distributedly* preserve the RF-link among them, they should move in the blue disk, so to maintain at least the critical distance allowing them to communicate [left part]. On the other hand,

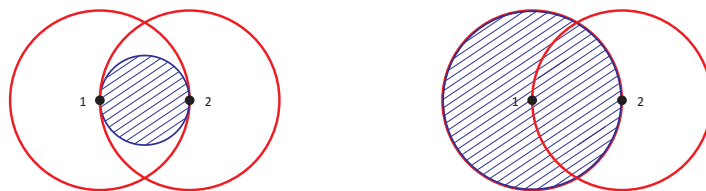


**Figure 5.5:** Graphical illustration of the connectivity-oriented motivation for demanding motion of one node at each step in a simple network of two nodes.

if we allow only to the right node to move, then, as shown in the right part of the figure, a quite larger domain is allowed. Although this is not a rule of thumb, restricting the nodes to move to one, although may delay the convergence process, it can amend for connectivity preservation while allow more flexibility during the network evolution [right part].

It should be noted that, knowledge of the  $2r$ -limited Delaunay neighbors of a node is crucial for evaluating distributedly control laws that are based on geometric partitioning of the space such as (4.6). Although it is up to the design of the control action in order to *maintain* connectivity among the  $2r$ -limited Delaunay neighbors, there are cases where connectivity cannot be *guaranteed/constructed*.

### 5.3 Distributed Control for Optimum Coverage while Maintaining Network Connectivity

Let us consider a simple network consisted of 2 nodes, with  $R = r$ , as shown in the left part of Fig. 5.6. Assuming control law (4.6), node 1 should not move since it already attains optimum coverage, while node 2 is moved towards the direction shown with the green arrow, as pushed away from the boundary. At this point the nodes do not have perception of each other. Node 2 will keep moving to the left until it reaches the configuration shown, while node 1 will still stay still. The main issue here is that both nodes “believe” that they have achieved optimal area–coverage, since they still are out of RF–range of each other (and do not have knowledge of existence of each other), while the real coverage performance of the network is less that the distributedly estimated one, as the union of the discs.

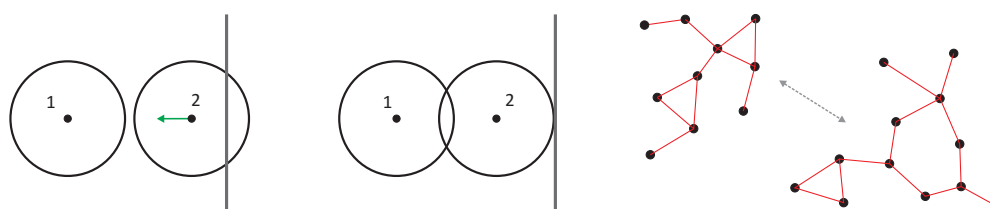


**Figure 5.6:** Graphical representation of topologies where connectivity among  $2r$ –limited Delaunay neighbors cannot be forced.

In fact, the nodes cannot do anything about these cases, since they have wrong local perception of the state of the network. Same scenarios is when the network is consisted of clusters of nodes without any “bridge”–nodes to allow interaction between the groups, as shown in the right part of Fig. 5.6. In such cases when these nodes ever come in range of each other, the control law will try and maintain such connectivity links. Thus, although connectivity among the  $2r$ –limited Delaunay neighbors can be *maintained*, it cannot be *enforced* in some cases, depending on the network topology.

### 5.3 Distributed Control for Optimum Coverage while Maintaining Network Connectivity

The objective of the suggested control scheme is to lead the network in such configurations where the sensed part of area  $\Omega$  under consideration is as high as possible, while simultaneously end–to–end connectivity is preserved. In general, coordination should be performed in a distributed way meaning that the node–to–move does not have global knowledge for the state of the whole network. In this section, radio–connectivity among two nodes is extended further

## 5. COVERAGE WITH CONSTRAINTS IN THE COMMUNICATION RANGE

---

than the standard case, i.e. that two nodes are connected (and thus exchange information), if they are within the radio-range among each other. Specifically, the term of  $N$ -hops connectivity is introduced (previous section), allowing two nodes to share data if there exists a valid  $N$ -hop corresponding communication path for information flow.

### 5.3.1 Motivation for extension of existing control laws

The presented results are based on the control scheme proposed by the authors in [21], which is suitable for optimizing the area-coverage performance in a mobile sensor network. For the limited sensing range in the nodes' performance model, the control action (4.6) leads a network in an area-optimal topology, following the gradient direction in order to achieve maximal-rate increase of the network's performance between time-steps. The main issue though is that the aforementioned scheme correlates the radio range with the sensing one as explained in Fig. 5.2 in order to guarantee distributed evaluation of the corresponding Voronoi cells.

Applying that control law in a network though where the nodes have RF-range less than twice the sensing one, can result in quite unsatisfactory performance, judging from the converged topologies. The modification presented in Algorithm 5.2 is the main basis of the control approaches following in the sequel, allowing for handling the communication constraints imposed, while ensuring distributed and correct evaluation of the corresponding  $r$ -limited Voronoi cells.

---

**Algorithm 5.2** Motion planning for coverage control in networks under non-trivial communication constraints (base pattern)

---

- 1: **loop**
- 2:   implement TX/RX loop as in Algorithm 5.1
- 3:   evaluate own  $V_i^r$  based on  $\mathcal{N}_i^{2r}$
- 4:   implement `FunctionMotionDirection()`
- 5:   perform line-search optimization along the selected direction as

$$\left\{ \begin{array}{l} \text{maximize} \quad \text{stepsize towards direction inside } V_i^r \\ \text{subject to :} \quad \text{connectivity not violated} \end{array} \right.$$

- 6: **end loop**
- 

We apply the scheme described in Algorithm 5.2 in a network of 10 nodes, where the sensing radius is equal to the RF one for visualization purposes. The `FunctionMotionDirection`

### 5.3 Distributed Control for Optimum Coverage while Maintaining Network Connectivity

(line 4) in this case is selected as the area–gradient one, given in (4.6). The nodes are set to move on condition that 2–hops connectivity in  $G_d^{2r}$  is maintained. Figure 5.7 depicts the initial configuration of the network along with the final one when the prescribed law is applied.

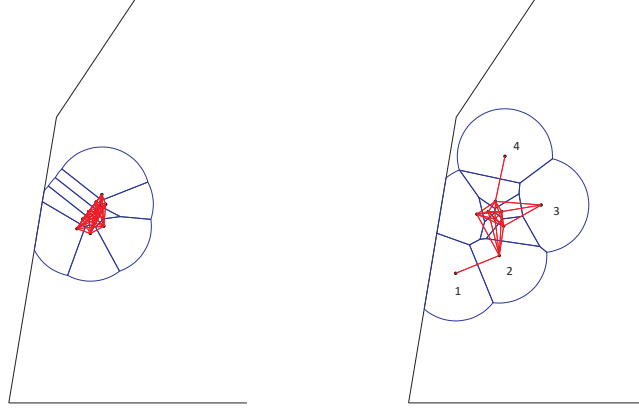


**Figure 5.7:** Coordination results derived via Algorithm 5.2. [Left] Initial network configuration. [Right] Final network state. Communication graph indicates 2–hops connectivity among the  $2r$ –limited Delaunay neighbors.

Observing the results, it is clear that, besides the fact that the demanded 2–hop connectivity is attained among the  $2r$ –limited Delaunay neighbors and the area function  $\mathcal{H}$  increases from one step to the other (due to the gradient–based nature of the control law), the final coverage performance of the network can be further increased. This issue appears due to two main reasons:

- some nodes do not move further since their motion along the area–maximization–gradient contradicts with connectivity preservation, and thus consist a “barrier” for the network (see enumerated nodes in right part of Fig. 5.7),
- the control action for some nodes corresponds to null, since their  $r$ –limited Voronoi cells do not contain any arc, resulting in their congestion in small areas (rest of the nodes).

This next two sections are dedicated in providing further extensions/modifications to achieve area–wise “better” topological configurations.

#### 5.3.2 Proposed Control Scheme – Modifications

The first step so to overcome the aforementioned problems is to categorize the nodes depending on the characteristics of their corresponding  $r$ –limited Voronoi cells. The motion planning

## 5. COVERAGE WITH CONSTRAINTS IN THE COMMUNICATION RANGE

scheme for each node can then be designed, dependent on the category a node belongs at, while determined via information from  $N$ -hops radio-connected nodes.

**Definition 5.4.** *In a network where the nodes' sensing performance is limited-range radial, let  $\mathcal{E}$  contain the set of nodes whose  $r$ -limited Voronoi cell contains at least one arc of the boundary of their sensing domain. Let these nodes be called exterior ones, formally defined as  $\mathcal{E} := \{j \in I_n : \partial V_j^r \cap \partial C_j \neq \emptyset\}$ . Univocally, we can define the set of interior nodes  $\mathcal{I} := I_n \setminus \mathcal{E}$ , containing the rest nodes of the network, that is the nodes whose  $r$ -limited Voronoi cell contains no arc.*

**Remark 5.1.** *The categorization proposed in Definition 5.4 can be performed in a distributed manner by the nodes themselves, as long as connectivity among the  $2r$ -limited Dealunay neighbors is maintained. Indeed, if a node knows its aforementioned neighbors, then it can evaluate its own  $r$ -limited Voronoi cell and thus identify the category it belongs at, managing properly its control action in the sequel.*

Examining Fig. 5.7 and taking into account the discussion at the end of the previous subsection, one can see that the exterior nodes are the ones to “block” network evolution by forming some kind of barrier, while the interior ones stay still according to gradient law, until they ever become exterior ones.

Figure 5.8 depicts the categorization of twelve nodes into interior and exterior ones. In or-

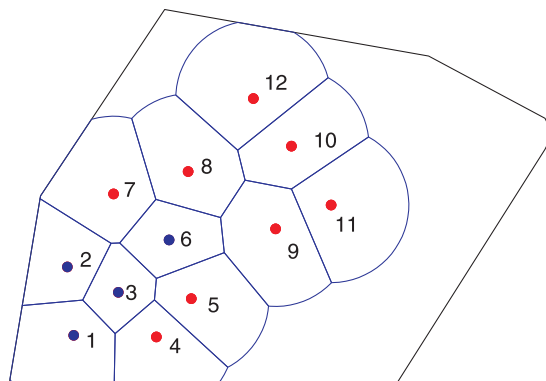


**Figure 5.8:** Categorization of nodes into interior and exterior ones. Blue (red) dots represent the interior (exterior) ones.

der to avoid the above issues, we propose some modifications/extensions to the original control scheme, based on Algorithm 5.2. According to the latter, which consists a connectivity-aware version of the original scheme, an exterior node checks the area-gradient direction in order to



### 5.3 Distributed Control for Optimum Coverage while Maintaining Network Connectivity

move and increase the overall network’s performance, without breaking any link that is used for connectivity among  $2r$ -limited Delaunay neighbors. These checks are performed inside the line-search optimization loop for determination of the appropriate step-size as already shown in Algorithm 5.2.

Apparently, according to Algorithm 5.2, if no valid step size is found along the scan direction that does not violate the connectivity demand, the node does not perform any motion. The problem with this concept is that it “locks” the exterior nodes at a configuration, where any infinitesimal motion along the optimum area-increase direction will break essential links in the network. In this chapter analysis, the search procedure does not end in this point, but we allow suboptimal direction-scan, too, in order to avoid reaching such spatial topologies. Particularly, the directions that deviate from the gradient one at any range within a maximum of 90 degrees can be selected, since these will also increase network’s coverage performance, though not in the optimal manner, as shown graphically in Fig. 5.9.

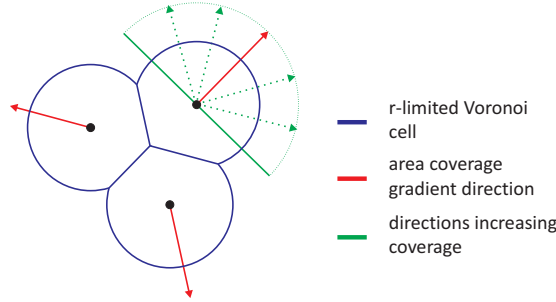


**Figure 5.9:** Graphical depiction of the suboptimal directions allowed in chapter 5 to avoid deadend-configurations, while preserving connectivity.

Considering the selection of the suboptimal directions, in the case where there is no non-zero step-size along the area-gradient direction that maintains connectivity, the directions closest to the latter are first examined, moving towards the outer directions during scanning procedure. Assuming a predefined angle-step  $\delta\theta$ , at the  $m$ -th iteration the direction scanned is set to

$$v_m = \mathbf{R}((-1)^m \lceil m/2 \rceil \delta\theta) \nabla \mathcal{H}, \quad |m/2 \delta\theta| \leq \pi/2, \quad (5.3)$$

where  $\lceil \cdot \rceil$  is the ceiling function,  $m$  is the iteration of the direction-scanning loop and  $\mathbf{R}(\cdot)$  is the standard rotation matrix as previously presented in section 4.4.2.

Considering proper control of the motion of interior nodes, in order to avoid being idle until they (ever) become exterior, we are based on the fact that infinitesimal motions do not affect

## 5. COVERAGE WITH CONSTRAINTS IN THE COMMUNICATION RANGE

---

the network's coverage. Apparently, that is also the main reason that the control law (4.6) is null for them. What we propose is to move in such a way so that they relax possible hard RF constraints that may have "locked" exterior nodes, and hence give them the opportunity to evolve in space for increasing network's performance. Considering that, they are selected to move in a direction towards their furthest  $2r$ -limited Delaunay neighbor. It should be noted that this motion is performed with the appropriate step-size so that  $N$ -hops connectivity is not violated in  $G_D^{2r}$ . That way, it is guaranteed that the overall network's coverage performance increases in a monotonic manner, a straightforward property of control action (4.6) [21, 45]. An algorithmic sketch of the described control scheme is presented in Algorithm 5.3

---

**Algorithm 5.3** Proposed control scheme based on interior/exterior nodes-categorization

---

```

1: loop
2:   implement TX/RX loop as in Algorithm 5.1
3:   evaluate own  $V_i^r$  based on  $\mathcal{N}_i^{2r}$ 
4:   identify own category (remark 5.1)
5:    $m := 0$ 
6:   if exterior node then
7:     evaluate search-direction via (5.3)
8:   else
9:     move towards own furthest  $2r$ -limited Delaunay neighbor
10:  end if
11:  perform line-search optimization along the selected direction as
      
$$\begin{cases} \text{maximize} & \text{stepsize towards direction inside } V_i^r \\ \text{subject to} & : \text{ connectivity not violated} \end{cases}$$

12:  if exterior node and no feasible step found then
13:     $m \leftarrow m + 1$ 
14:    go to 6
15:  end if
16: end loop

```

---

*On network end-to-end connectivity.* Before proceeding to the numerical results, an important issue on global connectivity in  $G_D^{2r}$  should be discussed. As already presented, the proposed control scheme maintains *local* connectivity in  $\mathcal{N}_i^{2r}$ , assuming that node  $i$  is the node that moves. Consequently, since only one node moves at a time-state, the only alteration to

### 5.3 Distributed Control for Optimum Coverage while Maintaining Network Connectivity

the connectivity graph is in the neighborhood of node  $i$ . However, when a node decides during its transition to drop a (redundant) link, even if does not affect connectivity in  $\mathcal{N}_i^{2r}$ , it must be assured that it will not affect global connectivity in  $G_d^{2r}$ , too, ensuring so that every other node will still be allowed to have information from its  $2r$ -limited Delaunay neighbors.

More specifically, the node-to-move decides to break a link via information from the set  $\mathcal{D}_i^N$ . Apparently if two node of the network utilize a link of  $i$  for preserving their  $N$ -hops connectivity among them, and node  $i$  knows about their existence, i.e. they belong to the set  $\mathcal{D}_i^N$ , then it will not break the aforementioned link, as it is vital for end-to-end connectivity of the network. The main question though is if this set is *sufficient* to guarantee that removal of this link will not violate *global* connectivity of the network. Since this is not trivially guaranteed when deciding via local information, this issue is formally stated and proven in the following lemma.

**Lemma 5.1.** *Consider a sensor network where each node has information from its  $N$ -hops afar nodes, that is the set  $\mathcal{D}_i^N$  for any arbitrary node  $i$ . If the node-to-move decides to drop a communication link during its transition to a new spot, deciding that it does not violate its connectivity with  $\mathcal{N}_i^{2r}$ , then it does not violate global  $N$ -hops connectivity among any two  $2r$ -limited Delaunay neighbors of the network, without needing to have global perception of the network.*

*Proof.* Assume that node  $i$  is the node that moves, and that at this time it has information from at-most  $N$ -hops-afar nodes, that is the set  $\mathcal{D}_i^N$  (Definition 5.3). Let  $d$  be the node with whom node  $i$  decides to abandon RF link (Fig. 5.10). Apparently, before the motion it holds  $i \longleftrightarrow d$ . What we need to prove is that, if there are two arbitrary nodes in the network that are  $2r$ -limited Delaunay neighbors (among them) and utilized the  $i$ - $d$  link for preserving  $N$ -hops connectivity among them, then both nodes are already known to node  $i$ .

Let  $j, k$  be the aforementioned two nodes in the network and the link  $i$ - $d$  is included in the  $N$ -hops-path between them, as being  $2r$ -limited Delaunay neighbors. The shortest path among the nodes  $j$  and  $k$  (including  $i$ - $d$  link) can be composed as shown in the two cases below:

- $j \longleftrightarrow q_1 \longleftrightarrow q_2 \dots q_m \longleftrightarrow d \longleftrightarrow i \longleftrightarrow q_{m+1} \longleftrightarrow q_{m+2} \dots q_{m+p} \longleftrightarrow k$  (a) or
- $j \longleftrightarrow q_1 \longleftrightarrow q_2 \dots q_m \longleftrightarrow i \longleftrightarrow d \longleftrightarrow q_{m+1} \longleftrightarrow q_{m+2} \dots q_{m+p} \longleftrightarrow k$  (b),

where  $m, p \in \mathbb{N}$ . For visualization purposes, topology-(a) is depicted graphically in Fig. 5.10. One can get topology-(b) just by swapping nodes  $i$  and  $d$ .

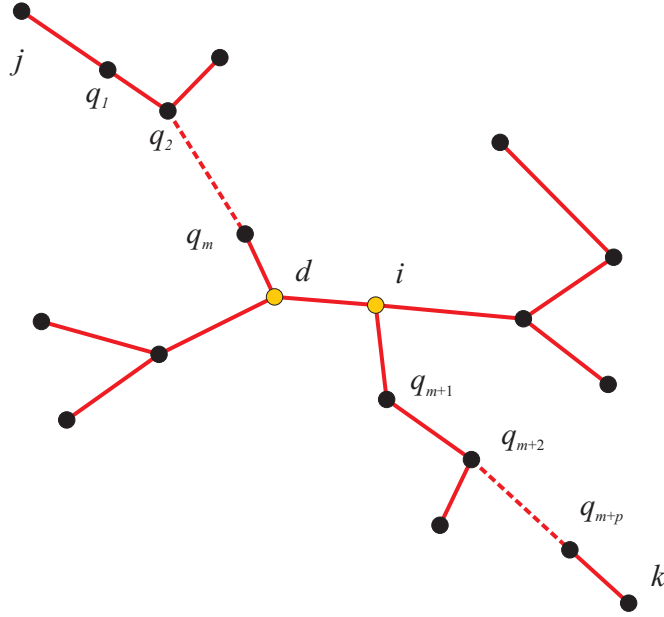


Figure 5.10: Notations concerning the proof of Lemma 5.1

Let us make the assumption that at least one node out of  $j, k$  is unknown to node  $i$ , which without loss of generality can be assumed as node  $j$ .

Topology-(a): Since  $j \in \mathcal{D}_k^N$ , as  $2r$ -limited Delaunay neighbors, enumerating the links in the path provides that  $(m+1)+1+(p+1) \leq N$ . Furthermore, since  $j$  is considered unknown to  $i$ , that is  $j \notin \mathcal{D}_i^N$ , it holds that the path from  $j$  to  $i$  has length at least  $N+1$ , that is  $m+2 \geq N+1$ . Utilizing the fact that  $m+p+3 \leq N$  we get  $m+2 \geq N+1 \Rightarrow m+p+3 > N+p+2 \Rightarrow N \geq N+p+2 \Rightarrow p \leq -2$ , leading in contradiction since  $p \in \mathbb{N}$ .

Topology-(b): The analysis in this case falls along the lines of the previous one. Again simple enumeration of links gives  $m+p+3 \leq N$ . In this case, though, the path from  $j$  to  $i$  consists of  $m+1$  links, instead of  $m+2$  previously. This results in  $m+1 \geq N+1$ . Working on the last expression, as before, provides  $m+1 \geq N+1 \Rightarrow m+p+3 > N+p+3 \Rightarrow N \geq N+p+3 \Rightarrow p \leq -3$ , which cannot hold as  $p \in \mathbb{N}$ .

Consequently, the original assumption is proven wrong and thus both nodes  $j$  and  $k$  are known to node  $i$  if they utilize the link  $i-d$  connectivity maintenance, that is  $j, k \in \mathcal{D}_i^N$ . This means that if two arbitrary nodes utilize the link for preserving  $N$ -hops connectivity among them, then they belong to the set of nodes that node  $i$  has perception of and thus can amend for not violating connectivity. But since nodes  $j, k$  are arbitrary, global connectivity among any two  $2r$ -limited Delaunay neighbors is guaranteed and this completes the proof.  $\square$

**Remark 5.2.** When the nodes are organized via the proposed control scheme (Algorithm 5.3),

### 5.3 Distributed Control for Optimum Coverage while Maintaining Network Connectivity

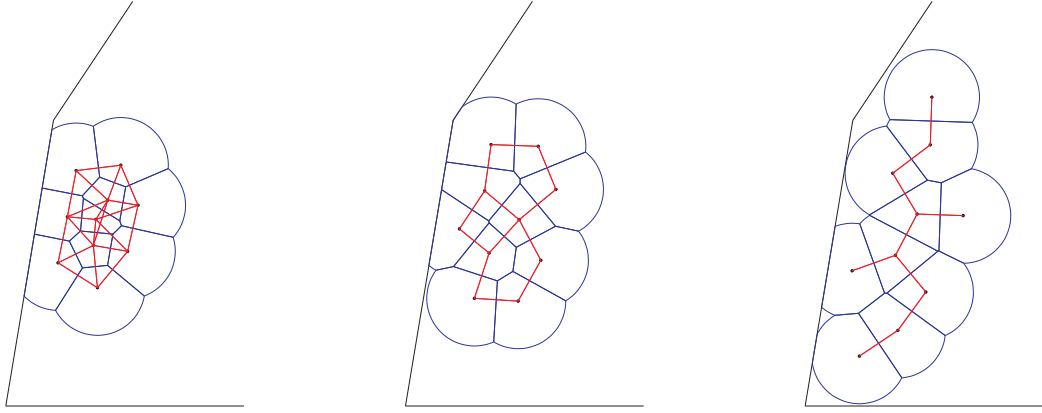


**Figure 5.11:** Converged state along with communication graph when 1-hop [left], 2-hops [middle] and 3-hops [right] connectivity is demanded.

*then if the network is initially end-to-end connected (Assumption 5.1), it will remain connected throughout evolution.*

Simulation results are presented in order to further verify the efficiency of the proposed control scheme. The area of interest is a convex compact planar set of total area  $\int_{\Omega} dx = 6.2 \text{ units}^2$ , which is identical to that used in [15] (also presented initially in Fig. 5.8). Let us assume the network consisting of  $n = 10$  nodes, identical to the one used in Fig. 5.7. These initial conditions will be utilized throughout the section for comparative analysis of the cases studied. The nodes are equipped with sensors of radius  $r = 0.2 \text{ units}$ , while their communication range is selected equal to sensing ( $R = r$ ) for visualization purposes. This is in fact a quite hard constraint imposed, comparing with the trivial case of  $R = 2r$ .

Comparative studies are presented in order to emphasize in the advantages provided by allowing multi-hopping inter-agent communication. Particularly, we examine the effect of the demanded  $N$ -hops connectivity in the network's coverage performance at the converged state, while applying the proposed connectivity-aware coordination scheme. During the study, the nodes were initially deployed in a way that Assumption 5.1 holds. The maximum possible coverage ratio is 20.6%, while the network initially senses 3.6% of the area. Simulations were conducted for different values of  $N$  hops allowed: 1, 2 and 3. The final network configuration in all three cases are presented in Fig. 5.11.

The effect of the allowed number of hops for connectivity preservation in the network's coverage performance is presented in Fig. 5.12. It is apparent that increasing the permitted number of hops among  $2r$ -limited Delaunay neighbors results in a significant increase in the

## 5. COVERAGE WITH CONSTRAINTS IN THE COMMUNICATION RANGE

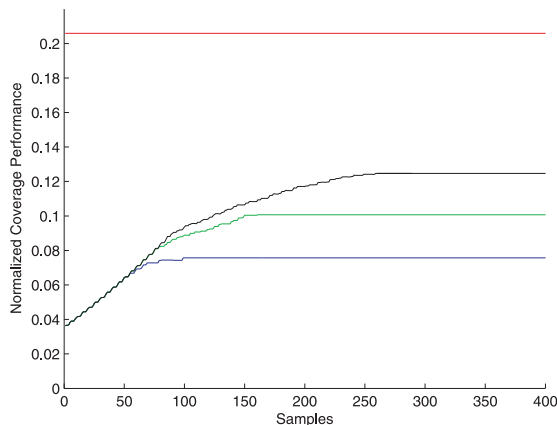


**Figure 5.12:** Effect of allowed number of hops for connectivity preservation in coverage performance [1-hop:blue, 2-hops:green, 3-hops:black].

percentage of the sensed area. However, maximum coverage performance cannot be achieved, since it is directly dependent on the sensing-to-radio radii ratio, encapsured in the overlapping among the nodes' sensing domains.

Besides the fact that fixed radio-range restrains the network from achieving maximum coverage performance, it can be seen that the network's performance index  $\mathcal{H}$  increases among any two consecutive time-steps. Note that at the time steps where network's coverage stays at same rate, it is the case where an interior node moves (one node at a time), trying to relax the critical-range constraints, rather than emphasize in increasing coverage, as explained at the design procedure.

It should be noted that in the case of 3-hops, there exist two nodes in the network (at the bottom-left side of the figure), which communicate via 4-hops instead of 3 (maximum allowed), while being  $2r$ -limited Delaunay neighbors. This is exactly the case that was depicted and discussed in Fig. 5.6; these nodes *became* neighbors during evolution, although not in  $N$ -hops-range, and did not abandon any link that used to preserve connectivity among them, instead. However, this issue does not have to do with the selected coordination scheme, but with a general fact that arises in RF-constraint networks.

### 5.3.3 Further heuristic extension

The achieved network's coverage performance, when the previously presented coordination scheme is applied may seem quite satisfactory given the imposed communication constraints. However, observing the final network configurations in Fig. 5.11, one could argue that an even

### 5.3 Distributed Control for Optimum Coverage while Maintaining Network Connectivity

better performance can be achieved, since there are nodes that still sense outside the area of interest. Apparently, if these nodes are to move away from the boundary, then the percentage of sensed area can be increased even more.

Even though this is not some general fact, it still applies to cases where the area under surveillance is quite larger than the maximum area that the nodes can sense. It should be noted that moving away from the boundary of the area of interest does not guarantee monotonic increase in the network's coverage as before, but may be dropped, when two consecutive time-steps are compared. Based on these remarks, an extended categorization of the nodes is proposed that takes into account contact with the area boundary, while coordination plan is modified accordingly, in order to amend for achieving possibly better results, in area-wise terms.

**Definition 5.5.** *In a network where the nodes' sensing performance is limited-range radial, let  $\bar{\mathcal{B}}$  contain the set of nodes whose  $r$ -limited Voronoi cell shares parts with the boundary of the region of interest. Let us call these as boundary nodes, defined as  $\bar{\mathcal{B}} := \{j \in I_n : \partial V_j^r \cap \partial \Omega \neq \emptyset\}$ . Let us define as interior nodes,  $\bar{\mathcal{I}}$ , the ones that their  $r$ -limited Voronoi cell does not contain any arc of the boundary of their sensing domain, while not belonging in the boundary-nodes category, that is  $\bar{\mathcal{I}} := \{j \in I_n \setminus \bar{\mathcal{B}} : \partial V_j^r \cap \partial \Omega = \emptyset\}$ . Univocally, the last set of exterior nodes  $\bar{\mathcal{E}} := I_n \setminus \{\bar{\mathcal{I}} \cup \bar{\mathcal{B}}\}$ , containing the rest nodes of the network, that is the nodes whose  $r$ -limited Voronoi cell contains at least one circular arc, while not being boundary node, though.*

Figure 5.13 depicts the categorization of twelve nodes into the above three categories, based not only on the existence of arcs on their  $r$ -limited Voronoi cell boundary, but based on the common parts with the boundary of the area under consideration. Apparently, these sets consist a tessellation of the nodes-set  $I_n$ .

Adding this extra category of boundary nodes, in comparison to the previous case, we select to plan their motion accordingly to the motivation that pushed us to discriminate them. More specifically, the latter are selected to move away from the boundary of the area  $\Omega$ , and particularly in the opposite direction of that of the closest point of  $\partial \Omega \cap \partial V_i^r$  to the node.

In accordance to the previously presented scheme, a (boundary) node moves with an appropriate step-size, as derived from the corresponding line-search, in the aforementioned direction providing that the demanded  $N$ -hops connectivity among its  $2r$ -limited Delaunay neighbors is maintained. In the case that no suitable step is found, the node stays idle. Although, the selection of the scheme invests in achieving a "better" final network configuration as far as coverage is concerned, it should be mentioned that monotonicity of the area evolution (3.15)

## 5. COVERAGE WITH CONSTRAINTS IN THE COMMUNICATION RANGE

---

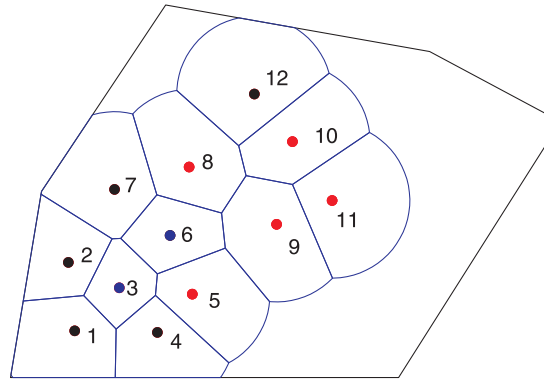


**Figure 5.13:** Categorization of nodes into interior(exterior)[boundary] nodes, denoted with blue(red)[black] dots.

is not guaranteed that way, since it is not selected to follow the gradient direction. This motion plan serves very well in cases where the area of interest is large enough, providing higher probability of achieving topological configurations with all nodes' sensing regions laying in the interior of the area of interest.

As for the interior and exterior nodes, accordingly, they are selected to move as described in section 5.3.2 on condition that, after their motions they should not be turned into boundary nodes. The extra restriction imposed arises from the need to prevent them from switching to boundary–category, since in that case the node will end in a cyclic loop. The main reason for this fact is the intuitive strategy followed for the boundary nodes' motion in order to assist the network achieve better area configurations, rather than contribute to coverage–increase directly. To avoid repetition, the control scheme in this section is not presented in some algorithmic form, since it shares most parts with the Algorithm 5.3, with the exception that boundary–nodes' motion is included as to move away from closest boundary point.

The control technique presented above is validated in the same sensor network as before, with exactly the same characteristics as in the previous case–study, that is same radii (sensing and radio ones), environment, initial conditions and connectivity restrictions (set at 2–hops). Figure 5.14 shows the network's initial configuration, the nodes' trajectories, along with the converged state.

Examining the results derived from that control scheme, in comparison to the results obtained before (for the 2–hops case), one can conclude that the network achieves better end–state coverage–performance, while connectivity maintenance demand still applies. However, due to the motion of boundary nodes heading away from the boundary, and not move with respect



### 5.3 Distributed Control for Optimum Coverage while Maintaining Network Connectivity

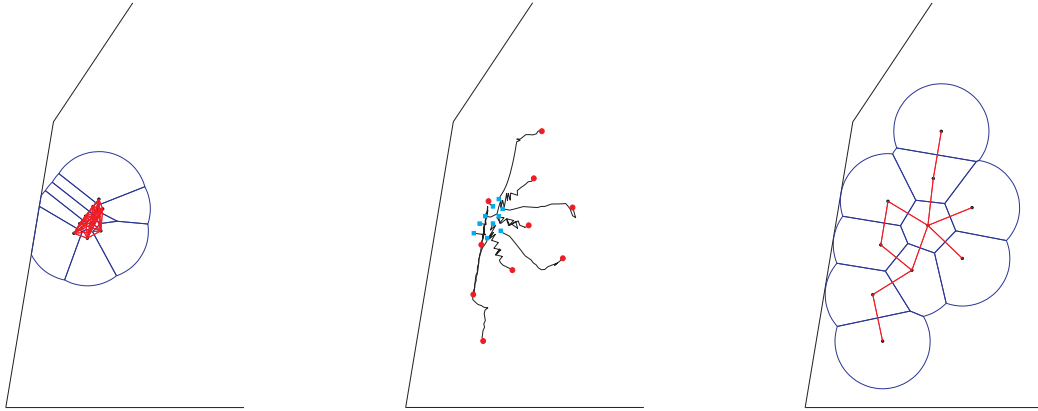


**Figure 5.14:** Coordination results derived via the heuristically extended control scheme. [Left] Initial network configuration. [Middle] network evolution. [Right] Final network state.

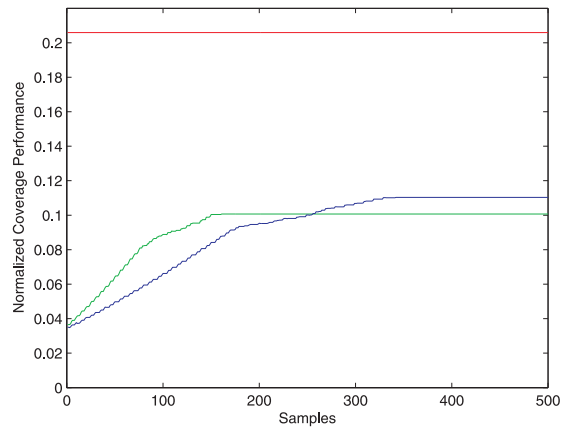


**Figure 5.15:** Percentage of sensed area during network evolution. Blue (green) line corresponds to Fig. 5.14 (5.11).

## 5. COVERAGE WITH CONSTRAINTS IN THE COMMUNICATION RANGE

---

to area–gradient–based headings, the percentage of sensed area is increased with reduced rate, compared to the green line in Fig. 5.12, which is also repeated for ease of comparison in Fig. 5.15. This is though the trade–off to balance in order to hopefully achieve configurations of better performance in coverage–terms.

### 5.4 Conclusions

In this chapter, two distributed coordination approaches were developed for controlling coverage performance of a mobile robotic network, when the nodes’ antenna range can take any arbitrary value, independently of the sensing range. In both proposed control schemes, the nodes plan their motion via information acquired from  $N$ –hops radio–connected nodes so that RF-connectivity among  $2r$ –limited Delaunay neighbors is retained. In the first scheme, the nodes are categorized based on the existence of arcs in their corresponding  $r$ –limited Voronoi cells, guaranteeing that the percentage of sensed area increases from one time–step to the other. In the sequel, an additional category is introduced based on contact with the boundary region, forcing the boundary nodes to plan their motions via the aspect of assisting the network to achieve a “better” (area–wise) final state, although monotonic increase in coverage during network evolution is not guaranteed that way. Simulation results were presented to confirm the efficiency of both control schemes in radio–range–constrained networks.

# 6

## Thesis Summary and Future Research Plans

### 6.1 Research Contribution

The purpose of this chapter is to summarize and discuss the main contribution topics of this thesis, along with providing insights on how the current results can be extended in the future. The main topic of research addressed is the possible ways to treat the area coverage problem in mobile robotic networks. The problem was initially approached for networks that evolve in discrete time by properly adjusting the motion of the node-to-move in order to ensure overall coverage increase [18]. It was shown that, although it suffers from relatively slow convergence due to the assumption of moving one node at each step, it can lead to optimal coverage performance [35]. The monotonic increase between each two consecutive steps is ensured by proper identification of future Delaunay neighbors based on a worst case scenario plan [36].

The case of heterogeneous networks was examined in the sequel, where the anisotropy was identified in the different radial sensing performance range of the nodes. The partitioning of the space was performed via a proposed pattern-based scheme that suits robotic teams with limited range sensory [37, 64], assigning convex domains of the configuration space among the members, in order to base their control action. A distributed control law was designed in order to lead a robotic team towards optimum surveillance of an area of interest, as based on the aforementioned proposed partitioning scheme [45].

The preceding work posed the main inspiration for treating coverage control in a combined “partitioning–development & controller–design” framework, allowing its extension for

## 6. THESIS SUMMARY AND FUTURE RESEARCH PLANS

---

swarms with heavily anisotropic sensing domains. At first stage, cooperative control action for networks with non-radial sensors has been examined, where the sensors were supposed to share the same heading (orientation) [65]. Based, on certain theorems for planar convex curves, a distributed control law was developed to lead the agents to optimal topology as far as the overall coverage is concerned [66]. The presented scheme was extended for networks with additional distance-like unevenness captured in the different scaling factors of the patterns [57].

Despite the fact that the aforementioned results were quite important in the overall distributed coverage concept, the assumption for common sensors orientation was still a hardly conservative factor. An innovative pattern-based partitioning is proposed in [67] in order to properly assign responsibility regions of the sensed configuration space among nodes with non-common sensor heading. Allowing rotation degree on the members' mobility, control action was designed so that it properly regulates both the nodes' positions and their orientations in order to achieve coverage optimal performance. The developed framework is suitable for any kind of sensory domain, making it quite attractive for real applications.

Although a communication range analysis followed each controller design in order to guarantee its distributed nature (since centralized schemes are somehow non realistic), it does not engulf the case of a-priori fixed radio-range for the nodes' communication devices. This problem is usually overcome by allowing the latter to be twice that of the sensing, assuming radial performance. The coverage problem was examined from an RF-constraint point of view, by imposing non-trivial assumptions in the overall problem formulation [68]. A combined control action was developed that allowed for simultaneous distributed optimization of the network's coverage and connectivity preservation, by properly manipulating redundant RF links [69] via self categorization of the nodes based on their topological state.

### 6.2 Extensions of current research

The results presented in this thesis have the potential to get extended or combined in order to form strategies that can be useful in more realistic applications. The pattern-based partitioning developed for the case of heterogeneous anisotropic sensors with rotation incorporated [67] is mainly applicable for any sensing pattern of the nodes, allowing it to become a core result for distributed control laws implemented the future. Although its complexity increases according to that of the pattern, it is the proper tool to get past the radial performance models.

Considering the rapid research development in the field of unmanned aerial vehicle control, the proposed coordination schemes can be almost directly applied for 3d space networks. Coverage control can be reformed as a continuous aerial surveillance problem for patrolling areas of interest for precaution or security applications. Challenging is the case when the footprint start to be treated as time-varying ones, where terms of convergence and optimal configuration need to be treated carefully.

Judging from the majority of the control algorithms for distributed coordination of groups of nodes, it is evident that incorporating different mobility models is still in research stage. Allowing nonholonomic constraints in the overall problem emphasizes in the need for applicability of the results in real experiments, while existence of radio constraints is something that cannot be neglected. A combined framework that can incorporate the above would form a significant advance in the current coverage formulation.

## **6. THESIS SUMMARY AND FUTURE RESEARCH PLANS**

---

# Curriculum Vitæ

Yiannis Stergiopoulos was born in Athens, Greece on October 20, 1982. He received his 5-years Diploma (magna cum laude) in Electrical & Computer Engineering from University of Patras in 2006 and was awarded for his performance during his studies by the Technical Chamber of Greece. His thesis was related to Input shaping Control of Oscillatory Electropneumatic Crane Systems, where he has published several articles on the corresponding field. In the summer of 2006 he started working on his doctoral thesis focusing in the field of Distributed Coverage Control in Mobile Robotic Networks, in the same institution. In 2011, in parallel with his PhD research studies, he obtained his 4-years degree in Mathematics (summa cum laude) at University of Patras. His main research interests include distributed optimization, coverage control, mobile robotic networks, input shaping and crane control.

## **List of Publications**, relevant to the subject of the PhD thesis

### **Journal articles**

- J1.** Y. Stergiopoulos, A. Tzes, "Spatially Distributed Area Coverage Optimisation in Mobile Robotic Networks with Arbitrary Convex Anisotropic Patterns," in *Automatica*, vol. 49, no. 1, pp. 232-237, 2013.
- J2.** Y. Stergiopoulos, Y. Kantaros, A. Tzes, "Distributed Control of Mobile Sensor Networks under RF Connectivity Constraints," in *International Journal of Distributed Sensor Networks*, Article ID 741821, doi: 10.1155/2012/741821, 2012.
- J3.** Y. Stergiopoulos, A. Tzes, "Decentralized Swarm Coordination: A Combined Coverage/Connectivity Approach," in *Journal of Intelligent and Robotic Systems*, vol. 64, no. 3-4, pp. 603-623, 2011.
- J4.** Y. Stergiopoulos, A. Tzes, "Convex Voronoi-inspired Space Partitioning for Heterogeneous Networks: A Coverage-oriented Approach," in *IET Control Theory and Applications*, vol. 4, no. 12, pp. 2802-2812, 2010.

## 6. THESIS SUMMARY AND FUTURE RESEARCH PLANS

---

### Conference articles

- C1.** Y. Stergiopoulos, A. Tzes, "Cooperative Positioning/Orientation Control of Mobile Heterogeneous Anisotropic Sensor Networks for Area Coverage," in *Proc. IEEE International Conference on Robotics & Automation*, pp. 1106-1111, Hong Kong, China, 2014.
- C2.** Y. Stergiopoulos, A. Tzes, "Autonomous Deployment of Heterogeneous Mobile Agents with Arbitrarily Anisotropic Sensing Patterns," in *Proc. 20<sup>th</sup> Mediterranean Conference on Control and Automation*, pp. 1585-1590, Barcelona, Spain, 2012.
- C3.** Y. Stergiopoulos, Y. Kantaros, A. Tzes, "Connectivity-aware Coordination of Robotic Networks for area Coverage Optimization," in *Proc. 2012 IEEE International Conference on Industrial Technology*, pp. 36-40, Athens, Greece, 2012.
- C4.** Y. Stergiopoulos, A. Tzes, "Coverage-oriented Coordination of Mobile Heterogeneous Networks," in *Proc. 19<sup>th</sup> Mediterranean Conference on Control and Automation*, pp. 175-180, Corfu, Greece, 2011.
- C5.** Y. Stergiopoulos, A. Tzes, "Decentralized Communication Range Adjustment Issues in MultiAgent Mobile Networks," in *Proc. 2010 American Control Conference*, pp. 1629-1634, Baltimore, USA, 2010.
- C6.** Y. Stergiopoulos, A. Tzes, "Convex Voronoi Space-Partitioning for Coverage Purposes in Heterogeneous Sensor Networks," in *Proc. 2009 IEEE European Control Conference*, pp. 2361-2366, Budapest, Hungary, 2009.
- C7.** Y. Stergiopoulos, A. Tzes, "Voronoi-based Coverage Optimization for Mobile Networks with Limited Sensing Range – A Directional Search Approach," in *Proc. 2009 American Control Conference*, pp. 2642-2647, Missouri, USA, 2009.



# References

- [1] *T-mote Sky Datasheet*, Moteiv/Sentilla Corporation, 11/13/2006. [Online]. Available: <http://www.sentilla.com>
- [2] *Polar Patterns*, Audio-Technica. [Online]. Available: <http://www.audio-technica.com>
- [3] J. Finke and K. Passino, “Stable cooperative vehicle distributions for surveillance,” *ASME Journal of Dynamic Systems, Measurement, and Control*, vol. 129, no. 5, pp. 597–608, 2007.
- [4] R. Murray, “Recent research in cooperative control of multivehicle systems,” *ASME Journal of Dynamic Systems, Measurement, and Control*, vol. 129, pp. 571–583, 2007.
- [5] J.-S. Li, H.-C. Kao, and J.-D. Ke, “Voronoi-based relay placement scheme for wireless sensor networks,” *IET Communications*, vol. 3, no. 4, pp. 530–538, 2009.
- [6] N. Leonard, D. Paley, F. Lekien, R. Sepulchre, D. Fratantoni, and R. Davis, “Collective motion, sensor networks, and ocean sampling,” *Proceedings of the IEEE*, vol. 95, no. 1, pp. 48–74, 2007.
- [7] Y. Guo and Z. Qu, “Coverage control for a mobile robot patrolling a dynamic and uncertain environment,” in *Proc. of World Congress on Intelligent Control and Automation*, China, 2004, pp. 1630–1635.
- [8] I. Hussein and D. Stipanović, “Effective coverage control for mobile sensor networks with guaranteed collision avoidance,” *IEEE Transactions on Control System Technology*, vol. 14, no. 4, pp. 642–657, 2007.
- [9] H. Chang, C. Lee, Y. Hu, and Y. Lu, “Multi-robot SLAM with topological/metric maps,” in *Proc. 2007 IEEE International Conference on Intelligent Robots and Systems*, San Diego, CA, 2007, pp. 1467–1472.
- [10] K. Alexis, G. Nikolakopoulos, A. Tzes, and L. Dritsas, *Applications of Intelligent Control to Engineering Systems*, ser. Intelligent Systems, Control and Automation: Science and Engineering. Springer Science, 2009, vol. 39, ch. 7: Coordination of Helicopter UAVs for Aerial Forest-Fire Surveillance, pp. 169–193.
- [11] J. Balasubramanian, J. Garcia-Fernandez, D. Isacoff, E. Spafford, and D. Zamboni, “An architecture for intrusion detection using autonomous agents,” in *Proc. of the 14<sup>th</sup> Annual Computer Security Applications Conference*, Phoenix, AZ, USA, 1998, pp. 13–24.
- [12] F. Bullo, J. Cortés, and S. Martinez, *Distributed Control of Robotic Networks*. Princeton University Press, 2009.
- [13] S. Martinez, J. Cortés, and F. Bullo, “Motion coordination with distributed information,” *IEEE Control Systems Magazine*, vol. 27, no. 4, pp. 75–88, 2007.

## REFERENCES

---

- [14] F. Aurenhammer and R. Klein, *Handbook of Computational Geometry*. Elsevier Publishing House, 1999, ch. 5: *Voronoi Diagrams*, pp. 201–290.
- [15] J. Cortés and F. Bullo, “Coordination and geometric optimization via distributed dynamical systems,” *SIAM Journal on Control and Optimization*, vol. 44, no. 5, pp. 1543–1574, 2005.
- [16] J. Cortés, S. Martinez, T. Karatas, and F. Bullo, “Coverage control for mobile sensing networks,” *IEEE Transactions on Robotics and Automation*, vol. 20, no. 2, pp. 243–255, 2004.
- [17] S. Boyd and L. Vandenberghe, *Convex Optimization*. Cambridge University Press, 2004.
- [18] J. Stergiopoulos and A. Tzes, “Voronoi-based coverage optimization for mobile networks with limited sensing range – a directional search approach,” in *Proc. 2009 American Control Conference*, Missouri, USA, 2009, pp. 2642–2647.
- [19] K. Laventall and J. Cortés, “Coverage control by robotic networks with limited-range anisotropic sensory,” in *Proc. of the 2008 American Control Conference*, Seattle, Washington, USA, 2008, pp. 2666–2671.
- [20] W. Sun and Y.-X. Yuan, *Optimization Theory and Methods: Nonlinear Programming*. Springer, 2006.
- [21] J. Cortés, S. Martinez, and F. Bullo, “Spatially-distributed coverage optimization and control with limited-range interactions,” *ESAIM: Control, Optimisation and Calculus of Variations*, vol. 11, no. 4, pp. 691–719, 2005.
- [22] Q. Du, V. Faber, and M. Gunzburger, “Centroidal Voronoi tessellations: Applications and algorithms,” *SIAM Review*, vol. 41, no. 4, pp. 637–676, 1999.
- [23] F. Aurenhammer and H. Edelsbrunner, “An optimal algorithm for constructing the weighted Voronoi diagram in the plane,” *Pattern Recognition*, vol. 17, no. 2, pp. 251–257, 1984.
- [24] A. Aggarwal, L. Guibas, J. Saxe, and P. Shor, “A linear-time algorithm for computing the Voronoi diagram of a convex polygon,” *Discrete & Computational Geometry*, vol. 4, no. 6, pp. 591–604, 1989.
- [25] F. Aurenhammer, “A new duality result concerning Voronoi diagrams,” *Discrete & Computational Geometry*, vol. 5, pp. 243–254, 1990.
- [26] —, “Power diagrams: Properties, algorithms and applications,” *Computational Geometry*, vol. 16, no. 1, pp. 78–96, 1987.
- [27] I. Emiris and M. Karavelas, “The predicates of the Apollonius diagram: Algorithmic analysis and implementation,” *Computational Geometry*, vol. 33, no. 1-2, pp. 18–57, 2006.
- [28] C. Friedrich, *Virtual Systems and Multimedia*, ser. Lecture Notes in Computer Science. Springer Berlin / Heidelberg, 2008, ch. 3, pp. 132–142.
- [29] Q. Du and D. Wang, “Anisotropic centroidal Voronoi tessellations and their applications,” *SIAM Journal of Scientific Computing*, vol. 26, no. 3, pp. 737–761, 2005.
- [30] A. Gusrialdi, S. Hirche, T. Hatanaka, and M. Fujita, “Voronoi based coverage control with anisotropic sensors,” in *Proc. of the 2008 American Control Conference*, Seattle, Washington, USA, 2008, pp. 736–741.

- 
- [31] L. Pimenta, V. Kumar, R. Mesquita, and G. Pereira, "Sensing and coverage for a network of heterogeneous robots," in *Proc. of the 47<sup>th</sup> Conference on Decision and Control*, Cancun, Mexico, 2008, pp. 3947–3952.
- [32] Y. Wang and I. Hussein, "Cooperative vision-based multi-vehicle dynamic coverage control for underwater applications," in *Proc. 16th IEEE International Conference on Control Applications*, Singapore, 2007, pp. 82–87.
- [33] A. Panousopoulou and A. Tzes, "On mobile agent positioning for wireless network reconfiguration," in *Proc. 6th International Symposium on Modeling and Optimization in Mobile, Ad Hoc, and Wireless Networks and Workshops WiOPT 2008*, Berlin, Germany, 2008, pp. 108–115.
- [34] H. Flanders, "Differentiation under the integral sign," *American Mathematical Monthly*, vol. 80, no. 6, pp. 615–627, 1973.
- [35] Y. Stergiopoulos and A. Tzes, "Decentralized swarm coordination: A combined coverage/connectivity approach," *Journal of Intelligent and Robotic Systems*, vol. 64, no. 3-4, pp. 603–623, 2011.
- [36] J. Stergiopoulos and A. Tzes, "Decentralized communication range adjustment issues in multiagent mobile networks," in *Proc. 2010 American Control Conference*, Baltimore, USA, 2010, pp. 1629–1634.
- [37] Y. Stergiopoulos and A. Tzes, "Convex Voronoi-inspired space partitioning for heterogeneous networks: A coverage-oriented approach," *IET Control Theory and Applications*, vol. 4, no. 12, pp. 2802–2812, 2010.
- [38] J. Le Ny and G. Pappas, "Sensor based robot deployment algorithms," in *Proc. IEEE Conference on Decision and Control*, Atlanta, GA, 2010.
- [39] A. Jadbabaie, J. Lin, and A. Morse, "Coordination of groups of mobile autonomous agents using nearest neighbor rules," *IEEE Transactions on Automatic Control*, vol. 48, no. 6, pp. 988–1001, 2003.
- [40] M. Zavlanos, H. Tanner, A. Jadbabaie, and G. Pappas, "Hybrid control for connectivity preserving flocking," *IEEE Transactions on Automatic Control*, vol. 54, no. 12, pp. 2869–2876, 2009.
- [41] M. Zavlanos and G. Pappas, "Distributed connectivity control of mobile networks," *IEEE Transactions on Robotics*, vol. 24, no. 6, pp. 1416–1428, 2008.
- [42] M. Zavlanos, M. Egerstedt, and G. Pappas, "Graph theoretic connectivity control of mobile robot networks," *Proc. of the IEEE*, vol. 99, no. 9, pp. 1525–1540, 2011.
- [43] M. Zavlanos, V. Preciado, A. Jadbabaie, and G. Pappas, "Spectral control of mobile robot networks," in *Proc. 2011 American Control Conference*, San Francisco, CA, 2011.
- [44] N. Bartolini, T. Calamoneri, T. La Porta, and S. Silvestri, "Autonomous deployment of heterogeneous mobile sensors," *IEEE Transactions on Mobile Computing*, vol. 10, no. 6, pp. 753–766, 2011.
- [45] Y. Stergiopoulos and A. Tzes, "Coverage-oriented coordination of mobile heterogeneous networks," in *Proc. of the 19<sup>th</sup> Mediterranean Conference on Control and Automation*, Corfu, Greece, 2011, pp. 175–180.
- [46] A. Getmanenko, "Helly-type theorems for plane convex curves," arXiv.org e-Print archive. [Online]. Available: <http://arxiv.org/abs/math.MG/0010311>

## REFERENCES

---

- [47] K.-J. Swanepoel, “Helly-type theorems for homothets of planar convex curves,” *Proc. of the American Mathematical Society*, vol. 131, no. 3, pp. 921–932, 2003.
- [48] I. Nourbakhsh, K. Sycara, M. Koes, M. Yong, M. Lewis, and S. Burion, “Human-robot teaming for search and rescue,” *IEEE Pervasive Computing*, vol. 4, no. 1, pp. 72–79, 2005.
- [49] J. Goodman, “On the largest convex polygon contained in a non-convex  $n$ -gon or how to peel a potato,” *Geometricae Dedicata*, vol. 11, no. 1, pp. 99–106, 1981.
- [50] J.-S. Chang and C.-K. Yap, “A polynomial solution for the potato-peeling problem,” *Discrete & Computational Geometry*, vol. 1, no. 1, pp. 155–182, 1986.
- [51] J.-M. Chassery and D. Coeurjolly, *Mathematical Morphology*. Springer Netherlands, 2006, ch. Optimal Shape and Inclusion Open Problems.
- [52] R. Forrest, “Interactive interpolation and approximation by Bézier polynomials,” *Computational Geometry*, vol. 15, no. 1, pp. 71–79, 1972.
- [53] T. Weise, *Global Optimization Algorithms — Theory and Application*, 2009. [Online]. Available: <http://www.it-weise.de>
- [54] D. Kandris, P. Tsioumas, A. Tzes, G. Nikolakopoulos, and D. Vergados, “Power conservation through energy efficient routing in wireless sensor networks,” *Sensors*, vol. 9, pp. 7320–7342, 2009.
- [55] B. Hexsel, N. Chakraborty, and K. Sycara, “Coverage control for mobile anisotropic sensor networks,” in *Proc. of the 2011 IEEE International Conference on Robotics and Automation*, Shanghai, China, 2011, pp. 2878–2885.
- [56] H. Imai, M. Iri, and K. Murota, “Voronoi diagram in the Laguerre geometry and its applications,” *SIAM Journal on Computing*, vol. 14, no. 1, pp. 93–105, 1985.
- [57] Y. Stergiopoulos and A. Tzes, “Autonomous deployment of heterogeneous mobile agents with arbitrarily anisotropic sensing patterns,” in *Proc. of the 20<sup>th</sup> Mediterranean Conference on Control and Automation*, Barcelona, Spain, 2012, pp. 1585–1590.
- [58] T. Razafindralambo and D. Simplot-Ryl, “Connectivity preservation and coverage schemes for wireless sensor network,” *IEEE Transactions on Automatic Control*, vol. 56, no. 10, 2011.
- [59] A. Panousopoulou and A. Tzes, “RF-power overlapping control for connectivity awareness in wireless ad-hoc and sensor networks,” in *Proc. 2nd IFAC Workshop on Distributed Estimation and Control in Networked Systems*, Annecy, France, 2010, pp. 275–280.
- [60] S. He, J. Chen, and Y. Sun, “Coverage and connectivity in duty-cycled wireless sensor network for event monitoring,” *IEEE Transactions on Parallel and Distributed Systems*, vol. 23, no. 3, 2012.
- [61] M. Zhong and C. Cassandras, “Distributed coverage control and data collection with mobile sensor network,” *IEEE Transactions on Automatic Control*, vol. 56, no. 10, 2011.
- [62] W. Li and C. G. Cassandras, “Distributed cooperative coverage control of sensor networks,” in *Decision and Control, 2005 and 2005 European Control Conference. CDC-ECC’05. 44th IEEE Conference on*. IEEE, 2005, pp. 2542–2547.

- [63] C. Godsil and G. Royle, *Algebraic Graph Theory*. New York: Springer-Verlag, 2001.
- [64] J. Stergiopoulos and A. Tzes, “Convex Voronoi space-partitioning for coverage purposes in heterogeneous sensor networks,” in *Proc. 2009 IEEE European Control Conference*, Budapest, Hungary, 2009, pp. 2361–2366.
- [65] Y. Stergiopoulos and A. Tzes, “Coordination of mobile networks for arbitrary sensing patterns,” in *Proc. IASTED International Conference on Control applications*, Crete, Greece, 2012, pp. 256–262.
- [66] —, “Spatially distributed area coverage optimisation in mobile robotic networks with arbitrary convex anisotropic patterns,” *Automatica*, vol. 49, no. 1, pp. 232–237, 2013.
- [67] —, “Cooperative positioning/orientation control of mobile heterogeneous anisotropic sensor networks for area coverage,” in *Proc. IEEE International Conference on Robotics & Automation*, Hong Kong, China, 2014, pp. 1106–1111.
- [68] Y. Stergiopoulos, Y. Kantaros, and A. Tzes, “Connectivity-aware coordination of robotic networks for area coverage optimization,” in *Proc. 2012 IEEE International Conference on Industrial Technology*, Athens, Greece, 2012, pp. 36–40.
- [69] —, “Distributed control of mobile sensor networks under RF connectivity constraints,” *International Journal of Distributed Sensor Networks*, vol. 2012, 7 pages, doi: 10.1155/2012/741821.

## REFERENCES

---

## **Declaration**

I herewith declare that I have produced this Thesis without the prohibited assistance of third parties and without making use of aids other than those specified; notions taken over directly or indirectly from other sources have been identified as such.

The thesis work was conducted from 13/07/2006 to 30/09/2014 under the supervision of Prof. Anthony Tzes at Electrical and Computer Engineering Department, University of Patras, Greece.

Patras,